In *The Wigner Distribution - Theory and Applications in Signal Processing*
W. Mecklenbräuker and F. Hlawatsch, Eds., Amsterdam: Elsevier, 1997, pp. 59-133.

The interference structure of the Wigner distribution and related time-frequency signal representations

F. Hlawatsch[a] and P. Flandrin[b]

[a]Inst. für Nachrichtentechnik u. Hochfrequenztechnik, Technische Universität Wien, Gusshausstrasse 25/389, A-1040 Vienna, Austria (fhlawats@email.tuwien.ac.at)

[b]Ecole Normale Superieure de Lyon, Laboratoire de Physique (URA 1325 CNRS), 46 allee d'Italie, 69364 Lyon Cedex 07, France (flandrin@physique.ens-lyon.fr)

Abstract

The interference terms (ITs) of the Wigner distribution (WD) dramatically affect WD analysis results and constitute a major problem in many WD applications. This tutorial chapter describes the geometry of ITs for both the WD itself and related time-frequency representations like the generalized Wigner distribution, the ambiguity function, and smoothed WD versions such as the pseudo Wigner distribution, the spectrogram, and the Choi-Williams distribution. The important classes of shift-invariant (Cohen-class) and shift-scale-invariant time-frequency representations are given special attention. Further aspects of ITs are also discussed, including relations with energetic signal parameters and the relevance of ITs to the definition of discrete-time WD versions.

1. INTRODUCTION

The interference structure of the Wigner distribution (WD) [1] strongly influences the results of WD-based signal analysis and restricts the WD's practical usefulness. It is thus of great theoretical and practical consequence, and a sound knowledge about the WD's interference structure is essential both for correctly interpreting WD results and for successfully applying the WD in practice. Let us illustrate this by an example. We wish to analyze, using the WD, a signal with sinusoidal frequency modulation. Since the WD is known to distribute the signal's energy over the time-frequency plane, we expect something like *Figure 1.a.* However, what we obtain is the result shown in *Figure 1.b.* We might then jump to the conclusion that the WD, in spite of its excellent mathematical properties, is not well fit for practical signal analysis. This conclusion, however, is not justified since also Figure 1.a was obtained using the WD. This seems paradoxical but can be explained as follows: the complexity (or, apparently, confusion) of Figure 1.b is caused by "inner interference terms" which have been suppressed in Figure 1.a by appropriate smoothing.

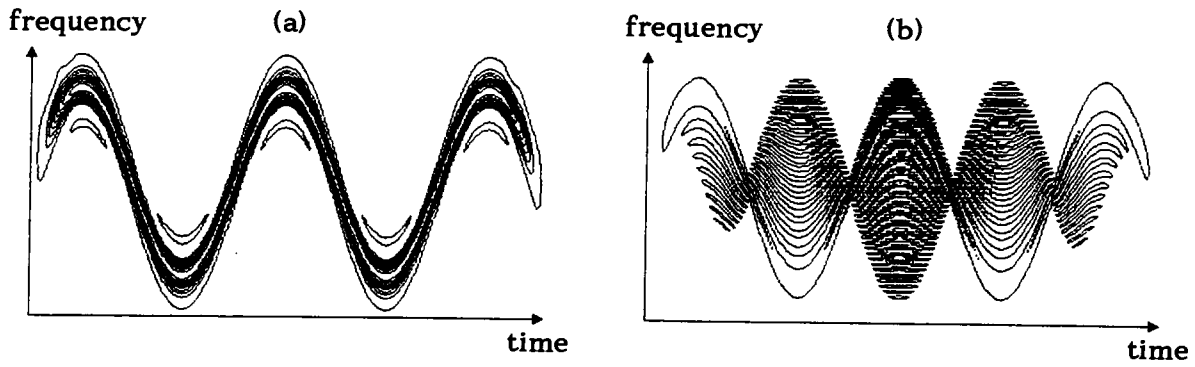

Figure 1. Time-frequency representation of sinusoidal frequency modulation: (a) expected result; (b) WD.

The example given shows the practical significance and relevance of interference terms (ITs). Indeed, two common practical situations call for some knowledge about the WD's interference structure. The first situation is that of "*prediction*:" based on some *a-priori* knowledge about the signal to analyze, we wish to predict what the signal's WD will look like, or what modifications of the WD we must employ to get a clear and readable WD result. In the second situation, that of "*interpretation*," we are given the WD of an unknown signal and wish to derive some information about the signal by interpreting various components and structures visible in the signal's WD.

Apart from its relevance to practical applications, the interference property of the WD is also interesting on theoretical grounds since it shows the high degree of organization and inner dependency inherent in the WD. The geometry of ITs highlights the WD's inherent symmetry and concentration and thus helps to explain why the WD is an ideal basis for time-frequency analysis. Indeed, time-frequency representations with quite similar mathematical properties (like, e.g., the WD and the Rihaczek distribution) will generally display one and the same signal in widely different ways; this can be nicely explained in terms of the different "interference geometries" of these representations. Finally, the WD's interference structure also has a bearing on the problem of time discretization. Specifically, it shows that the WD must generally be sampled twice as fast as the signal itself. Also, the aliasing components in the discrete-time WD can be interpreted as ITs.

One of the first accounts of the WD's interference structure has been given in [2], where the name "interference" is introduced. Other customary names are "cross terms," "ghost terms," or "phantom terms." We stress, however, that not all interference phenomena can be considered as bilinear cross terms; this is related to the distinction between "outer" and "inner" interference (see Section 5). Outer ITs of the WD, their characterization by means of the ambiguity function, and their attenuation by smoothing are discussed in [3]. Another study [4] investigates the geometric and energetic properties of ITs and extends the interference principle to monocomponent signals by introducing the concept of inner interference. For the class of amplitude-/frequency-modulated signals, the stationary-phase method has been used for an analytic derivation of the ITs' geometry [2,5], and characteristic

structures of ITs have been described by means of catastrophe theory [5,6]. In [7], the geometry of interference is discussed for the family of *generalized Wigner distributions* which is attractive from a theoretical viewpoint, and it has been shown that, inside this family, the WD is optimal with respect to interference geometry. A number of papers describe the ITs of smoothed WD versions like the *pseudo Wigner distribution* and the *spectrogram* and discuss the attenuation of ITs by means of time-frequency smoothing, e.g., [8-21]. This survey of previous work does not pretend to be exhaustive: since interference is a prominent feature of the WD, it is discussed, more or less explicitly, in many other papers as well.

This chapter is intended to be a tutorial exposition of the topic which encompasses many of the results and insights gained so far. We believe such a comprehensive treatment to be valuable especially for those who plan to use the WD as an analysis tool and wish to know what results they may expect and what modifications of the WD they will have to employ.

The chapter is organized in two parts. In Part I, the interference structure of the WD is considered. Part II studies the interference structure of some time-frequency representations related to the WD.

Note. In all figures showing results of the WD and related time-frequency representations, the time axis is horizontal and the frequency axis is vertical. In contour-line plots, only positive heights are indicated by contour lines since this yields a clearer display of the oscillatory interference terms as compared to plotting both positive and negative heights.

PART I - WIGNER DISTRIBUTION

Based on the WD's quadratic superposition principle, the ITs of the WD are first introduced in Section 2 as bilinear cross terms arising in the case of a multicomponent signal. This type of interference, termed "outer" interference, is further considered in Sections 3 and 4. Section 3 studies the geometry of outer ITs and shows that this geometry depends on the time-frequency locations of the interfering signal components. Based on the WD's marginal properties, energetic aspects of outer ITs are discussed in Section 4. Section 5 then extends the interference principle to the case of monocomponent signals by introducing the concept of "inner" interference. Outer and inner ITs are shown to possess identical geometric properties. Using the method of stationary phase, the laws of interference geometry are re-derived analytically for the class of amplitude-/frequency-modulated signals in Section 6. Section 7 uses results from catastrophe theory for studying characteristic singularities of ITs. Finally, Section 8 demonstrates the relevance of ITs in the context of discrete-time WD versions.

2. OUTER INTERFERENCE

The outer interference terms of the WD are a consequence of the WD's bilinear (or quadratic) structure; they occur in the case of multicomponent signals and can

be identified mathematically with quadratic cross terms.

Some WD fundamentals. The *cross-WD* of two signals x(t), y(t) with Fourier transforms X(f), Y(f) is defined as [1]

$$W_{x,y}(t,f) \triangleq \int_\tau x(t+\tfrac{\tau}{2})y^*(t-\tfrac{\tau}{2})\, e^{-j2\pi f\tau}\, d\tau = \int_\upsilon X(f+\tfrac{\upsilon}{2})Y^*(f-\tfrac{\upsilon}{2})\, e^{j2\pi t\upsilon}\, d\upsilon ,$$

with t and f denoting time and frequency, respectively. (Integrals go from $-\infty$ to ∞ unless stated otherwise.) The *auto-WD* of a single signal x(t) is defined as $W_x(t,f) \triangleq W_{x,x}(t,f)$. Both the cross-WD and auto-WD will be briefly called WD. From the WD's hermiticity property $W_{y,x}(t,f) = W^*_{x,y}(t,f)$, it follows that auto-WDs are real-valued even for complex signals. They may hence be represented graphically as surfaces over a time-frequency plane.

The WD can be interpreted as a distribution of the signals' *energy*

$$E_{x,y} \triangleq \int_t x(t)\, y^*(t)\, dt = \int_f X(f)\, Y^*(f)\, df$$

over the time-frequency plane. This is expressed mathematically by the well-known *marginal properties*

$$\int_f W_{x,y}(t,f)\, df = p_{x,y}(t) , \quad \int_t W_{x,y}(t,f)\, dt = P_{x,y}(f) , \quad \int_t\int_f W_{x,y}(t,f)\, dt\, df = E_{x,y} , \qquad (2.1)$$

which show that the *time-domain energy density* (instantaneous power) $p_{x,y}(t) = x(t)y^*(t)$ and the *frequency-domain energy density* (spectral energy density) $P_{x,y}(f) = X(f)Y^*(f)$ are "marginal densities" of the WD, and that, consequently, the WD's integral over the entire time-frequency plane yields the signals' energy. Still, a pointwise interpretation of the WD as a joint "time-frequency energy density" is not possible; such a concept is prohibited by the uncertainty principle [22]. Therefore, if the auto-WD $W_x(t,f)$ of a signal x(t) is large at a certain point (t,f) of the time-frequency plane, this does not necessarily mean that the signal x(t) has energy around this point. Indeed, it is this fact that motivates and necessitates the distinction between *WD signal terms* and *WD interference terms.*

A further important WD property is the property of *time-frequency shift invariance*: if the signals x(t) and y(t) are shifted with respect to time by t_0 and with respect to frequency by f_0,

$$x_0(t) = x(t-t_0)\, e^{j2\pi f_0 t} , \qquad y_0(t) = y(t-t_0)\, e^{j2\pi f_0 t} ,$$

then their WD is likewise shifted by t_0 and f_0,

$$W_{x_0,y_0}(t,f) = W_{x,y}(t-t_0,f-f_0) . \qquad (2.2)$$

Quadratic superposition and outer interference terms. It has just been shown that the WD is intimately related with the energy densities p(t), P(f) and the energy E. These signal parameters having a bilinear structure (quadratic structure in the "auto" case y(t)=x(t)), it is not surprising that also the WD has a bilinear (quadratic) struc-

ture. This fact is of particular significance in the case of multicomponent signals. Let us consider an N-component signal comprising N signal components $c_k x_k(t)$ with complex coefficients c_k,

$$x(t) = \sum_{k=1}^{N} c_k x_k(t) \ . \tag{2.3}$$

The auto-WD of the N-component signal x(t) can then be expressed as

$$W_x(t,f) = \sum_{k=1}^{N} \sum_{l=1}^{N} c_k c_l^* W_{x_k,x_l}(t,f) = \sum_{k=1}^{N} W_k^{(S)}(t,f) + \sum_{\substack{k=1 \\ (l>k)}}^{N} \sum_{l=1}^{N} W_{kl}^{(I)}(t,f) \ , \tag{2.4}$$

where

$$W_k^{(S)}(t,f) \triangleq |c_k|^2 \, W_{x_k}(t,f)$$

is the WD *signal term* corresponding to the k-th signal component $c_k x_k(t)$, and

$$W_{kl}^{(I)}(t,f) \triangleq c_k c_l^* W_{x_k,x_l}(t,f) + c_l c_k^* W_{x_l,x_k}(t,f) = 2\,\mathrm{Re}\left\{ c_k c_l^* W_{x_k,x_l}(t,f) \right\}$$

is the outer WD *interference term* (IT) corresponding to the k-th and l-th signal components $c_k x_k(t)$ and $c_l x_l(t)$. There is obviously $W_{kl}^{(I)}(t,f) = W_{lk}^{(I)}(t,f)$. According to the quadratic superposition law (2.4), the WD of an N-component signal consists of N signal terms and $\binom{N}{2} = \frac{N(N-1)}{2}$ ITs. Each signal component generates a signal term, and each *pair* of signal components generates an IT. While the number of signal terms thus grows linearly with the number N of signal components, the number of ITs grows *quadratically* with N.

3. INTERFERENCE GEOMETRY

The distinction between signal terms and outer ITs is not merely a formal one; typically, signal and interference terms are WD structures with qualitatively different geometric appearance. It will be seen that ITs are characterized, and distinguished from signal terms, by their *oscillation*; furthermore, the time-frequency location of ITs follows from the time-frequency locations of the corresponding signal terms. These geometric properties of ITs will be called the *interference geometry* of the WD.

Time-frequency location of outer ITs - the outer interference formula. We first discuss the *time-frequency location* of outer ITs. According to Section 2, the outer IT of two signals $x_1(t)$, $x_2(t)$ (we suppress the coefficients c_1, c_2 for simplicity) is given by $W_{12}^{(I)}(t,f) = 2\mathrm{Re}\{W_{x_1,x_2}(t,f)\}$. Suppose that the effective time-frequency supports of the corresponding signal terms $W_1^{(S)}(t,f) = W_{x_1}(t,f)$ and $W_2^{(S)}(t,f) = W_{x_2}(t,f)$ are the time-frequency regions R_1 and R_2, respectively. This means that the signal terms are approximately zero outside the respective region R_1 or R_2. What is the effective time-frequency support of the IT? A pointwise construction of the IT's time-frequency support, denoted by R_{12}, can be based on the *outer interference formula* of the WD [4]

$$|W_{x_1,x_2}(t,f)|^2 = \int_\tau \int_\upsilon W_{x_1}(t+\tfrac{\tau}{2}, f+\tfrac{\upsilon}{2})\, W_{x_2}(t-\tfrac{\tau}{2}, f-\tfrac{\upsilon}{2})\, d\tau\, d\upsilon \qquad (3.1)$$

which expresses the magnitude of the signals' cross-WD in terms of the signals' auto-WDs. Let (t_1,f_1) and (t_2,f_2) be two time-frequency points inside the time-frequency supports R_1 and R_2, respectively. We introduce the *center point* (t_{12},f_{12}), the *time lag* τ_{12}, and the *frequency lag* υ_{12} by

$$t_{12} \triangleq \frac{t_1+t_2}{2}\ , \quad f_{12} \triangleq \frac{f_1+f_2}{2}\ ; \qquad \tau_{12} \triangleq t_1-t_2\ , \quad \upsilon_{12} \triangleq f_1-f_2$$

so that, conversely,

$$t_1 = t_{12}+\frac{\tau_{12}}{2}\ , \quad f_1 = f_{12}+\frac{\upsilon_{12}}{2}\ ; \qquad t_2 = t_{12}-\frac{\tau_{12}}{2}\ , \quad f_2 = f_{12}-\frac{\upsilon_{12}}{2}\ .$$

(*These definitions of t_{12}, f_{12}, τ_{12}, and υ_{12} will remain valid throughout this work.*) The outer interference formula (3.1) then shows that the cross-WD $W_{x_1,x_2}(t,f)$ may be nonzero at the center point (t_{12},f_{12}). The center point will thus belong to the IT's support R_{12}.

The above result can be summarized as follows: *if the signal terms are nonzero around two points (t_1,f_1) and (t_2,f_2), respectively, then the corresponding IT must be expected to be nonzero around the center point (t_{12},f_{12}).* Based on this simple law, the IT's time-frequency support R_{12} may be constructed pointwise, as is shown in *Figure 2*: it is the collection of all center points (t_{12},f_{12}) for which $(t_1,f_1) \in R_1$ and $(t_2,f_2) \in R_2$. Note that the IT always lies inside a hull which is drawn around the two signal terms according to Figure 2.

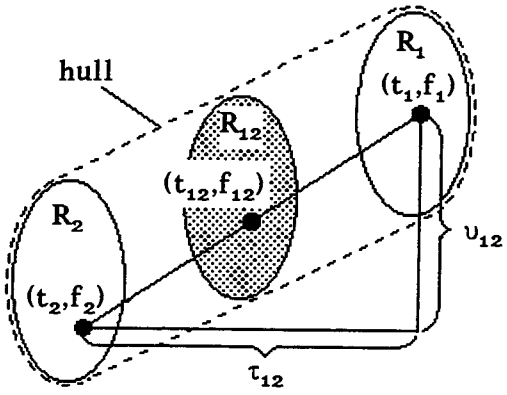

Figure 2. Pointwise construction of IT support R_{12}.

Oscillation of outer ITs. While the interference formula (3.1) gives a fairly complete characterization of the IT's time-frequency support, it does not say anything about the IT's *shape*. Indeed, an analytical treatment of this question seems to be difficult in the general case. We therefore consider the simple special situation where the interfering signals are identical apart from time-frequency shifts. This

situation allows a simple mathematical analysis and yet highlights the crucial feature of ITs, namely, their oscillation.

Let $x_0(t)$ be a signal which we assume to be centered around the time-frequency origin (0,0) for simplicity. From $x_0(t)$, we derive the signals

$$x_1(t) = x_0(t-t_1)\, e^{j2\pi f_1 t} \quad , \qquad x_2(t) = x_0(t-t_2)\, e^{j2\pi f_2 t}$$

by shifting $x_0(t)$ to the time-frequency locations (t_1,f_1) and (t_2,f_2), respectively. We may thus say that the two signals $x_1(t)$ and $x_2(t)$ are identical apart from the fact that they occur at different time-frequency locations. For the two-component signal $x(t) = c_1x_1(t) + c_2x_2(t)$, signal and interference terms are easily calculated: we obtain

$$W_1^{(S)}(t,f) = |c_1|^2\, W_{x_0}(t-t_1, f-f_1) \quad , \qquad W_2^{(S)}(t,f) = |c_2|^2\, W_{x_0}(t-t_2, f-f_2) \tag{3.2}$$

for the signal terms, and

$$W_{12}^{(I)}(t,f) = F(t-t_{12}, f-f_{12}) \, , \qquad F(t,f) = 2\,|c_1||c_2|\, W_{x_0}(t,f)\, \cos\left[2\pi(\upsilon_{12}t - \tau_{12}f) + \varphi_{12}\right] \tag{3.3}$$

with

$$\varphi_{12} = \arg\{c_1\} - \arg\{c_2\} + 2\pi\,\upsilon_{12}\,t_{12}$$

for the outer IT of the signal components $c_1x_1(t)$ and $c_2x_2(t)$. This result is illustrated in *Figure 3* for a Gaussian signal $x_0(t)$. According to (3.2), the signal terms equal the WD of $x_0(t)$ apart from scale factors and time-frequency shifts which reflect the time-frequency locations of the signals $x_1(t)$ and $x_2(t)$ in accordance with the WD's shift invariance property (2.2). The IT (3.3), on the other hand, is shifted to the *center point* (t_{12},f_{12}); we here observe the geometry described by the outer interference formula. The cosine factor in (3.3) expresses an *oscillation* whose "frequencies" in the time and frequency direction are given by the frequency and time lags υ_{12} and τ_{12}, respectively. This, in particular, implies that a large distance between the signal terms in the time (frequency) direction entails a faster IT oscillation in the frequency (time) direction. In a contour-line plot like Figure 3, the

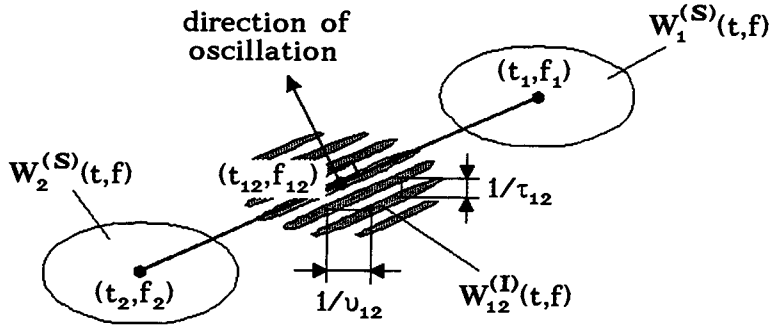

Figure 3. Interference geometry of WD.

direction of oscillation will be vertical to the line connecting the two signal terms irrespective of the graphical time and frequency scales. The *envelope* of the oscillatory IT surface is given by the WD of $x_0(t)$; it is independent of the time and frequency lags τ_{12} and υ_{12} and thus independent of the signal terms' time-frequency locations. The cosine modulation of (3.3) causes the IT to be partly negative. Finally, the *phase* of the oscillation depends on the difference of the phases of the coefficients c_1 and c_2.

While the IT's envelope only depends on the signal $x_0(t)$, the IT's time-frequency location and oscillation geometry merely depend on the time-frequency locations (t_1,f_1) and (t_2,f_2) of the interfering signal terms and on the phases of the signal coefficients c_1 and c_2. Note that the phases of the coefficients c_1 and c_2 do not show up in the signal terms; they are present in the IT only. As a simple example, we compare the two two-component signals $x^+(t) = x_1(t)+x_2(t)$ and $x^-(t) = x_1(t)-x_2(t)$ which differ merely with respect to the phase of c_2. In spite of this difference, the WD signal terms corresponding to the components of $x^+(t)$ and $x^-(t)$ are identical; however, the phases of the ITs' oscillation differ by π which corresponds to a change of sign of the entire IT. It is thus seen that the IT contains an important piece of information which is not contained in the signal terms.

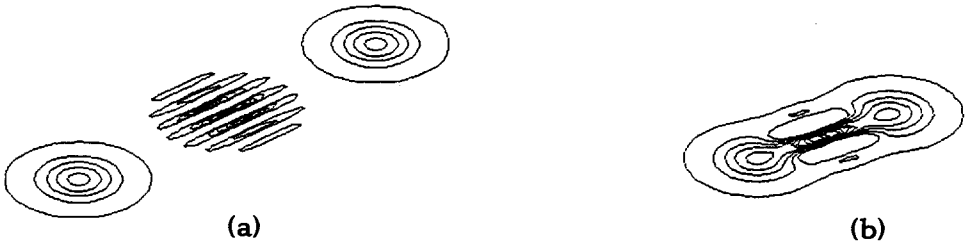

Figure 4. WD of two-component signal (Gaussian signal components): (a) isolated IT; (b) IT overlaps with signal terms.

Signal terms and IT will appear as isolated WD components only if the time lag τ_{12} and/or frequency lag υ_{12} of the interfering signal components is sufficiently large. If τ_{12} and υ_{12} are both small, then the IT may overlap with the associated signal terms, and signal terms and IT are not nicely separated. These two situations are compared in *Figure 4*. Note, also, that an IT is *oscillatory* only if the interfering signal components occupy essentially *different* regions of the time-frequency plane such that $\tau_{12}\neq 0$ and/or $\upsilon_{12}\neq 0$. If, on the other hand, the signal components occupy essentially the same time-frequency region ($R_1 \approx R_2$, which results in $\tau_{12}\approx 0$ and $\upsilon_{12}\approx 0$), the IT will not oscillate. Let us consider an extreme example to illustrate this situation. Obviously, any signal $x(t)$ may be decomposed as $x(t) = c_1x_1(t) + c_2x_2(t)$ with $x_1(t) = x_2(t) = x(t)$ and $c_2 = 1-c_1$. This is a completely artificial signal decomposition without any physical significance; the signal components are identical apart from factors and hence occupy the same time-frequency region. The WD signal terms and the IT here are

$$W_1^{(S)}(t,f) = |c_1|^2 W_x(t,f) , \qquad W_2^{(S)}(t,f) = |1-c_1|^2 W_x(t,f) ,$$

$$W_{12}^{(I)}(t,f) = 2|c_1||1-c_1| W_x(t,f) \cos\varphi$$

with $\varphi = \arg\{c_1\} - \arg\{1-c_1\}$. Signal terms and IT are thus seen to be identical apart from different factors; in particular, the IT does not exhibit any oscillation. From its appearance, it cannot be distinguished from a signal term (unless c_1 is chosen such that $\cos\varphi < 0$). This (extreme) example shows that a meaningful distinction between signal terms and outer ITs is possible only if the underlying signal decomposition is physically meaningful in the sense that the individual signal components are essentially "time-frequency disjoint."

Extension of interference geometry. So far, the WD's interference geometry has been studied for the special case where the interfering signal components are identical apart from time-frequency shifts. This assumption, while allowing a straightforward mathematical analysis, appears to be rather unrealistic. Still, it turns out that the results derived with this assumption are relevant also in the general case where the interfering signals are completely different.

In the general case, the laws of interference geometry are still valid but have to be applied "locally." This is best explained using a simple example. *Figure 5* shows the WD of a two-component signal consisting of a Gaussian signal and a complex sinusoid. The signal components are here quite different, and the WD signal terms accordingly have different shapes. To construct the IT by local application of the laws of interference geometry, we proceed as follows: we choose two points (t_1,f_1) and (t_2,f_2), one point inside each signal term. Midway between these two points, i.e., around the center point (t_{12},f_{12}), the IT will generally be nonzero; furthermore, it will *oscillate* with a local oscillation direction vertical to the line connecting the two "signal points" (t_1,f_1) and (t_2,f_2). The local oscillation "frequency" in the time (frequency) direction again equals the frequency lag υ_{12} (time lag τ_{12}) between the signal points.

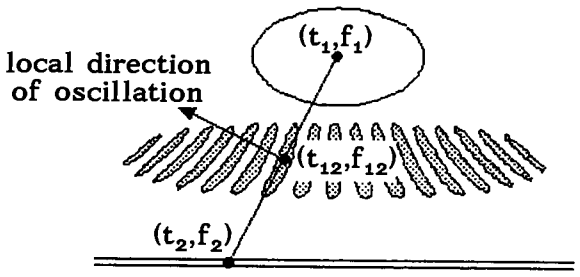

Figure 5. Local application of interference geometry.

An analytical derivation and justification of this construction scheme seems to be difficult in the general case. However, an approximate analysis can be performed

in the special situation where the signal components are sinusoids with amplitude and frequency modulation (see Section 6).

Finite-support properties. We finally consider the case where the interfering signal components $x_1(t)$ and $x_2(t)$ have finite time supports $[t_{1a},t_{1b}]$ and $[t_{2a},t_{2b}]$, respectively, i.e., they are zero outside the respective intervals. Due to the WD's finite-support property [1], the WD signal terms are then likewise zero outside these intervals. The IT can be shown to be zero outside the interval $[t_{12,a},t_{12,b}]$, where $t_{12,a} = (t_{1a}+t_{2a})/2$ and $t_{12,b} = (t_{1b}+t_{2b})/2$. This result is consistent with the general interference geometry. Similarly, if the signal components $x_1(t)$ and $x_2(t)$ are bandlimited in frequency intervals $[f_{1a},f_{1b}]$ and $[f_{2a},f_{2b}]$, respectively, the same is true for the WD signal terms, and the IT is restricted to the "interference band" $[f_{12,a},f_{12,b}]$ with $f_{12,a} = (f_{1a}+f_{2a})/2$ and $f_{12,b} = (f_{1b}+f_{2b})/2$.

4. ENERGETIC INTERPRETATION OF INTERFERENCE TERMS

Sometimes it is argued that ITs do not possess any "real physical significance" and that they are "artifacts" of the signal representation WD. We now discuss some relations of outer ITs with physically observable signal properties and physically measurable signal parameters.

Energy quantities, quadratic superposition, and marginal properties. Specifically, we investigate the "energy content" of outer ITs and the ITs' contribution to the physically significant energy quantities $p_{x,y}(t) = x(t)y^*(t)$, $P_{x,y}(f) = X(f)\,Y^*(f)$, and $E_{x,y} = \int p_{x,y}(t)\,dt = \int P_{x,y}(f)\,df$. Our discussion will be based on the WD's marginal properties (2.1),

$$\int_f W_{x,y}(t,f)\,df = p_{x,y}(t)\,, \quad \int_t W_{x,y}(t,f)\,dt = P_{x,y}(f)\,, \quad \int\!\!\int_{t\,f} W_{x,y}(t,f)\,dt\,df = E_{x,y}\,, \qquad (4.1)$$

which state that the energy quantities p(t), P(f), and E can be derived from the WD W(t,f) by integration with respect to t and/or f. Exactly as the WD, the energy quantities have bilinear (quadratic) structure and thus obey the same quadratic superposition principle. Let us consider the "auto case" y(t)=x(t) and assume the signal x(t) to be N-component as in (2.3). For the auto-energy $E_x=E_{x,x}$, for example, the quadratic superposition law then reads (cf. (2.4))

$$E_x = \sum_{k=1}^{N} E_k^{(S)} + \sum_{\substack{k=1 \\ (l>k)}}^{N} \sum_{l=1}^{N} E_{kl}^{(I)}\,. \qquad (4.2)$$

Analogously to the WD, the energy E_x comprises N "signal terms" $E_k^{(S)} = |c_k|^2 E_{x_k}$ and $\binom{N}{2} = \frac{N(N-1)}{2}$ cross or "interference" terms $E_{kl}^{(I)} = 2\,\mathrm{Re}\{c_k c_l^* E_{x_k,x_l}\}$. The marginal properties of the WD hold for both signal and interference terms *separately*: in the case of the energy, for example, we obtain

$$\int\!\!\int_{t\,f} W_k^{(S)}(t,f)\,dt\,df = E_k^{(S)}\,, \qquad \int\!\!\int_{t\,f} W_{kl}^{(I)}(t,f)\,dt\,df = E_{kl}^{(I)}\,. \qquad (4.3)$$

Analogous relations exist for the energy densities $p_x(t)$ and $P_x(f)$.

Energy content of outer ITs - orthogonality and time-frequency disjointness. Inserting (4.3) into (4.2), the energy of the N-component signal x(t) can be written in a way that involves the WD's signal and interference terms:

$$E_x = \sum_{k=1}^{N} \left[\iint_{t\,f} W_k^{(S)}(t,f)\,dt\,df \right] + \sum_{\substack{k=1 \\ (l>k)}}^{N} \sum_{l=1}^{N} \left[\iint_{t\,f} W_{kl}^{(I)}(t,f)\,dt\,df \right] .$$

This shows that, in general, both WD signal terms *and ITs* contribute to the signal's energy via their integrals. An IT's "energy content" (measured by its time-frequency integral) is not necessarily zero, which suggests that some physical significance can be attributed to ITs.

Still, the oscillatory shape of ITs indicates that an IT's time-frequency integral will generally be small as compared to that of signal terms: positive and negative contributions will tend to cancel each other. It is interesting to study the case where an IT's energy content is *exactly zero* [4]. Since the cross-energy $E_{x,y}$ of two signals x(t), y(t) equals the signals' inner product (x,y),

$$E_{x,y} = \int_t x(t)\,y^*(t)\,dt = (x,y) ,$$

an outer IT's energy content can be written as

$$\iint_{t\,f} W_{kl}^{(I)}(t,f)\,dt\,df = 2\,\mathrm{Re}\left\{ c_k c_l^*(x_k,y_l) \right\} .$$

Thus, a sufficient (though not necessary) condition for an IT to have zero energy content is the *orthogonality* $(x_k,x_l)=0$ of the interfering signals.

An important special case of orthogonality is time-frequency disjointness. We call two signals x(t), y(t) *time-frequency disjoint* if their WDs occupy different regions in the time-frequency plane and, consequently, do not overlap. Mathematically, this implies that the time-frequency supports R_x of x(t) and R_y of y(t) are disjoint and that, consequently, $W_x(t,f)\,W_y(t,f) \equiv 0$. Note that two signals may be time-frequency disjoint without being either time-disjoint ($x(t)y(t) \equiv 0$ or, equivalently, $p_x(t)p_y(t) \equiv 0$) or frequency-disjoint ($X(f)Y(f) \equiv 0$ or $P_x(f)P_y(f) \equiv 0$). Such a situation is shown in *Figure 6* for the case of two chirp signals (i.e., linear FM signals) with identical chirp rates: the WDs of the signals x(t) and y(t) are disjoint whereas the signals themselves overlap in both time domain and frequency domain.

Signals which are time-frequency disjoint are also orthogonal (the converse need not be true, as is demonstrated by the signals $x(t) = \sin(2\pi f_0 t)$ and $y(t) = \cos(2\pi f_0 t)$ which are orthogonal without being time-frequency disjoint). This follows immediately from *Moyal's formula* [1]

$$\iint_{t\,f} W_x(t,f)\,W_y(t,f)\,dt\,df = |(x,y)|^2$$

according to which $W_x(t,f)W_y(t,f) \equiv 0$ entails $(x,y) = 0$. We then conclude, finally, that *the IT of two time-frequency disjoint signals has zero energy content.*

In most practical situations, the exact version of time-frequency disjointness is too restrictive and must be replaced by an approximate version. Indeed, it is well

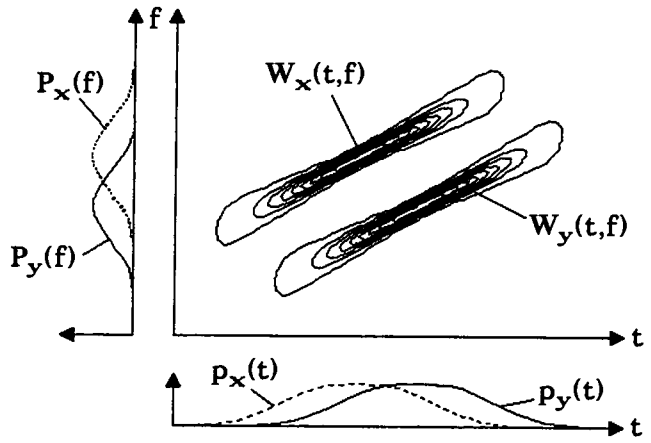

Figure 6. Time-frequency disjoint signals.

known that the WD cannot be strictly confined to a finite time-frequency region; thus, the situation illustrated in Figure 6 will generally correspond to an *approximate* time-frequency disjointness. Take, for example, the case of two time-frequency shifted Gaussian signals. The WD of a Gaussian signal is itself a two-dimensional Gaussian which, strictly speaking, occupies the entire time-frequency plane; however, it decays fast and is hence negligible outside a suitably chosen elliptical time-frequency contour. This means that the WDs of two Gaussian signals overlap irrespective of the signals' time-frequency distance; the signals are therefore not time-frequency disjoint in the strict sense. On the other hand, the overlap is negligible whenever the two Gaussians are sufficiently distant in the time-frequency plane: when this is the case, the signals are "approximately time-frequency disjoint." Our discussion has been based on the exact version of time-frequency disjointness, but the results are most significant in the "approximate" situation.

Beat effect and comb-filter effect. Even in those cases where an outer IT has zero energy content, it may be physically significant in the sense that it can be associated with a physically observable signal property. The link is again provided by the marginal relations of the WD. We consider two simple situations which illustrate this point. The first situation is that of two signal components which overlap in the time domain but are displaced in frequency. In the simplest case, the components $x_1(t)$ and $x_2(t)$ of the two-component signal $x(t) = c_1x_1(t) + c_2x_2(t)$ are complex sinusoids

$$x_1(t) = e^{j2\pi f_1 t}, \qquad x_2(t) = e^{j2\pi f_2 t} \tag{4.4}$$

with different frequencies ($f_1 \neq f_2$). The signal's instantaneous power (time-domain energy density) is

$$p_x(t) = |c_1|^2 + |c_2|^2 + 2|c_1||c_2|\cos(2\pi \upsilon_{12} t + \varphi_{12})$$

or, in more detail,

$$p_1^{(S)}(t) = |c_1|^2 , \qquad p_2^{(S)}(t) = |c_2|^2 , \qquad p_{12}^{(I)}(t) = 2|c_1||c_2|\cos\left(2\pi\upsilon_{12}t + \varphi_{12}\right)$$

with $\varphi_{12} = \arg\{c_1\} - \arg\{c_2\}$. The power shows an oscillation with frequency equal to the difference $\upsilon_{12} = f_1 - f_2$ of the signal frequencies f_1, f_2. If the signal frequencies are close, then this oscillation effect can be interpreted as an amplitude modulation of the two-component signal x(t); this is then known as the *beat* of the signal components $x_1(t)$ and $x_2(t)$. Note that this beat is expressed by the power's IT $p_{12}^{(I)}(t)$ which can be related to the WD's IT $W_{12}^{(I)}(t,f)$ via the interference-term version of the first marginal property

$$\int_f W_{12}^{(I)}(t,f)\,df = p_{12}^{(I)}(t).$$

Indeed, the signal terms and the IT of the WD are

$$W_1^{(S)}(t,f) = |c_1|^2\,\delta(f-f_1) , \qquad W_2^{(S)}(t,f) = |c_2|^2\,\delta(f-f_2) , \tag{4.5}$$

$$W_{12}^{(I)}(t,f) = 2|c_1||c_2|\,\delta(f-f_{12})\cos\left(2\pi\upsilon_{12}t + \varphi_{12}\right) . \tag{4.6}$$

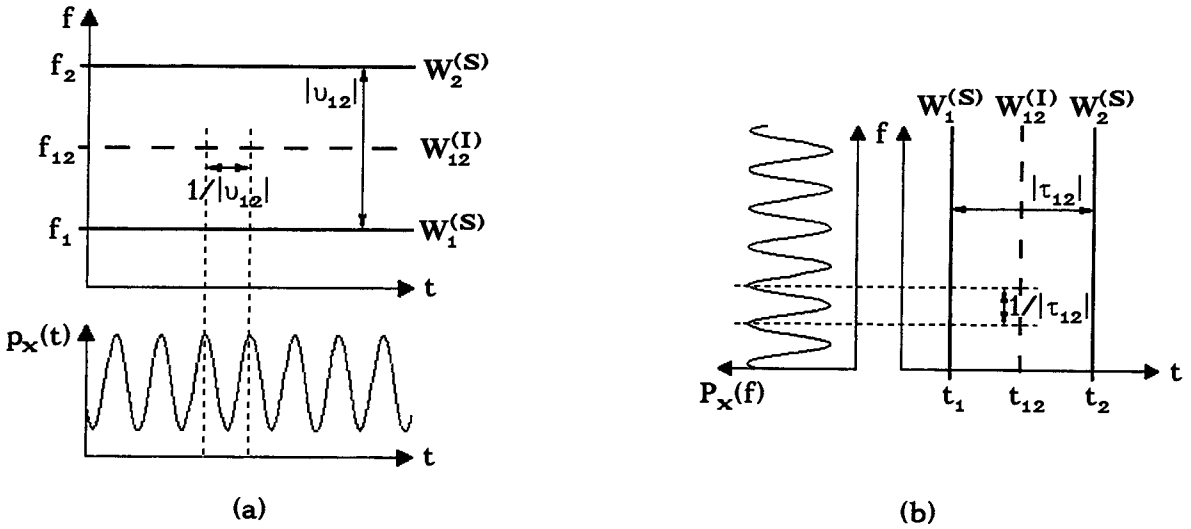

Figure 7. (a) The beat effect, (b) the comb-filter effect.

The WD signal terms are two time-invariant "spectral lines" at the signal frequencies f_1 and f_2. The outer IT, on the other hand, occurs at the center frequency $f_{12} = (f_1+f_2)/2$ and oscillates in the time direction with the beat frequency $\upsilon_{12} = f_1 - f_2$. The signal's WD and power are shown in *Figure 7.a.* We notice that *in the WD, the signal's beat is expressed by the IT, and only by the IT.* The IT is thus recognized to express a physically observable and significant signal property. In a certain sense, the occurrence of outer ITs in the WD is *enforced* by the marginal properties:

if the WD did not contain an oscillatory IT like (4.6) but only the stationary signal terms (4.5), then its integral with respect to frequency would be equally constant. Since the power itself is oscillatory, the first marginal property $\int W_{x,y}(t,f)\,df = p_{x,y}(t)$ could not be satisfied. Hence, the marginal property necessitates the existence of an oscillatory IT in the WD. While the marginal property does not completely define the IT's geometrical shape, it certainly defines the IT's oscillation.

The second situation is the time-frequency dual of the beat effect. We again assume a two-component signal $x(t) = c_1 x_1(t) + c_2 x_2(t)$, where the two signal components $x_1(t)$ and $x_2(t)$ now overlap in the frequency domain but are displaced in time. In the simplest case, the signal components are impulses at times t_1 and t_2,

$$x_1(t) = \delta(t-t_1) \quad , \qquad x_2(t) = \delta(t-t_2) \; .$$

This is indeed the time-frequency dual of (4.4) since the signal components of (4.4) are impulses in the frequency domain. We here compare the signal's spectral energy density

$$P_x(f) = |c_1|^2 + |c_2|^2 + 2\,|c_1|\,|c_2| \cos\left(2\pi\tau_{12} f - \varphi_{12}\right) \quad , \qquad \varphi_{12} = \arg\{c_1\} - \arg\{c_2\} \; ,$$

with the signal's WD

$$W_x(t,f) = |c_1|^2\,\delta(t-t_1) + |c_2|^2\,\delta(t-t_2) + 2\,|c_1|\,|c_2|\,\delta(t-t_{12}) \cos\left(2\pi\tau_{12} f - \varphi_{12}\right) \tag{4.7}$$

which is shown in *Figure 7.b*. The spectral energy density $P_x(f)$ *oscillates* with a "frequency" which equals the time lag $\tau_{12} = t_1 - t_2$ between the signal's impulse locations t_1, t_2. Suppose that the two-component signal $x(t) = c_1 x_1(t) + c_2 x_2(t)$ is interpreted as the impulse response of a linear time-invariant filter, with a "main peak" $c_1\delta(t-t_1)$ and an "echo" $c_2\delta(t-t_2)$. Due to the oscillation of $P_x(f)$, the filter's frequency response is that of a *comb filter*. In the WD, the filter's comb filter property is expressed by the IT

$$W_{12}^{(I)}(t,f) = 2\,|c_1|\,|c_2|\,\delta(t-t_{12}) \cos\left(2\pi\tau_{12} f - \varphi_{12}\right) \tag{4.8}$$

which occurs at the center time $t_{12} = (t_1+t_2)/2$ and shows the "comb-filter" oscillation with "frequency" $\tau_{12} = t_1 - t_2$.

The "beat effect" and the "comb-filter effect" are two basic situations which occur frequently in practical signal analysis. For the sake of simplicity, we have studied these situations with the assumption of extremely simple signal components (impulses in the frequency or time domain). However, the results can be generalized to the case of more complicated signal components. For the beat effect, it is essential that the signal components overlap in the time domain and occur at different frequencies; in the time interval of overlap, the power will then show an oscillation which is expressed in the WD by the oscillatory IT. The comb-filter effect is the time-frequency dual of the beat effect.

5. INNER INTERFERENCE

Outer ITs have been introduced as quadratic cross terms of the WD in the case where the signal to be analyzed is multicomponent. We have seen that the most important characteristic of outer ITs is their *oscillation* and partial negativity and, further, that the ITs' time-frequency support and oscillation geometry depend in a simple way on the time-frequency supports of the associated signal terms.

Monocomponent signals and inner ITs. Any given signal can be decomposed, and thus considered as multicomponent, in an infinity of ways. However, there are signals where a "natural" decomposition is impossible. We shall call such signals *monocomponent*. Even in the case of monocomponent signals, the WD generally contains interference terms which obey the same geometrical laws as the outer ITs considered so far; in particular, they are again oscillatory. These ITs of monocomponent signals will be termed *inner interference terms*. Inner ITs cannot be considered as quadratic cross terms of the WD since an adequate multicomponent signal model is not available.

We will now introduce inner ITs by studying a simple but characteristic example. Let us start with the Gaussian signal $x_g(t) = e^{-at^2}$, $a > 0$. Clearly, the signal is monocomponent: we could, for example, decompose it by simply cutting through the time axis; however, this would certainly be an entirely arbitrary and artificial procedure which is in no way motivated by the signal itself. The Gaussian's WD, shown schematically in *Figure 8.a*, is a two-dimensional Gaussian; it is strictly positive and non-oscillatory.

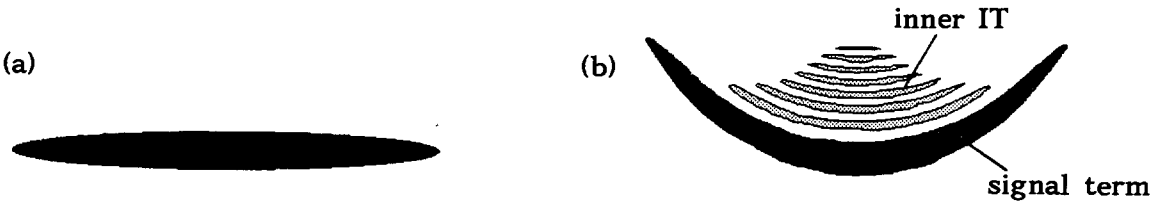

Figure 8. Inner interference: (a) WD of Gaussian signal; (b) WD of "twisted" Gaussian signal (occurrence of inner ITs).

Let us now apply a time-frequency "twist" to our Gaussian by introducing quadratic frequency modulation. The new signal is

$$x(t) = x_g(t)\, e^{j\varphi(t)}, \qquad \varphi(t) = \frac{b}{3}t^3,$$

with the instantaneous frequency

$$f_i(t) \triangleq \frac{1}{2\pi}\varphi'(t) = \frac{1}{2\pi}bt^2$$

being a quadratic function of time. The signal's WD is shown in *Figure 8.b*. We realize that the (originally Gaussian) WD is itself twisted according to the curvature of the instantaneous frequency; besides, there now exist oscillatory and partly

negative WD components. Indeed, the WD can be split into a "signal term" which occurs along the instantaneous-frequency curve and an oscillatory "inner interference term" located on the concave side of the instantaneous-frequency curve.

Geometry of inner ITs. The shape of the inner IT is consistent with the laws of interference geometry as derived previously for outer interference. As in the general case of outer interference, the laws of interference geometry must here be applied *locally* as follows: midway between two time-frequency points (t_1,f_1) and (t_2,f_2) of the signal term, i.e., around the center point (t_{12},f_{12}), the inner IT's local oscillation "frequency" in the time (frequency) direction equals the frequency lag $\upsilon_{12} = f_1 - f_2$ (time lag $\tau_{12} = t_1 - t_2$) between the two "signal points" (t_1,f_1) and (t_2,f_2). The IT's local direction of oscillation is thus again vertical to the line connecting the signal points. This, in fact, is exactly the same construction scheme as in the case of outer interference; the only difference is that now both "signal points" belong to one and the same signal component and, consequently, to one and the same WD signal term.

In a certain sense, there is no difference between inner and outer interference: the essential point is that the signal has energy contributions at different time-frequency locations; these energy contributions will then "interfere" and cause an oscillatory IT around the center point. For this mechanism, it is quite immaterial whether these energy contributions correspond to different signal components (case of outer interference) or to one and the same signal component (case of inner interference). In the first case, there exists an explicit multicomponent signal model; in the latter case, such a model cannot be found. In any case, ITs are characterized by their oscillation and partial negativity. Indeed, the local negativity of the WD can be considered as an interference phenomenon.

As in the case of outer interference, a mathematical description of the geometry of inner ITs seems to be difficult in general. However, an indication of the inner IT's time-frequency support is given by the "inner interference formula" [2,4]

$$\left[W_x(t,f)\right]^2 = \int_\tau \int_\upsilon W_x\left(t+\tfrac{\tau}{2}, f+\tfrac{\upsilon}{2}\right) W_x\left(t-\tfrac{\tau}{2}, f-\tfrac{\upsilon}{2}\right) d\tau\, d\upsilon \qquad (5.1)$$

which is derived from the outer interference formula (3.1) by letting $x_1(t) = x_1(t) = x(t)$. The inner interference formula expresses the high degree of symmetry and organization inherent in (auto) WD surfaces; it shows that the WD values at different points of the time-frequency plane are not independent and thus highlights the redundancy of the signal representation WD.

We can use the inner interference formula (5.1) for answering the following question: if the effective support of a WD signal term is the time-frequency region R_S, what is the effective support R_I of the associated inner IT? Based on (5.1), the time-frequency region R_I can be constructed pointwise as discussed in Section 3 for the case of outer interference: if the two time-frequency points (t_1,f_1) and (t_2,f_2) are inside R_S, then the center point (t_{12},f_{12}) will be inside R_I (see *Figure 9*). This, in particular, implies that an inner IT always lies inside a hull drawn around the signal term as shown in Figure 9.

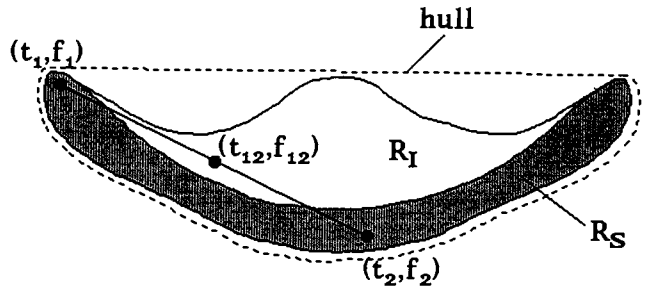

Figure 9. Pointwise construction of time-frequency support of inner IT.

6. THE STATIONARY-PHASE APPROXIMATION

In the case of sinusoids with amplitude modulation (AM) and frequency modulation (FM), the *method of stationary phase* [23] can be applied for a characterization of inner and outer ITs and for an analytical derivation of the WD's interference geometry. This approach, which has been proposed in [2] and worked out in [5,7], provides a mathematical foundation of the laws of interference geometry for a comparatively large and interesting class of signals.

Let us start with *inner* interference. We consider a complex monocomponent AM-FM signal

$$x(t) = a(t)\, e^{j\varphi(t)}, \qquad a(t)\geq 0, \qquad \varphi(t)\in\mathbb{R} \tag{6.1}$$

with *instantaneous amplitude* (envelope) a(t) *and instantaneous phase* $\varphi(t)$. We assume that the instantaneous amplitude a(t) is slowly varying as compared to the oscillatory FM factor $e^{j\varphi(t)}$. For our discussion, the *instantaneous frequency* $f_i(t) = \frac{1}{2\pi}\varphi'(t)$ will be most important since it closely corresponds to the geometry of the WD surface (the *signal term*, and thus the signal's energy, is located along the curve of instantaneous frequency).

The stationary-phase approximation. The WD of the AM-FM signal (6.1) can be written as

$$W_x(t,f) = \int_\tau L(t;\tau)\, e^{j\Phi(t,f;\tau)}\, d\tau \tag{6.2}$$

with

$$L(t;\tau) = a\left(t+\tfrac{\tau}{2}\right) a\left(t-\tfrac{\tau}{2}\right), \qquad \Phi(t,f;\tau) = \varphi\left(t+\tfrac{\tau}{2}\right) - \varphi\left(t-\tfrac{\tau}{2}\right) - 2\pi f\tau\ .$$

The WD is thus recognized as an *oscillatory integral* which can be calculated in an approximate way by the *method of stationary phase* [23]. To evaluate (6.2) at a given time-frequency point (t_o,f_o), we define the function $\Phi_o(\tau) \triangleq \Phi(t_o,f_o;\tau)$ and consider the values τ_i for which the first derivative of $\Phi_o(\tau)$ vanishes. Let us suppose that the equation $\Phi_o'(\tau) = 0$ has n solutions τ_i and that all "stationary points" τ_i satisfy $\Phi_o''(\tau_i) \neq 0$. The stationary-phase approximation of $W_x(t_o,f_o)$ is then given by

$$W_x(t_o,f_o) \approx \sum_{i=1}^{n} R_o(\tau_i)\, e^{j\Psi_o(\tau_i)} \tag{6.3}$$

with

$$R_o(\tau) \triangleq \frac{L(t_o;\tau)}{\sqrt{|\Phi_o''(\tau)|}} , \qquad \Psi_o(\tau) \triangleq \Phi_o(\tau) + \frac{\pi}{4}\,\mathrm{sign}\{\Phi_o''(\tau)\} . \tag{6.4}$$

We see that each stationary point τ_i yields a contribution to $W_x(t_o,f_o)$. If $\Phi_o'(\tau) = 0$ does not have any solution, then the stationary-phase approximation vanishes, $W_x(t_o,f_o) \approx 0$. If, finally, a solution τ_i to $\Phi_o'(\tau) = 0$ does not satisfy $\Phi_o''(\tau_i) \neq 0$, then the corresponding contribution to (6.3) diverges and, in fact, the stationary-phase approximation (6.3) is not valid. It is easily seen that the stationary points τ_i always occur by pairs: if a certain τ is a stationary point, i.e., satisfies $\Phi_o'(\tau) = 0$ and $\Phi_o''(\tau) \neq 0$, then $-\tau$ is a stationary point as well. The number n of stationary points τ_i is thus even, and the stationary-phase approximation (6.3) can be rewritten as

$$W_x(t_o,f_o) \approx 2 \sum_{i=1}^{n/2} R_o(\tau_i) \cos \Psi_o(\tau_i) , \qquad \tau_i > 0 , \tag{6.5}$$

where now only the positive τ_i are included. This expression is consistent with the real-valuedness of the auto-WD.

Interference geometry. We now give a geometrical interpretation of the relations $\Phi_o'(\tau) = 0$, $\Phi_o''(\tau) \neq 0$ specifying the stationary points τ_i for a given time-frequency point (t_o,f_o). These equations can be rewritten in terms of the instantaneous frequency $f_i(t)$ and its derivative $f_i'(t)$ as

$$f_o = \frac{f_i(t_o+\frac{\tau}{2}) + f_i(t_o-\frac{\tau}{2})}{2} , \qquad f_i'(t_o+\tfrac{\tau}{2}) \neq f_i'(t_o-\tfrac{\tau}{2}) . \tag{6.6}$$

The first equation of (6.6) is simply a restatement of the WD's interference geometry. This is easily seen by letting

$$t_1 = t_o+\tfrac{\tau}{2} , \qquad t_2 = t_o-\tfrac{\tau}{2} , \qquad f_1 = f_i(t_o+\tfrac{\tau}{2}) = f_i(t_1) , \qquad f_2 = f_i(t_o-\tfrac{\tau}{2}) = f_i(t_2) ,$$

so that $t_o = t_{12} = (t_1+t_2)/2$, $\tau = \tau_{12} = t_1-t_2$, and the first equation of (6.6) reduces to $f_o = f_{12} = (f_1+f_2)/2$. This can now be interpreted as follows: at a given time-frequency point (t_o,f_o), the WD will be nonzero only if two points (t_1,f_1) and (t_2,f_2) *on the instantaneous-frequency curve* $f_i(t)$ can be found such that (t_o,f_o) is the center point (t_{12},f_{12}) of (t_1,f_1) and (t_2,f_2) (cf. *Figure 10*). Any pair of points on the instantaneous-frequency curve for which (t_o,f_o) is center point gives a stationary point $\pm\tau$, with $\tau = \tau_{12} = t_1-t_2$, and thus produces a distinct contribution to the (real-valued) stationary-phase approximation (6.5). For the stationary-phase approximation to be valid, the second equation of (6.6), $f_i'(t_1) \neq f_i'(t_2)$, must be satisfied; this equation simply requires that the *slopes* of the instantaneous-frequency curve $f_i(t)$ must not be equal at the points t_1 and t_2.

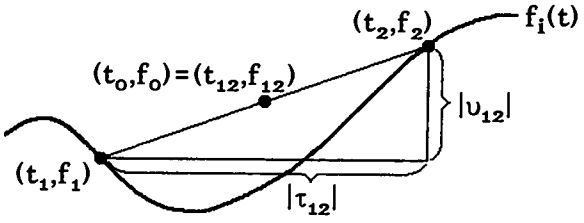

Figure 10. Consistency of stationary-phase approximation with interference geometry.

If the WD is evaluated on the instantaneous-frequency curve, i.e., (t_0,f_0) is chosen such that $f_0 = f_i(t_0)$, then the symmetry conditions $t_0 = t_{12}$, $f_0 = f_{12}$ have a trivial solution $t_1 = t_2 = t_0$, $f_1 = f_2 = f_0$ which corresponds to τ=0: the points (t_1,f_1) and (t_2,f_2) here coalesce. Obviously, the requirement of different slopes is then not satisfied, and the stationary-phase approximation is not valid.

Intuitively, it is rather clear that the WD signal term is located along the curve of instantaneous frequency. The stationary-phase approximation (6.5) cannot be used for calculating this signal term, but it allows an approximate calculation of the inner IT. If (t_1,f_1) and (t_2,f_2) are two points of the signal term, i.e., on the instantaneous-frequency curve, then the corresponding "interference point" is the center point $(t_0,f_0) = (t_{12},f_{12})$. If, for the sake of simplicity, we assume that no other pair of points on the instantaneous-frequency curve has the same center point, then the stationary-phase approximation has only a single contribution,

$$W_x(t_{12},f_{12}) \approx 2\,R_0(\tau_{12})\cos\Psi_0(\tau_{12}) =$$

$$= 2\frac{a(t_1)\,a(t_2)}{\sqrt{\frac{\pi}{2}\left|f_i'(t_1)-f_i'(t_2)\right|}}\cos\left[\varphi(t_1)-\varphi(t_2)-2\pi f_{12}\tau_{12}+\varphi_0\right] \qquad (6.7)$$

with $\varphi_0 = \frac{\pi}{4}\,\mathrm{sign}\{f_i'(t_1)-f_i'(t_2)\}$. This is an approximate expression for the inner IT at the center point (t_{12},f_{12}). We note, in particular, that (6.7) is proportional to $a(t_1)\,a(t_2)$, the product of the instantaneous signal amplitudes at the interfering points t_1 and t_2. Furthermore, (6.7) is inversely proportional to $|f_i'(t_1)-f_i'(t_2)|$, the difference between the slopes of the instantaneous-frequency curve at t_1 and t_2: increasing parallelism of slopes yields a larger WD value at the center point (t_{12},f_{12}). In the case of exact parallelism, $f_i'(t_1) = f_i'(t_2)$, the stationary-phase approximation (6.7) is infinite and not valid.

Apart from the location and local amplitude of the IT, also the IT's oscillation can be derived by means of the stationary-phase approximation (6.7). To obtain an indication of the local behavior of the WD around the center point (t_{12},f_{12}), we replace t_0 by $t_0+\Delta t$ and f_0 by $f_0+\Delta f$, where $|\Delta t|$ and $|\Delta f|$ are assumed to be small. We consider τ_{12} as fixed and both $a(t)$ and $f_i'(t)$ as locally constant around t_1 and t_2. Furthermore, we use the linear approximation $\varphi(t+\Delta t) \approx \varphi(t) + \varphi'(t)\,\Delta t = \varphi(t) + 2\pi f_i(t)\,\Delta t$. With this, (6.7) yields

$$W_x(t_{12}+\Delta t, f_{12}+\Delta f) \approx 2\frac{a(t_1)\,a(t_2)}{\sqrt{\frac{\pi}{2}\left|f_i'(t_1)-f_i'(t_2)\right|}} \cos\left[2\pi\left(\upsilon_{12}\Delta t - \tau_{12}\Delta f\right)+\psi_o\right]$$

with $\tau_{12}=t_1-t_2$, $\upsilon_{12}=f_1-f_2=f_i(t_1)-f_i(t_2)$, and $\psi_o=\varphi(t_1)-\varphi(t_2)-2\pi f_{12}\tau_{12}+\varphi_o$. We recognize an oscillation as predicted by the laws of interference geometry: around the center point (t_{12},f_{12}), the local oscillation "frequency" in the time (frequency) direction equals the frequency lag $\upsilon_{12}=f_1-f_2$ (time lag $\tau_{12}=t_1-t_2$) between the interfering points (t_1,f_1) and (t_2,f_2); the direction of oscillation is again vertical to the line connecting these points. This geometry is illustrated in *Figure 11.*

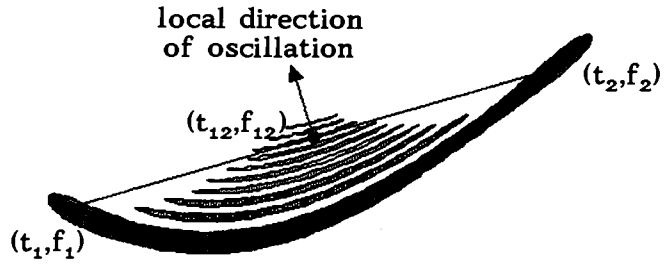

Figure 11. Local oscillation of IT.

Outer Interference. All of the results derived above for inner interference can be reformulated for the case of outer interference. We assume an N-component signal with signal components of the AM-FM type,

$$x(t) = \sum_{k=1}^{N} x_k(t) , \qquad x_k(t) = a_k(t)\, e^{j\varphi_k(t)} . \tag{6.8}$$

For the sake of simplicity, the signal components' coefficients c_k are assumed to be included in the instantaneous amplitudes $a_k(t)$ and the instantaneous phases $\varphi_k(t)$. The outer IT of the k-th and l-th signal component is

$$W_{kl}^{(I)}(t,f) = 2\,\mathrm{Re}\left\{W_{x_k,x_l}(t,f)\right\} = 2\,\mathrm{Re}\left\{\int_\tau L_{kl}(t;\tau)\, e^{j\Phi_{kl}(t,f;\tau)}\, d\tau\right\}$$

with

$$L_{kl}(t;\tau) = a_k\left(t+\tfrac{\tau}{2}\right) a_l\left(t-\tfrac{\tau}{2}\right) , \qquad \Phi_{kl}(t,f;\tau) = \varphi_k\left(t+\tfrac{\tau}{2}\right) - \varphi_l\left(t-\tfrac{\tau}{2}\right) - 2\pi f\tau \quad .$$

The outer IT is thus expressed as the real part of an oscillatory integral which can again be approximated by means of the stationary-phase method. As the derivations are completely analogous to the previously discussed case of inner interference, we shall not further elaborate the case of outer interference. Similar to the case of inner interference, the stationary-phase approximation is again consistent with the local application of the laws of interference geometry as described in Section 3.

Real-valued signal. A real-valued AM-FM signal

$$x(t) = a(t)\cos\varphi(t)$$

can be written as a two-component complex-valued AM-FM signal,

$$x(t) = a_1(t)\, e^{j\varphi_1(t)} + a_2(t)\, e^{j\varphi_2(t)}$$

with $a_1(t) = a_2(t) = \frac{1}{2}a(t)$, $\varphi_1(t) = \varphi(t)$, and $\varphi_2(t) = -\varphi(t)$. It can thus be regarded as a special case of the multicomponent signal (6.8). The instantaneous frequencies of the two signal components satisfy $f_{i,2}(t) = -f_{i,1}(t)$. This symmetry with respect to frequency is also visible in the signal terms and the outer IT of the WD: it is easily shown that $W_2^{(S)}(t,f) = W_1^{(S)}(t,-f)$ and $W_{12}^{(I)}(t,-f) = W_{12}^{(I)}(t,f)$.

7. SINGULARITIES OF INTERFERENCE TERMS

According to (6.4), the stationary-phase approximation (6.3) diverges when a stationary point τ is such that $\Phi_0''(\tau) = 0$. This is especially the case when $\tau = 0$, i.e., when the time-frequency point of evaluation, (t_0,f_0), lies on the instantaneous-frequency curve $f = f_i(t)$.

As shown in *Figure 12*, this curve corresponds to the exact border between two regions with dramatically different behaviors: within the shaded area, *two* distinct stationary points $\pm\tau$ exist, leading to a non-zero stationary-phase approximation, whereas outside this area, *no* stationary point exists and the approximated WD is negligible. This sudden change in behavior which occurs when passing through the boundary of the shaded area (and which corresponds to the coalescence of two stationary points) is expressed by the local divergence of the stationary-phase approximation; following [24,6,7], it can be viewed as a "catastrophe" of the WD.

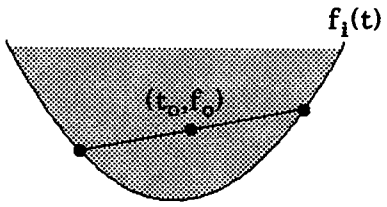

Figure 12. Stationary-points area.

Catastrophes of WD. Catastrophe theory (CT) [25], which provides a qualitative framework for describing sudden changes in systems, can be used for evaluating oscillatory integrals such as (6.2). In a very general manner, CT states that the qualitative behavior of an oscillatory integral only depends on the singularities of the phase function $\Phi_0(\tau)$, i.e., on how the successive derivatives of $\Phi_0(\tau)$ vanish. Since the desired description is essentially qualitative, the approach of CT is to replace the true phase function by a standard ("generic") phase function which possesses the same structure concerning singularities.

This results in both a qualitative *description*, which holds even when the stationary-phase approximation breaks down, and a *classification* of possible geometrical

structures, which only involves a reduced number of typical cases associated to "elementary" catastrophes. The number of these typical cases depends on the dimension of the problem, i.e., on the number of parameters controlling the phase. In the case of the WD considered here, $\Phi_o(\tau) = \Phi(t_o,f_o;\tau)$ depends on one variable, the integration variable τ, and two parameters, the evaluation time t_o and frequency f_o. As a remarkable consequence, CT tells us that *only two* elementary catastrophes may occur and lead to essential contributions [24]. This corresponds to the following situations associated with the successive derivatives of $\Phi_o(\tau)$.

(i) Stationary-points areas. Stationary-points areas comprise those points (t_o,f_o) for which there exist two distinct values $\pm\tau$ such that

$$\Phi_o'(\tau) = 0 \quad , \qquad \Phi_o''(\tau) \neq 0 \quad .$$

This is just the case where the stationary-phase approximation holds (cf. Section 6); hence, the stationary-points area is the shaded region in Figure 12.

(ii) Fold lines. Fold lines, the first elementary catastrophe of the WD, consist of those points (t_o,f_o) for which

$$\Phi_o'(\tau) = 0 \quad , \qquad \Phi_o''(\tau) = 0 \quad , \qquad \Phi_o'''(\tau) \neq 0 \quad ,$$

which implies that

$$f_o = \frac{f_i(t_o+\frac{\tau}{2}) + f_i(t_o-\frac{\tau}{2})}{2} \quad , \qquad f_i'(t_o+\tfrac{\tau}{2}) = f_i'(t_o-\tfrac{\tau}{2}) \quad , \qquad f_i''(t_o+\tfrac{\tau}{2}) \neq -f_i''(t_o-\tfrac{\tau}{2}) \, . \tag{7.1}$$

Thus, fold lines consist of chord midpoints for which the slopes of $f_i(t)$ at the corresponding chord endpoints are equal and the curvatures of $f_i(t)$ at these endpoints do not have equal magnitudes and opposite signs. As shown in *Figure 13*, there are two types of fold lines: (a) the instantaneous-frequency curve $f = f_i(t)$, for which $\tau = 0$, and (b) a "ghost curve" $f = \tilde{f}_i(t)$, for which $\tau \neq 0$. This ghost structure is obviously related to the inner interference mechanism.

Figure 13. Fold lines.

In the vicinity of $f_i(t)$, a "transitional" approximation of the WD can be obtained by expanding the instantaneous phase $\Phi_o(\tau)$ to the third order, which corresponds to expanding the instantaneous frequency $f_i(t)$ to the second order around t_o [2]. This leads to

$$W_x(t,f) \approx W_a(t,f) \underset{f}{*} \left[-\frac{1}{\varepsilon(t)} \mathrm{Ai}\left(\frac{1}{\varepsilon(t)}(f-f_i(t))\right)\right] \quad \text{with} \quad \varepsilon(t) = \sqrt[3]{\frac{f_i''(t)}{32\pi^2}} \tag{7.2}$$

where $W_a(t,f)$ is the WD of the AM part a(t), $\overset{*}{f}$ denotes convolution with respect to the frequency variable, and

$$\mathrm{Ai}(y) = \int_u e^{j(yu+u^3/3)}\,du \tag{7.3}$$

is the *Airy function* [26], the characteristic function of the fold catastrophe (see *Figure 14*). From this result, we conclude that, locally, the WD of an FM signal generally exhibits a fast decay on the convex side of $f_i(t)$ and oscillatory fringes (inner interference terms) on its concave side. Note that the Airy-function approximation does not diverge on $f_i(t)$; it is thus a refinement of the stationary-phase approximation. Furthermore, it can be checked from (7.3) that the Airy function has its centroid, but not its maximum, located at the origin $y = 0$ (cf. Figure 14.b). This implies that the frequency $f = f_i(t)$ corresponds to the "center of gravity" of the WD with respect to the frequency variable but does not equal the maximum of the WD, which is slightly displaced towards the concave side of $f_i(t)$.

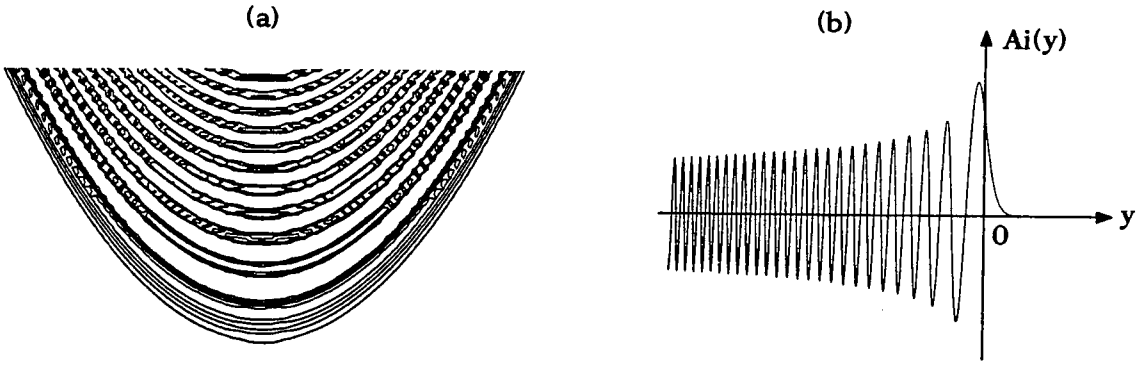

Figure 14. (a) Quadratic FM model, (b) Airy function.

The Airy-function approximation (7.2) depends (via the parameter $\varepsilon(t)$) on the local curvature $f_i''(t)$ of $f_i(t)$. If this curvature vanishes (local linear FM approximation or local chirp approximation), then insertion of the limit identity

$$\lim_{\varepsilon \to 0} \frac{1}{\varepsilon}\,\mathrm{Ai}\left(\frac{y}{\varepsilon}\right) = \delta(y)$$

into (7.2) yields

$$W_x(t,f) \approx W_a(t, f-f_i(t)) ,$$

which is exactly the WD of a linear FM signal (chirp signal) with amplitude modulation a(t).

(iii) Cusp points. Cusp points are the second elementary WD catastrophe. They are characterized by

$$\Phi_o'(\tau) = 0 \ , \quad \Phi_o''(\tau) = 0 \ , \quad \Phi_o'''(\tau) = 0 \ , \quad \Phi_o''''(\tau) \neq 0 \ ,$$

and are hence singularities of fold lines (see (7.1)) for which

$$f_i''(t_o+\tfrac{\tau}{2}) = -f_i''(t_o-\tfrac{\tau}{2}) \ .$$

Since the curvatures of $f_i(t)$ at the chord endpoints must now have equal magnitudes but opposite signs, cusp points can only occur on "ghost" fold lines. An example (corresponding to a two-component signal) is given in *Figure 15.*

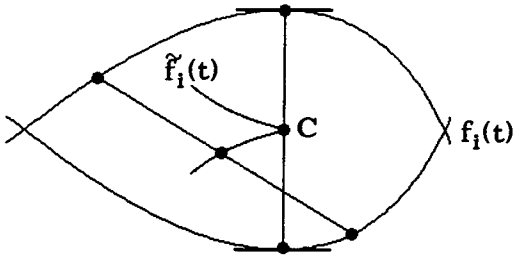

Figure 15. Cusp point (C).

At cusp points, the WD is peaked and its local geometry is governed by a two-dimensional special function called the *Pearcey function,*

$$Pe(t,f) = \int_u e^{j(tu-fu^2/2+u^4/8)}\,du \ ,$$

which is characteristic of the cusp catastrophe.

The three situations discussed - stationary-points areas, fold lines, and cusp points - essentially exhaust the possible situations in the two-parameter case of the WD. We note that points of higher-order singularities, which are midpoints of an *infinity* of chords, could also be considered. These occur in the case of perfectly symmetrical instantaneous-frequency curves $f_i(t)$, and at these points, the WD is highly peaked (see *Figure 16*). An example is the case of a linear FM signal. However, such situations are *unstable* in the sense that the slightest change in the perfect symmetry structure destroys the high-order singularity and reduces it to one of the previous situations.

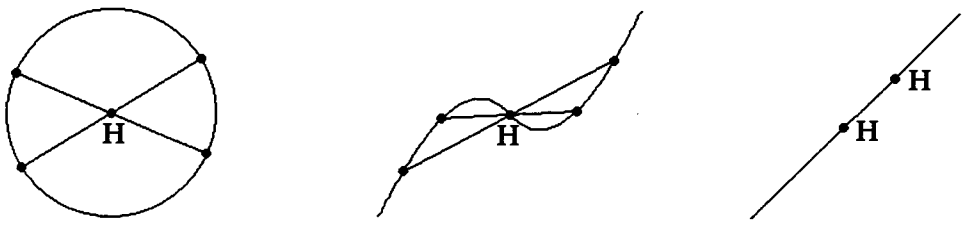

Figure 16. Points of higher-order singularities (H).

8. SAMPLING AND ALIASING

If signal processing is performed on a digital computer, then discrete-time signals have to be used, and a discrete-time version of the WD has then to be found which operates on the discrete signal samples. The definition of such a discrete-time WD is not straightforward, and several approaches are possible. However, a basic requirement is that the discrete-time WD is a time-sampled version of the continuous-time WD, where the sampling is done "properly" such that the continuous-time WD can be recovered via the usual reconstruction procedure. In this section, we study aspects of the WD's interference geometry which are relevant to the definition of a discrete-time WD.

Minimal WD sampling rate. We first discuss the minimal rate at which the WD must be sampled in the time direction. Let us consider signals $x(t)$ which are bandlimited to frequencies $|f| < F/2$; the signals' total bandwidth is thus F. (We have assumed a signal band centered at the frequency origin $f = 0$; however, our discussion can easily be reformulated for other band locations, e.g., $0 < f < F$.) According to the sampling theorem, the minimal sampling rate which allows the signal $x(t)$ to be recovered from its samples is the Nyquist rate $R_N = F$.

In order to determine the minimal time sampling rate for the WD, we have to investigate the WD's variation in the time direction. This time variation is governed by the oscillatory ITs of signal components displaced with respect to frequency. According to the WD's interference geometry, the IT oscillation frequency in the time direction equals the frequency distance of the interfering signal components. The fastest oscillation will hence occur when the signal components' frequency distance is maximal, i.e., when the signal components are located at the band edges $\pm F/2$. This "worst case" situation can be modelled by the signal components

$$x_1(t) = x_0(t)\, e^{j2\pi\frac{F-\varepsilon}{2}t} \quad , \qquad x_2(t) = x_0(t)\, e^{-j2\pi\frac{F-\varepsilon}{2}t} \quad , \tag{8.1}$$

where $x_0(t)$ is a narrowband lowpass signal bandlimited to $|f| < \varepsilon/2$. According to (8.1), the signals $x_1(t)$ and $x_2(t)$ are obtained by shifting the lowpass signal $x_0(t)$ to the band edges $\pm F/2$ of our signal band $|f| < F/2$ (see *Figure 17*). Note that $x_1(t)$ and $x_2(t)$ are properly bandlimited to $|f| < F/2$ and can thus be sampled at the Nyquist rate $R_N = F$.

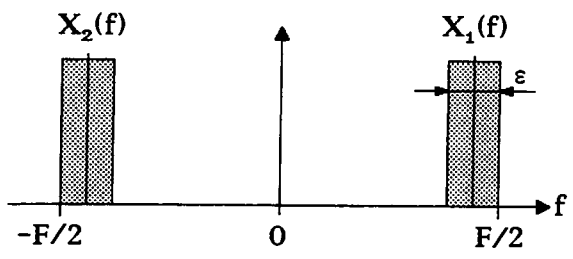

Figure 17. "Worst case" signal components with fastest IT oscillation.

The outer IT of the signal components $x_1(t)$ and $x_2(t)$,

$$W_{12}^{(I)}(t,f) = 2\, W_{x_0}(t,f) \cos\left[2\pi(F-\varepsilon)t\right] , \tag{8.2}$$

oscillates in the time direction with frequency F-ε. To sample (8.2) with respect to time such that the sampling condition is met, the sampling rate R_{WD} must satisfy $R_{WD} > 2(F-\varepsilon)$ which tends to 2F for $\varepsilon \to 0$. This shows that sampling the WD at the Nyquist rate, $R_N = F$, is not sufficient: *the WD must be sampled with respect to time at (at least) twice the Nyquist rate.*

WD aliasing as an interference phenomenon. We next consider the discrete-time version $x_d(n) = x(nT)$ (with $n \in \mathbb{Z}$) of a continuous-time signal x(t). The discrete-time signal $x_d(n)$ is derived from x(t) by sampling with sampling period T or sampling rate $R = 1/T$.

The most popular definition of a discrete-time WD (DTWD) is [27]

$$W_{x_d}^{(d)}(n,\Theta) = 2 \sum_m x_d(n+m)\, x_d^*(n-m)\, e^{-j4\pi\Theta m} ,$$

where n is the discrete time index and Θ is a normalized frequency parameter. It can be shown [27] that $W_{x_d}^{(d)}(n,\Theta)$ is a sampled (with respect to time) and periodic (with respect to frequency) version of the continuous-time WD $W_x(t,f)$,

$$W_{x_d}^{(d)}(n,\Theta) = R \sum_{k'} W_x\left[nT,\, R\cdot\left(\Theta - k'\tfrac{1}{2}\right)\right] , \qquad R = 1/T . \tag{8.3}$$

The sampling period T is that of the signals themselves; signals and WD are thus sampled at the same sampling rate $R = 1/T$. On the other hand, an inconvenient inconsistency exists with respect to frequency: while the Fourier transform

$$X_d(\Theta) \triangleq \sum_n x_d(n)\, e^{-j2\pi\Theta n} = R \sum_k X\left(R\cdot(\Theta - k)\right) \tag{8.4}$$

of the discrete-time signal $x_d(n)$ is derived from the Fourier transform X(f) of the continuous-time signal x(t) by periodic continuation with frequency period 1 (corresponding to the sampling rate R), the DTWD (8.3) is derived from the continuous-time WD by periodic continuation with frequency period 1/2 (corresponding to one half of the sampling rate, R/2). This means that, in general, the DTWD will feature aliasing with respect to the frequency variable. The aliasing components in (8.3) are given by the terms with $k' = 2k+1$,

$$a_k(n,\Theta) = R\, W_x\left[nT,\, R\cdot\left(\Theta - (2k+1)\tfrac{1}{2}\right)\right] = R\, W_x\left[nT,\, R\cdot\left(\Theta - (k+\tfrac{1}{2})\right)\right] . \tag{8.5}$$

We now show that the aliasing components $a_k(n,\Theta)$ can be interpreted as an interference phenomenon. In order to characterize the effects of signal sampling within the framework of the continuous-time WD, we use the following "continuous-time" version of sampling [28],

$$x_s(t) \triangleq x(t) \sum_n \delta(t-nT) = \sum_n x_d(n)\, \delta(t-nT) ,$$

where the signal samples $x_d(n)$ appear as the weights of sampling pulses $\delta(t-nT)$ occurring at the sample instances $t=nT$. The Fourier transform of $x_s(t)$,

$$X_s(f) = R \sum_k X(f-kR), \tag{8.6}$$

is a periodic version of the Fourier transform $X(f)$ of $x(t)$, with period equal to the sampling rate $R=1/T$. Indeed, the Fourier transforms $X_s(f)$ in (8.6) and $X_d(\Theta)$ in (8.4) are equivalent, $X_d(\Theta) = X_s(R\Theta)$. Transforming (8.6) into the time domain shows that $x_s(t)$ can be interpreted as a multicomponent signal comprising an infinite number of signal components $x_k(t) = Rx(t)e^{j2\pi(kR)t}$ which are derived from the original signal $x(t)$ via frequency shifts by integer multiples of the sampling rate R. The effects of signal sampling on the WD can now easily be described invoking the WD's interference geometry: two versions $x_i(t)$ and $x_j(t)$ of $x(t)$ shifted to frequency locations $f_i = iR$ and $f_j = jR$, respectively, cause an outer IT of the WD which is located around the center frequency $f_{ij} = \frac{f_i+f_j}{2} = (i+j)\frac{R}{2}$.

Two cases have now to be distinguished: if i+j is *even*, $\frac{i+j}{2} = k$ with $k \in \mathbb{Z}$, then the center frequency f_{ij} coincides with the frequency location kR of the signal component $x_k(t)$. The IT $W_{ij}^{(I)}(t,f)$ will then correspond, with respect to its frequency location, to the spectral component $X(f-kR)$ of $x_s(t)$. If, on the other hand, i+j is *odd*, $\frac{i+j}{2} = k+1/2$ with $k \in \mathbb{Z}$, then the center frequency f_{ij} equals the "half-integer" frequency location (k+1/2)R. The IT $W_{ij}^{(I)}(t,f)$ then does not correspond to any spectral component of $x_s(t)$ - rather, it is located midway between the adjacent spectral components $X(f-kR)$ and $X(f-(k+1)R)$ of $x_s(t)$. In this latter case, which is illustrated in *Figure 18*, the IT forms part of that aliasing term of the WD which is located around frequency (k+1/2)R.

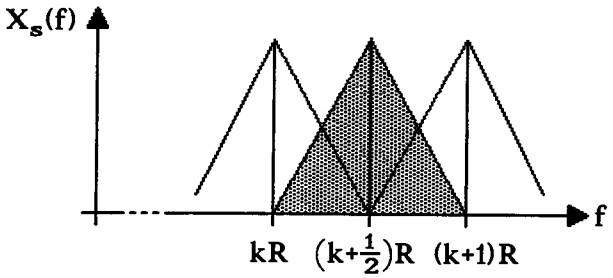

Figure 18. Equivalence of aliasing and interference.

Let us take a closer look at the way WD aliasing terms are made up by outer ITs. To produce the k-th aliasing term $a_k(n,\Theta)$ of (8.5), i.e., the aliasing term around frequency (k+1/2)R, we have to collect all ITs with center frequency $f_{ij} = (k+1/2)R$. Two signal components $x_i(t)$ and $x_j(t)$ will create an outer IT at $f_{ij} = (k+1/2)R$ if $i = k+m$ and $j = k-m+1$ with $m \in \mathbb{Z}$; their IT then is

$$W^{(I)}_{k+m,\,k-m+1}(t,f) = 2R^2\, W_x(t, f-(k+1/2)R)\, \cos\left[2\pi(2m-1)Rt\right].$$

Adding all these ITs yields

$$\sum_m W^{(I)}_{k+m,\,k-m+1}(t,f) = 2R^2\, W_x(t,\, f-(k+1/2)R) \sum_m \cos\left[2\pi(2m-1)R\,t\right] =$$

$$= R \sum_m (-1)^m\, W_x\Big(m\tfrac{T}{2},\, f-(k+1/2)R\Big)\, \delta\Big(t-m\tfrac{T}{2}\Big)\ . \qquad (8.7)$$

It is interesting that the continuous-time WD is here sampled with sampling period T/2, i.e., at sampling instances which are spaced twice as fine as the sampling instances of the signal [28]. The signal's sampling instances nT are obtained for m even, $m = 2n$; the weights $w_n^{(k)}(f)$ of the sampling pulses $\delta(t-nT)$ of (8.7) are here given by

$$w_n^{(k)}(f) = R\, W_x\big(nT,\, f-(k+1/2)R\big)\ . \qquad (8.8)$$

At these sampling instances, the discrete-time WD $W^{(d)}_{x_d}(n,\Theta)$ is defined. Comparing the k-th aliasing term $a_k(n,\Theta)$ (see (8.5)) of $W^{(d)}_{x_d}(n,\Theta)$, i.e., the aliasing term located around frequency $\Theta = k+1/2$, with (8.8), we finally recognize that this aliasing term is equal to the IT weight $w_n^{(k)}(f)$,

$$a_k(n,\Theta) = w_n^{(k)}(R\Theta).$$

This shows that the aliasing components of the DTWD can in fact be interpreted as ITs caused by interference of the various spectral components of the sampled signal.

PART II - RELATED TIME-FREQUENCY REPRESENTATIONS

In the context of the WD, certain other time-frequency representations are of theoretical and practical interest. Just as the WD itself, these representations have bilinear (quadratic) structure and will contain outer ITs whenever the signal under investigation is multicomponent. The interference principle can again be extended to inner interference in the case of monocomponent signals. However, the geometry of ITs may be quite different from the interference geometry of the WD. The purpose of Part II of this chapter is to investigate the similarities and differences of the interference geometries of various representations.

Section 9 studies the *generalized Wigner distribution* (GWD) and shows that, due to the GWD's interference geometry, GWD results are typically more difficult to interpret than WD results. The interference geometry of the *ambiguity function* is considered in Section 10; the results obtained will form a basis for discussing smoothed WD versions in Section 13. In Section 11, the class of *shift-invariant time-frequency representations* (Cohen's class) is considered, and the oscillation of ITs is shown to be a common characteristic of this class. The subclass of *shift-scale-invariant time-frequency representations* is shown in Section 12 to possess some remarkable properties with respect to interference geometry. Finally, Section 13 considers *smoothed versions of the WD* and discusses specific representations like the *smoothed pseudo Wigner distribution*, the *spectrogram*, and the *Choi-Williams distribution*.

9. GENERALIZED WIGNER DISTRIBUTION

The generalized Wigner distribution (GWD) is a family of bilinear time-frequency representations which can be considered as a natural generalization of the WD, with the WD being itself a special case. Most of the desirable mathematical properties satisfied by the WD are satisfied by the GWD as well. For this reason, the GWD family is theoretically an interesting alternative to the WD. From a practical viewpoint, however, the GWD is generally inferior to the WD since GWD results are typically much more difficult to interpret than WD results. It is the purpose of this section to demonstrate that this inferiority of the GWD is a direct consequence of the GWD's *interference geometry* which, in general, shows characteristic differences from the interference geometry of the WD.

Definition of GWD. The GWD is defined as [29,2,7]

$$W_{x,y}^{(\alpha)}(t,f) = \int_\tau x(t+\alpha^+\tau)\, y^*(t-\alpha^-\tau)\, e^{-j2\pi f\tau}\, d\tau = \int_\upsilon X(f+\alpha^-\upsilon)\, Y^*(f-\alpha^+\upsilon)\, e^{j2\pi t\upsilon}\, d\upsilon$$

where $\alpha^+ + \alpha^- = 1$. We may thus write $\alpha^+ = \frac{1}{2}+\alpha$, $\alpha^- = \frac{1}{2}-\alpha$ with a real-valued α which is the *parameter* of the GWD family. Obviously, the WD is a special case of the GWD; it is obtained with the symmetrical choice $\alpha = 0$ for which $\alpha^+ = \alpha^- = 1/2$. Another special case is the *Rihaczek distribution* (RD) [30,29,2]

$$R_{x,y}(t,f) = \int_\tau x(t+\tau)\, y^*(t)\, e^{-j2\pi f\tau}\, d\tau = X(f)\, y^*(t)\, e^{j2\pi tf}$$

for which $\alpha = 1/2$ or $\alpha^+ = 1$ and $\alpha^- = 0$. As a practically important difference from the WD, we note that auto-GWDs (with the exclusion of the WD case $\alpha = 0$) are not real-valued.

Since the auto-GWD is a quadratic signal representation, it obeys the same quadratic superposition principle as the WD. For an N-component signal with signal components $c_k x_k(t)$, the auto-GWD again consists of N signal terms

$$W_k^{(\alpha)(S)}(t,f) \triangleq |c_k|^2\, W_{x_k}^{(\alpha)}(t,f)$$

and $\binom{N}{2} = \frac{N(N-1)}{2}$ ITs

$$W_{kl}^{(\alpha)(I)}(t,f) \triangleq c_k c_l^*\, W_{x_k,x_l}^{(\alpha)}(t,f) + c_l c_k^*\, W_{x_l,x_k}^{(\alpha)}(t,f) \qquad (l>k)\ ,$$

where it is easily shown that

$$W_{x_l,x_k}^{(\alpha)}(t,f) = W_{x_k,x_l}^{(-\alpha)*}(t,f)\ .$$

We also note that the GWD satisfies the marginal and shift-invariance properties which have been discussed in the context of the WD in Section 2.

Interference geometry of GWD. The interference geometry of the GWD depends on the GWD parameter α. To study this dependence, we first consider the outer interference of two time-domain impulses $x_1(t) = \delta(t-t_1)$ and $x_2(t) = \delta(t-t_2)$. Signal

terms and IT are here obtained as

$$W_1^{(\alpha)(S)}(t,f) = |c_1|^2\,\delta(t-t_1)\,, \qquad W_2^{(\alpha)(S)}(t,f) = |c_2|^2\,\delta(t-t_2)\,,$$

$$W_{12}^{(\alpha)(I)}(t,f) = |c_1||c_2|\left[\delta[t-(t_{12}-\alpha\tau_{12})]\,e^{j(-2\pi\tau_{12}f+\varphi_{12})} + \delta[t-(t_{12}+\alpha\tau_{12})]\,e^{j(2\pi\tau_{12}f-\varphi_{12})}\right]$$

with $\varphi_{12} = \arg\{c_1\} - \arg\{c_2\}$. This is illustrated in *Figure 19.* We note that the signal terms are independent of the GWD parameter α; consequently, they equal the signal terms of the WD (cf. (4.7)). The IT, on the other hand, depends on α; it consists of two impulsive subterms located at time points $t_{12} \pm \alpha\tau_{12}$. With respect to the frequency f, the IT subterms oscillate with "frequency" $\tau_{12} = t_1 - t_2$; this oscillation is independent of α. The IT oscillation is the same as in the WD case; specifically, it will be faster for increasing time distance $|\tau_{12}|$ between the interfering signal components. A difference from the WD case is that the oscillation now corresponds to a *complex* sinusoid. We recognize that the GWD parameter α determines the *location* of the IT: for larger $|\alpha|$, the IT subterms will be more distant from the center point $t_{12} = (t_1+t_2)/2$.

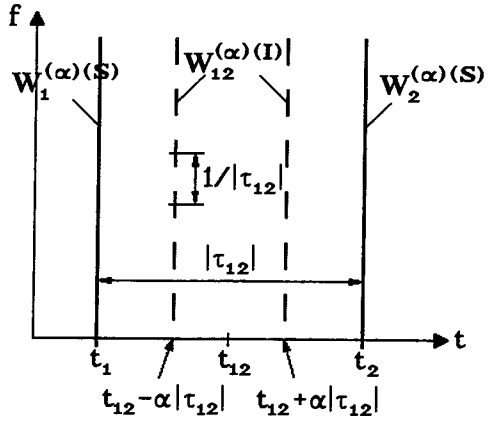

Figure 19. Signal terms and IT of GWD for the superposition of two impulses.

In the WD case (α=0), the IT subterms coalesce at the center point t_{12}, and we obtain a single real-valued IT (cf. (4.8))

$$W_{12}^{(I)}(t,f) = 2\,|c_1||c_2|\,\delta(t-t_{12})\cos\left(2\pi\tau_{12}f - \varphi_{12}\right)\,.$$

Another interesting special case is the RD (α=1/2) for which the IT subterms occur exactly at the signal (and thus signal term) locations t_1 and t_2,

$$R_{12}^{(I)}(t,f) = |c_1||c_2|\left[\delta(t-t_2)\,e^{j(-2\pi\tau_{12}f+\varphi_{12})} + \delta(t-t_1)\,e^{j(2\pi\tau_{12}f-\varphi_{12})}\right].$$

Dual results are obtained for the interference of two complex sinusoids (frequency-domain impulses) $x_1(t) = e^{j2\pi f_1 t}$ and $x_2(t) = e^{j2\pi f_2 t}$.

A joint time-frequency description of the GWD's interference geometry can again be obtained by considering the case of two time-frequency shifted versions $x_1(t) = x_0(t-t_1)e^{j2\pi f_1 t}$, $x_2(t) = x_0(t-t_2)e^{j2\pi f_2 t}$ of a signal $x_0(t)$. In this case, the GWD's signal terms are

$$W_1^{(\alpha)(S)}(t,f) = |c_1|^2 \, W_{x_0}^{(\alpha)}(t-t_1,f-f_1) , \qquad W_2^{(\alpha)(S)}(t,f) = |c_2|^2 \, W_{x_0}^{(\alpha)}(t-t_2,f-f_2) , \tag{9.1}$$

and the IT is obtained as

$$W_{12}^{(\alpha)(I)}(t,f) = \tag{9.2}$$

$$= |c_1||c_2| \left[F^{+}\big(t-(t_{12}-\alpha\tau_{12}),f-(f_{12}+\alpha\upsilon_{12})\big) + F^{-}\big(t-(t_{12}+\alpha\tau_{12}),f-(f_{12}-\alpha\upsilon_{12})\big)\right]$$

where

$$F^{\pm}(t,f) \triangleq W_{x_0}^{(\alpha)}(t,f) \; e^{\pm j[2\pi(\upsilon_{12}t-\tau_{12}f)+\varphi_{12}^{\pm}]} \tag{9.3}$$

with

$$\varphi_{12}^{\pm} = \arg\{c_1\} - \arg\{c_2\} + 2\pi\upsilon_{12}(t_{12} \mp \alpha\tau_{12}) .$$

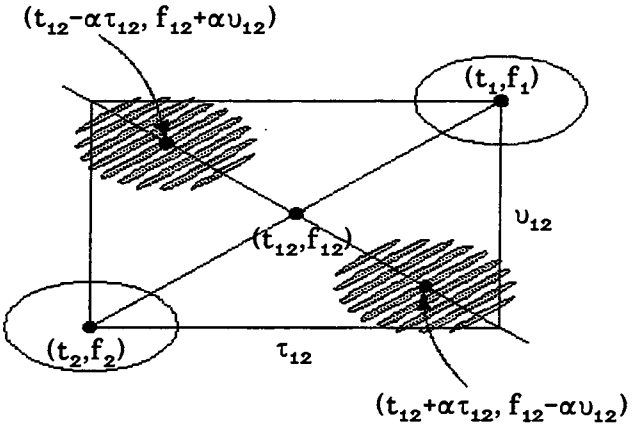

Figure 20. Interference geometry of GWD (schematic).

The geometry of this result is shown in *Figure 20.* Due to the GWD's shift invariance, the signal terms (9.1) are simply time-frequency shifted versions of the GWD of the signal $x_0(t)$. While the exact shape of the signal terms thus depends on the GWD parameter α, the signal terms' overall time-frequency locations are independent of α and always equal the true time-frequency locations (t_1,f_1) and (t_2,f_2) of the interfering signals.

The time-frequency location of the IT, on the other hand, depends on α: according to (9.2), the IT consists of two subterms located around time-frequency points $(t_{12}-\alpha\tau_{12}, f_{12}+\alpha\upsilon_{12})$ and $(t_{12}+\alpha\tau_{12}, f_{12}-\alpha\upsilon_{12})$. The distance of the IT subterms from the center point (t_{12},f_{12}) is thus proportional to $|\alpha|$. Eq. (9.3) shows that the IT subterms

are oscillatory, where the oscillation characteristic is identical with that of the WD. Specifically, the oscillation "frequencies" in the time and frequency directions again equal the frequency lag υ_{12} and time lag τ_{12}, respectively. Similar to the WD case, the envelopes of the oscillatory IT subterms are given by the GWD of $x_0(t)$.

In the special case of the WD, the two IT subterms coalesce and yield a single real-valued IT which is located around the center point (t_{12},f_{12}) (cf. (3.3)). In the case of the RD, the IT subterms are located around the time-frequency points (t_1,f_2) and (t_2,f_1); signal terms and IT subterms thus form the corners of a rectangle with center point (t_{12},f_{12}) and lateral lengths τ_{12}, υ_{12}. *Figure 21* compares the interference geometries of the WD and the RD.

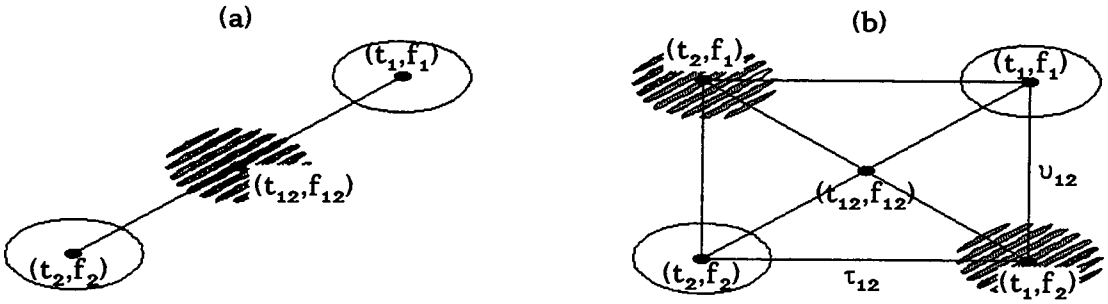

Figure 21. Interference geometries of (a) the WD and (b) the RD (schematic).

Interference formulae and inner interference. In general, the interfering signals will not be equal apart from time-frequency shifts. The GWD's interference geometry is still valid in the general case, but it has to be applied *locally* as explained in Section 3 for the WD. A partial mathematical foundation of this local application of interference geometry is provided by the GWD's *outer interference formula* [7]

$$\left|W^{(\alpha)}_{x_1,x_2}(t,f)\right|^2 = \int_\tau\int_\upsilon W^{(\alpha)}_{x_1}(t+\alpha^+\tau, f+\alpha^-\upsilon)\, W^{(\alpha)*}_{x_2}(t-\alpha^-\tau, f-\alpha^+\upsilon)\, d\tau\, d\upsilon \qquad (9.4)$$

which is a generalization of the WD's outer interference formula (3.1). With

$$t_1 = t+\alpha^+\tau\ , \quad t_2 = t-\alpha^-\tau\ , \quad f_1 = f+\alpha^-\upsilon\ , \quad f_2 = f-\alpha^+\upsilon$$

or, conversely,

$$t = t_{12}-\alpha\tau_{12}\ , \quad f = f_{12}+\alpha\upsilon_{12}\ , \quad \tau = \tau_{12}\ , \quad \upsilon = \upsilon_{12}\ ,$$

the GWD's outer interference formula implies the following: if the auto-GWDs $W^{(\alpha)}_{x_1}(t,f)$ and $W^{(\alpha)}_{x_2}(t,f)$ are nonzero around the time-frequency points (t_1,f_1) and (t_2,f_2), respectively, then the cross-GWD $W^{(\alpha)}_{x_1,x_2}(t,f)$ will generally be nonzero around the time-frequency point $(t_{12}-\alpha\tau_{12},f_{12}+\alpha\upsilon_{12})$. Since the outer IT of the signals $x_1(t)$ and $x_2(t)$ is given by $W^{(\alpha)(I)}_{12}(t,f) = W^{(\alpha)}_{x_1,x_2}(t,f)+W^{(\alpha)}_{x_2,x_1}(t,f)$, this can be interpreted as follows: two points (t_1,f_1) and (t_2,f_2) of the GWD signal terms $W^{(\alpha)}_{x_1}(t,f)$ and $W^{(\alpha)}_{x_2}(t,f)$, respectively, create two interference components around the points $(t_{12}-\alpha\tau_{12},f_{12}+\alpha\upsilon_{12})$ and $(t_{12}+\alpha\tau_{12},f_{12}-\alpha\upsilon_{12})$. The geometry of signal and interference

points equals that of Figure 20. As in the WD case, the GWD's interference formula characterizes the location of ITs but does not describe the ITs' oscillation.

So far, the interference geometry of the GWD has been discussed for outer interference. However, as in the special case of the WD, it also applies to *inner interference*. An indication of this fact is given by the GWD's *inner interference formula*

$$\left|W_x^{(\alpha)}(t,f)\right|^2 = \int_\tau \int_\upsilon W_x^{(\alpha)}(t+\alpha^+\tau, f+\alpha^-\upsilon)\, W_x^{(\alpha)*}(t-\alpha^-\tau, f-\alpha^+\upsilon)\, d\tau\, d\upsilon$$

which is derived from the outer interference formula (9.4) with $x_1(t) = x_2(t) = x(t)$. Analogously to the WD case, the geometries of inner and outer interference are the same; the only difference lies in the fact that, for inner interference, the interfering time-frequency points (t_1,f_1) and (t_2,f_2) belong to one and the same signal component (or GWD signal term).

Also for the GWD, the stationary-phase method can be used for an analytical derivation of the laws of interference geometry when the signals are of the AM-FM type (6.1). This is a straightforward extension of the discussion given in Section 6 and does not furnish any new aspects. We will not, therefore, enlarge on this point and refer the reader to [7] for details.

Optimality of WD. As demonstrated above, the GWD's interference geometry critically depends on the GWD parameter α. The WD case (α=0) is optimal in the sense that the ITs here occupy a time-frequency region with minimal area; the ITs of the WD have thus maximal time-frequency concentration. This optimality of the WD with respect to interference geometry is the reason why WD results are generally more easily interpreted than the results of other GWD representations.

We shall consider a simple example where the superior performance of the WD is most pronounced. The signal to be analyzed is the linear FM (chirp) signal

$$x(t) = a(t)\, e^{j2\pi\frac{c}{2}t^2} \qquad (a(t)\geq 0,\ c\in\mathbb{R})$$

with instantaneous frequency

$$f_i(t) = ct\ .$$

We assume that the AM part a(t) is a lowpass signal whose effective time support is the interval $[t_1,t_2]$. The WD of x(t) is obtained as

$$W_x(t,f) = W_a(t, f-ct)\ .$$

Since a(t) is a lowpass signal, $W_a(t,f)$ will be concentrated around f = 0, and $W_x(t,f)$ will thus be concentrated along the instantaneous-frequency line $f_i(t) = ct$. This behavior is illustrated in *Figure 22.a.* The interference-geometric interpretation according to Figure 21.a is that all inner IT components fall onto the instantaneous-frequency-line, and thus onto the signal term; therefore, a separate IT does not occur.

It is clear that this ideal behavior cannot be obtained with GWDs other than the WD. As an example, the RD of x(t) is shown in *Figure 22.b.* Using the stationary-phase method, the following approximation can be derived,

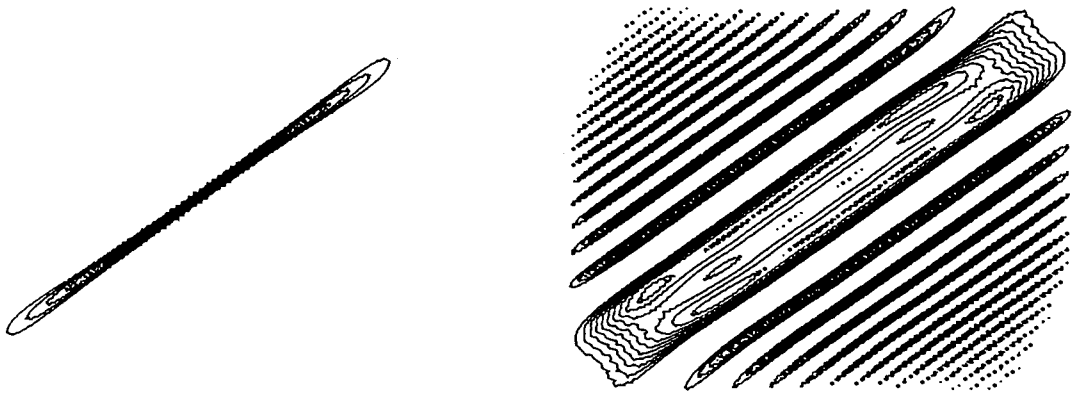

(a) (b)

Figure 22. (a) WD and (b) real part of RD of chirp signal.

$$R_x(t,f) \approx C\ a(t)\, a\left(\frac{f}{c}\right) e^{-j\frac{\pi}{c}(f-ct)^2} ,$$

where C is a complex constant. We see that $R_x(t,f)$ is oscillatory and effectively concentrated inside the time-frequency rectangle $[t_1,t_2] \times [ct_1,ct_2]$. In the frequency direction, the oscillation grows faster with increasing distance between f and $f_i(t) = ct$. This behavior is consistent with the interference geometry of the RD as shown in Figure 21.b: the inner ITs fill the rectangular time-frequency region defined by the end-points (t_1,ct_1) and (t_2,ct_2) of the chirp's signal term.

This example shows that the results obtained with the WD and other GWDs may be dramatically different; this difference is due to the different interference geometries of these representations. Our discussion also shows that the real part of the RD (also known as "instantaneous power spectrum") is by no means free of interference, and thus refutes an incorrect claim made in [31].

10. AMBIGUITY FUNCTION

In this section, we study the *ambiguity function* (AF) which is the Fourier transform of the WD. While the time-frequency representations considered so far (WD and GWD) can be interpreted as time-frequency energy distributions, the interpretation of the AF is that of a time-frequency correlation.

As may be expected, the AF's interference geometry is totally different from the interference geometry of the WD or GWD. The interest of the AF for our discussion stems from the fact that, being the Fourier transform of the WD, the AF allows a convenient description of smoothed WD versions like the pseudo Wigner distribution, the spectrogram, and the Choi-Williams distribution. This description will be used extensively in Section 13.

Definition and properties. The AF is defined as [29,14,32,33]

$$A_{x,y}(\tau,\upsilon) \triangleq \int_t x\left(t+\frac{\tau}{2}\right) y^*\left(t-\frac{\tau}{2}\right) e^{-j2\pi\upsilon t}\, dt = \int_f X\left(f+\frac{\upsilon}{2}\right) Y^*\left(f-\frac{\upsilon}{2}\right) e^{j2\pi\tau f}\, df ,$$

where τ and υ denote the time lag and frequency lag, respectively. The AF is essentially the two-dimensional Fourier transform of the WD,

$$A_{x,y}(\tau,\upsilon) = \int\int_{t\,f} W_{x,y}(t,f)\, e^{-j2\pi(\upsilon t-\tau f)}\, dt\, df \quad . \tag{10.1}$$

Due to this duality relation, there exists a corresponding property of the AF to each property of the WD. For example, the WD's shift invariance property (2.2) transforms into the following version of shift invariance: if

$$x_0(t) = x(t-t_0)\, e^{j2\pi f_0 t} \quad , \qquad y_0(t) = y(t-t_0)\, e^{j2\pi f_0 t} \quad ,$$

then

$$A_{x_0,y_0}(\tau,\upsilon) = A_{x,y}(\tau,\upsilon)\, e^{j2\pi(f_0\tau-t_0\upsilon)} \quad . \tag{10.2}$$

We see that a time-frequency shift of the signals causes the AF to be modulated by an oscillatory factor, instead of being shifted by t_0 and f_0 as in the WD case. As a further example, the WD's hermiticity $W_{y,x}(t,f) = W^*_{x,y}(t,f)$ transforms into

$$A_{y,x}(\tau,\upsilon) = A^*_{x,y}(-\tau,-\upsilon)\,;$$

it thus follows that auto-AFs are generally complex-valued but satisfy the symmetry property $A^*_x(-\tau,-\upsilon) = A_x(\tau,\upsilon)$.

Since the auto-AF is a quadratic signal representation, the quadratic superposition principle applies: for an N-component signal with signal components $c_k x_k(t)$, the auto-AF consists of N signal terms

$$A^{(S)}_k(\tau,\upsilon) \triangleq |c_k|^2\, A_{x_k}(\tau,\upsilon)$$

and $\binom{N}{2} = \frac{N(N-1)}{2}$ ITs

$$A^{(I)}_{kl}(\tau,\upsilon) \triangleq c_k c_l^*\, A_{x_k,x_l}(\tau,\upsilon) + c_l c_k^*\, A_{x_l,x_k}(\tau,\upsilon) =$$

$$= c_k c_l^*\, A_{x_k,x_l}(\tau,\upsilon) + c_l c_k^*\, A^*_{x_k,x_l}(-\tau,-\upsilon) \qquad (l>k) \quad ,$$

which satisfy the symmetry property of the auto-AF

$$A^{(I)*}_{kl}(-\tau,-\upsilon) = A^{(I)}_{kl}(\tau,\upsilon) \quad .$$

Interference geometry. The Fourier transform relation (10.1) connecting the WD and the AF holds for signal terms and ITs separately,

$$A^{(S)}_k(\tau,\upsilon) = \int\int_{t\,f} W^{(S)}_k(t,f)\, e^{-j2\pi(\upsilon t-\tau f)}\, dt\, df \quad , \qquad A^{(I)}_{kl}(\tau,\upsilon) = \int\int_{t\,f} W^{(I)}_{kl}(t,f)\, e^{-j2\pi(\upsilon t-\tau f)}\, dt\, df \quad ,$$

and thus relates the signal terms (ITs) of the AF with the corresponding signal terms (ITs) of the WD. From the properties of the Fourier transform, there follows a duality of the interference geometries of the WD and the AF.

Specifically, if a WD signal term occurs around the time-frequency location (t_1,f_1), then the corresponding AF signal term will be located around the origin $\tau=0$, $\upsilon=0$ of the (τ,υ)-plane since the WD signal term is essentially non-oscillatory. Furthermore, the AF signal term will oscillate in the τ direction with frequency f_1 and in the υ direction with "frequency" t_1.

An IT of the WD caused by WD signal terms located around (t_1,f_1) and (t_2,f_2) occurs around the center point (t_{12},f_{12}); the corresponding IT of the AF will hence oscillate in the τ direction with frequency f_{12} and in the υ direction with "frequency" t_{12}. Furthermore, the IT of the WD oscillates in the t direction with frequency $\pm\upsilon_{12}$ and in the f direction with "frequency" $\pm\tau_{12}$; the corresponding IT of the AF will hence be located around the points $(\tau_{12},\upsilon_{12})$ and $(-\tau_{12},-\upsilon_{12})$ in the (τ,υ)-plane.

We now illustrate these general laws by considering the simple situations previously discussed in the context of the WD and GWD. We first study the interference of two time-domain impulses $x_1(t) = \delta(t-t_1)$ and $x_2(t) = \delta(t-t_2)$. The AF's signal terms and outer IT are here obtained as

$$A_1^{(S)}(\tau,\upsilon) = |c_1|^2\,\delta(\tau)\,e^{-j2\pi t_1\upsilon}, \qquad A_2^{(S)}(\tau,\upsilon) = |c_2|^2\,\delta(\tau)\,e^{-j2\pi t_2\upsilon},$$

$$A_{12}^{(I)}(\tau,\upsilon) = |c_1||c_2|\left[\delta(\tau-\tau_{12})\,e^{j(-2\pi t_{12}\upsilon+\varphi_{12})} + \delta(\tau+\tau_{12})\,e^{j(-2\pi t_{12}\upsilon-\varphi_{12})}\right]$$

with $\varphi_{12} = \arg\{c_1\} - \arg\{c_2\}$. With respect to the time lag variable τ, the signal terms are impulses located at the origin $\tau = 0$; with respect to the frequency lag variable υ, they oscillate with "frequency" equal to the signals' time locations t_1 and t_2, respectively. The IT consists of two impulsive subterms located at time lags τ_{12} and $-\tau_{12}$, where $|\tau_{12}| = |t_1-t_2|$ is the distance between the signals' time locations. The IT subterms, too, oscillate with respect to υ; the oscillation "frequency" is the signals' center time $t_{12} = (t_1+t_2)/2$. This is illustrated in *Figure 23.* Dual results are obtained for the case of two complex sinusoids (frequency-domain impulses) $x_1(t) = e^{j2\pi f_1 t}$ and $x_2(t) = e^{j2\pi f_2 t}$.

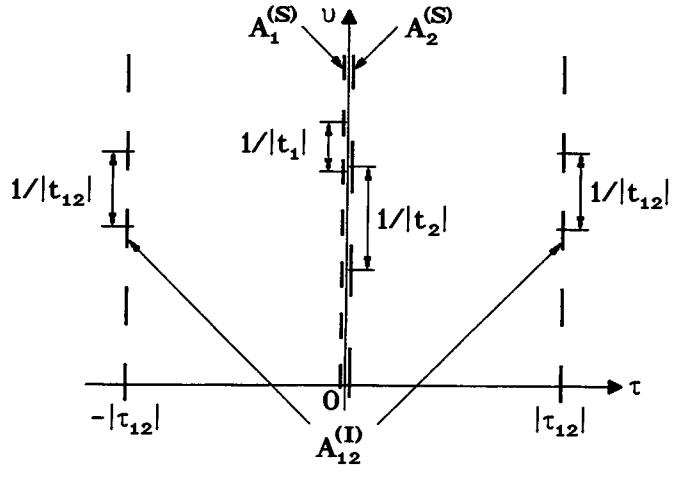

Figure 23. Signal terms and IT of AF for the superposition of two impulses.

We next consider the time-frequency shifted signal versions $x_1(t) = x_0(t-t_1)e^{j2\pi f_1 t}$ and $x_2(t) = x_0(t-t_2)e^{j2\pi f_2 t}$. The signal terms of the AF are obtained as

$$A_1^{(S)}(\tau,\upsilon) = |c_1|^2 A_{x_0}(\tau,\upsilon)\, e^{j2\pi(f_1\tau - t_1\upsilon)}, \qquad A_2^{(S)}(\tau,\upsilon) = |c_2|^2 A_{x_0}(\tau,\upsilon)\, e^{j2\pi(f_2\tau - t_2\upsilon)},$$

and the outer IT is

$$A_{12}^{(I)}(\tau,\upsilon) = |c_1||c_2| \left[F^{+}(\tau-\tau_{12},\upsilon-\upsilon_{12}) + F^{-}(\tau+\tau_{12},\upsilon+\upsilon_{12}) \right]$$

where

$$F^{\pm}(\tau,\upsilon) \triangleq A_{x_0}(\tau,\upsilon)\, e^{j[2\pi(f_{12}\tau - t_{12}\upsilon) \pm \varphi_{12}]}$$

with

$$\varphi_{12} = \arg\{c_1\} - \arg\{c_2\} + 2\pi f_{12}\tau_{12} .$$

This result is illustrated in *Figure 24*. The signal terms occur essentially around the origin of the (τ,υ)-plane; due to the AF's shift invariance property (10.2), they are simply modulated versions of $A_{x_0}(\tau,\upsilon)$. The outer IT consists of two subterms located around the points $(\tau_{12},\upsilon_{12})$ and $(-\tau_{12},-\upsilon_{12})$, where $\tau_{12} = t_1 - t_2$ and $\upsilon_{12} = f_1 - f_2$ are (respectively) the time lag and frequency lag between the interfering signal components or, equivalently, between the corresponding WD signal terms. Both IT subterms are oscillatory, with oscillation "frequency" in the τ direction (υ direction) equal to the center frequency f_{12} (center time t_{12}) of the interfering signal components or WD signal terms.

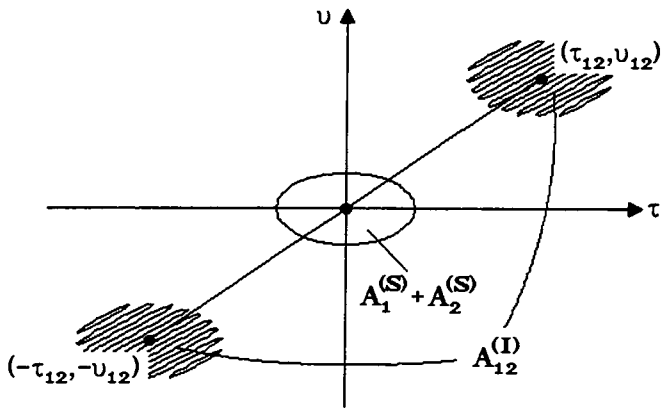

Figure 24. Interference geometry of AF.

These simple laws describe the interference geometry of the AF. We note that the AF's interference geometry is indeed the dual of the interference geometry of the WD: in the WD case, an IT's time-frequency location is (t_{12},f_{12}) and the oscillation "frequencies" are given by $(\tau_{12},\upsilon_{12})$ and $(-\tau_{12},-\upsilon_{12})$. With the AF, this is the other way around: the IT's location in the time-frequency-lag plane is $(\tau_{12},\upsilon_{12})$ and $(-\tau_{12},-\upsilon_{12})$ and its oscillation "frequencies" are (t_{12},f_{12}).

Interference formulae and inner interference. When the interfering signals are not identical except for time-frequency shifts, the laws of interference geometry have again to be applied *locally*, which allows a pointwise construction of ITs. A partial mathematical foundation of this principle is given by the AF's *outer interference formula*

$$|A_{x_1,x_2}(\tau,\upsilon)|^2 = \iint_{t\,f} W_{x_1}(t+\tfrac{\tau}{2},f+\tfrac{\upsilon}{2})\, W_{x_2}(t-\tfrac{\tau}{2},f-\tfrac{\upsilon}{2})\, dt\, df \qquad (10.3)$$

which relates the magnitude of the cross-AF with the corresponding WD signal terms. The interference formula supports the AF's interpretation as a time-frequency correlation and, also, the local application of the AF's interference geometry. In particular, it provides an answer to the following question: if the effective time-frequency supports of two signals $x_1(t)$ and $x_2(t)$ are given by regions R_1 and R_2 of the time-frequency plane, respectively (i.e., the WD signal terms are approximately zero outside these regions), what is the effective support region $\hat{R}_{12}$ of the AF's outer IT in the time-frequency-lag plane? Based on the outer interference formula (10.3), we can construct $\hat{R}_{12}$ pointwise as follows: we choose a point (t_1,f_1) inside R_1 and a point (t_2,f_2) inside R_2. Then $(\tau_{12},\upsilon_{12})$ and $(-\tau_{12},-\upsilon_{12})$, with $\tau_{12} = t_1-t_2$ and $\upsilon_{12} = f_1-f_2$, are points of the IT support region $\hat{R}_{12}$ (see *Figure 25*).

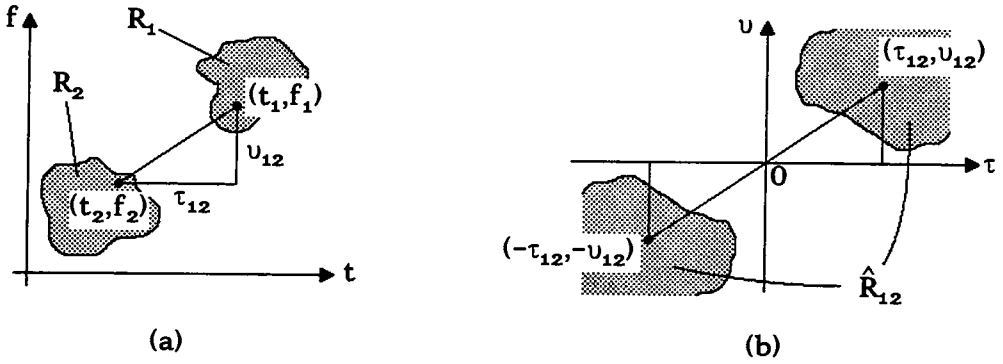

Figure 25. Pointwise construction of AF's IT support $\hat{R}_{12}$: (a) signal terms of WD; (b) IT of AF.

The interference geometry of the AF can again be reformulated for *inner interference* in a straightforward manner, the only difference being that both signal points (t_1,f_1) and (t_2,f_2) then belong to the same signal component or WD signal term. The AF's *inner interference formula*

$$|A_x(\tau,\upsilon)|^2 = \iint_{t\,f} W_x(t+\tfrac{\tau}{2},f+\tfrac{\upsilon}{2})\, W_x(t-\tfrac{\tau}{2},f-\tfrac{\upsilon}{2})\, dt\, df\ ,$$

which is derived from (10.3) by letting $x_1(t) = x_2(t) = x(t)$, permits a pointwise construction of the effective support region of the AF's inner ITs. Let R_x be the effective time-frequency support of the signal $x(t)$ such that the WD of $x(t)$ is approximately zero outside R_x. We choose two different points (t_1,f_1) and (t_2,f_2) inside R_x.

The points $(\tau_{12},\upsilon_{12})$ and $(-\tau_{12},-\upsilon_{12})$, with $\tau_{12} = t_1-t_2$ and $\upsilon_{12} = f_1-f_2$, will then belong to the effective support $\hat{R}_x$ of the AF of $x(t)$.

In any case, the WD is a convenient basis for a schematic construction of the AF's inner or outer ITs since all relevant parameters $(\tau_{12}, \upsilon_{12}, t_{12}, f_{12})$ are readily obtained from the WD signal terms.

11. THE SHIFT-INVARIANT CLASS

The class of bilinear (quadratic) time-frequency representations (TFRs) can be split into two subclasses distinguished by different modes of interpretation [34]: (i) the subclass of "energetic" TFRs which, conceptually, can be interpreted as distributions of the signal's energy over the time-frequency plane ((t,f)-plane); (ii) the subclass of "correlative" TFRs which can be interpreted as joint time-frequency correlation functions and, consequently, are functions of the time lag τ and frequency lag υ. So far, we have encountered specimens of both subclasses: the WD $W_{x,y}(t,f)$ and, more generally, the GWD $W^{(\alpha)}_{x,y}(t,f)$ are energetic TFRs whereas the AF $A_{x,y}(\tau,\upsilon)$ is a correlative TFR.

Bilinearity and shift invariance. In the following, we concentrate on the energetic subclass of bilinear TFRs. We consider a TFR $C_{x,y}(t,f)$ which is *bilinear*, i.e., the auto-TFR $C_x(t,f) \triangleq C_{x,x}(t,f)$ is quadratic and thus satisfies the quadratic superposition law: for an N-component signal $x(t)$ with signal components $c_k x_k(t)$, the TFR $C_x(t,f)$ consists of N signal terms

$$C^{(S)}_k(t,f) \triangleq |c_k|^2 C_{x_k}(t,f)$$

and $\binom{N}{2} = \frac{N(N-1)}{2}$ ITs

$$C^{(I)}_{kl}(t,f) \triangleq c_k c_l^* C_{x_k,x_l}(t,f) + c_l c_k^* C_{x_l,x_k}(t,f) \qquad (l>k) \ .$$

Apart from the bilinear (quadratic) structure, we also require that $C_{x,y}(t,f)$ is *shift-invariant* (cf. (2.2)): if

$$x_o(t) = x(t-t_o)\, e^{j2\pi f_o t} \quad \text{and} \quad y_o(t) = y(t-t_o)\, e^{j2\pi f_o t} \ ,$$

then

$$C_{x_o,y_o}(t,f) = C_{x,y}(t-t_o, f-f_o) \ .$$

The class of bilinear shift-invariant TFRs is well known as the "bilinear Cohen class" [34,35,14]. The WD and GWD are members of this class. To each shift-invariant TFR $C_{x,y}(t,f)$, we define its "correlative dual" $\hat{C}_{x,y}(\tau,\upsilon)$ as the Fourier transform

$$\hat{C}_{x,y}(\tau,\upsilon) = \iint_{t\,f} C_{x,y}(t,f)\, e^{-j2\pi(\upsilon t-\tau f)}\, dt\, df \ . \qquad (11.1)$$

Comparing with (10.1), we note that the correlative dual of the WD is the AF.

Kernels of shift-invariant TFRs. It can be shown that any bilinear shift-invariant TFR $C_{x,y}(t,f)$ can be written in four different though equivalent ways [29,34,14]:

(i) as the Fourier transform of a "time-dependent pseudo correlation function" $\tilde{r}_{x,y}(t,\tau)$ with respect to the time-lag variable τ,

$$C_{x,y}(t,f) = \int_{\tau} \tilde{r}_{x,y}(t,\tau)\, e^{-j2\pi f\tau}\, d\tau$$

with

$$\tilde{r}_{x,y}(t,\tau) = \int_{t'} \varphi_c(t-t',\tau)\, x\left(t'+\tfrac{\tau}{2}\right) y^*\left(t'-\tfrac{\tau}{2}\right) dt' ,$$

where $\varphi_c(t,\tau)$ will be called the *time kernel* of the TFR C;

(ii) as the inverse Fourier transform of a "frequency-dependent pseudo spectral correlation function" $\tilde{R}_{x,y}(f,\upsilon)$ with respect to the frequency-lag variable υ,

$$C_{x,y}(t,f) = \int_{\upsilon} \tilde{R}_{x,y}(f,\upsilon)\, e^{j2\pi t\upsilon}\, d\upsilon$$

with

$$\tilde{R}_{x,y}(f,\upsilon) = \int_{f'} \Phi_c(f-f',\upsilon)\, X\left(f'+\tfrac{\upsilon}{2}\right) Y^*\left(f'-\tfrac{\upsilon}{2}\right) df' ,$$

where $\Phi_c(f,\upsilon)$ is the *frequency kernel* of C;

(iii) as the convolution of the WD with the *Wigner kernel* $\psi_c(t,f)$,

$$C_{x,y}(t,f) = \int_{t'}\int_{f'} \psi_c(t-t',f-f')\, W_{x,y}(t',f')\, dt'\, df' ; \qquad (11.2)$$

(iv) as the Fourier transform (inversion of (11.1))

$$C_{x,y}(t,f) = \int_{\tau}\int_{\upsilon} \hat{C}_{x,y}(\tau,\upsilon)\, e^{j2\pi(t\upsilon-f\tau)}\, d\tau\, d\upsilon , \qquad (11.3)$$

where the correlative dual $\hat{C}_{x,y}(\tau,\upsilon)$ of C is given by the product of the AF and the *ambiguity kernel* $\Psi_c(\tau,\upsilon)$,

$$\hat{C}_{x,y}(\tau,\upsilon) = \Psi_c(\tau,\upsilon)\, A_{x,y}(\tau,\upsilon) . \qquad (11.4)$$

The time kernel $\varphi_c(t,\tau)$, frequency kernel $\Phi_c(f,\upsilon)$, Wigner kernel $\psi_c(t,f)$, and ambiguity kernel $\Psi_c(\tau,\upsilon)$ are all interrelated by one-dimensional and two-dimensional Fourier transforms according to *Figure 26.* In particular, the Wigner kernel $\psi_c(t,f)$ and the ambiguity kernel $\Psi_c(\tau,\upsilon)$ are related by the general duality relation connecting energetic and correlative TFRs (cf. (11.1)),

$$\Psi_c(\tau,\upsilon) = \int_{t}\int_{f} \psi_c(t,f)\, e^{-j2\pi(\upsilon t-\tau f)}\, dt\, df .$$

Any one of these four kernels provides a complete and compact characterization of the TFR C. For example, the kernels of the GWD $W^{(\alpha)}_{x,y}(t,f)$ are

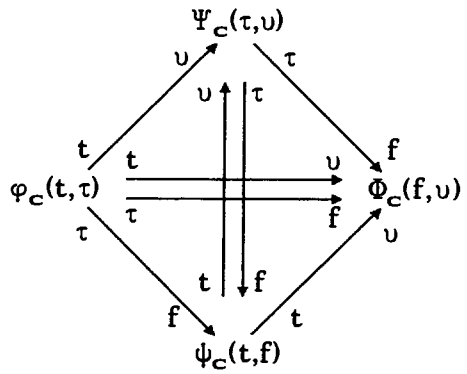

Figure 26. Fourier transform relationships of kernels of shift-invariant TFR.

$$\varphi_{W(\alpha)}(t,\tau) = \delta(t+\alpha\tau)\,, \qquad \Phi_{W(\alpha)}(f,\upsilon) = \delta(f-\alpha\upsilon)\,,$$
$$\psi_{W(\alpha)}(t,f) = \frac{1}{|\alpha|}\, e^{j2\pi\frac{tf}{\alpha}}\,, \qquad \Psi_{W(\alpha)}(\tau,\upsilon) = e^{j2\pi\alpha\tau\upsilon}\,, \tag{11.5}$$

and for the WD ($\alpha = 0$), we obtain

$$\varphi_W(t,\tau) = \delta(t)\,, \qquad \Phi_W(f,\upsilon) = \delta(f)\,, \qquad \psi_W(t,f) = \delta(t)\,\delta(f)\,, \qquad \Psi_W(\tau,\upsilon) \equiv 1\,.$$

Interference geometry. The geometric properties of the ITs of different shift-invariant TFRs may be quite different. There exists, however, a feature of interference geometry common to all shift-invariant TFRs, namely, the ITs' *oscillation.*

To illustrate this feature, we first consider the interference of two time-domain impulses $x_1(t) = \delta(t-t_1)$ and $x_2(t) = \delta(t-t_2)$. In this case, the signal terms and the IT can be written in terms of the time kernel $\varphi_C(t,\tau)$ as follows:

$$C_1^{(S)}(t,f) = |c_1|^2\,\varphi_C(t-t_1,0)\,, \qquad C_2^{(S)}(t,f) = |c_2|^2\,\varphi_C(t-t_2,0)\,,$$

$$C_{12}^{(I)}(t,f) = |c_1||c_2|\left[\varphi_C(t-t_{12},\tau_{12})\; e^{j(-2\pi\tau_{12}f+\varphi_{12})} + \varphi_C(t-t_{12},-\tau_{12})\; e^{j(2\pi\tau_{12}f-\varphi_{12})}\right]$$

with $\varphi_{12} = \arg\{c_1\} - \arg\{c_2\}$. We note that the signal terms are obtained by shifting the time kernel with $\tau = 0$, $\varphi_C(t,0)$, to the impulse locations $t = t_1$ and $t = t_2$, respectively. The signal terms are independent of frequency.

The IT consists of two subterms which are obtained by shifting the time kernel with (respectively) $\tau = \tau_{12}$ and $\tau = -\tau_{12}$ to the center time point $t = t_{12}$. This, however, does not necessarily imply that the IT subterms are indeed located around t_{12} (e.g., in the case of the GWD with $\varphi_{W(\alpha)}(t,\tau) = \delta(t+\alpha\tau)$, the IT subterms will be located at time points $t_{12}-\alpha\tau_{12}$ and $t_{12}+\alpha\tau_{12}$). The IT subterms both oscillate with respect to frequency; the oscillation "frequency" is τ_{12} and $-\tau_{12}$, respectively. Just as in the case of the WD or GWD, the IT's oscillation will thus be faster for increasing time distance $|\tau_{12}| = |t_1-t_2|$ between the interfering signal components. This type of IT oscillation is thus a common feature of all bilinear shift-invariant TFRs.

Dual results are obtained in the case of two complex sinusoids (frequency-domain impulses) $x_1(t) = e^{j2\pi f_1 t}$ and $x_2(t) = e^{j2\pi f_2 t}$. Here, signal terms and IT can be written in terms of the frequency kernel $\Phi_c(f,\upsilon)$:

$$C_1^{(S)}(t,f) = |c_1|^2 \Phi_c(f-f_1,0) , \qquad C_2^{(S)}(t,f) = |c_2|^2 \Phi_c(f-f_2,0) ,$$

$$C_{12}^{(I)}(t,f) = |c_1||c_2| \left[\Phi_c(f-f_{12},\upsilon_{12})\, e^{j(2\pi\upsilon_{12}t+\varphi_{12})} + \Phi_c(f-f_{12},-\upsilon_{12})\, e^{-j(2\pi\upsilon_{12}t+\varphi_{12})} \right] .$$

The discussion is analogous; in particular, the IT now oscillates in the time direction with frequency $\pm\upsilon_{12}$, where $|\upsilon_{12}| = |f_1-f_2|$ is the frequency distance between the interfering signal components.

We finally study the interference of two time-frequency shifted versions $x_1(t) = x_0(t-t_1)e^{j2\pi f_1 t}$, $x_2(t) = x_0(t-t_2)e^{j2\pi f_2 t}$ of a signal $x_0(t)$. Due to shift invariance, the signal terms are

$$C_1^{(S)}(t,f) = |c_1|^2 C_{x_0}(t-t_1,f-f_1) , \qquad C_2^{(S)}(t,f) = |c_2|^2 C_{x_0}(t-t_2,f-f_2) .$$

For the IT, we find

$$C_{12}^{(I)}(t,f) = |c_1||c_2| \left[F^{+}(t-t_{12},f-f_{12}) + F^{-}(t-t_{12},f-f_{12}) \right] \tag{11.6}$$

where

$$F^{\pm}(t,f) = C_{x_0}^{\pm}(t,f)\, e^{\pm j[2\pi(\upsilon_{12}t-\tau_{12}f)+\varphi_{12}]}$$

with

$$\varphi_{12} = \arg\{c_1\} - \arg\{c_2\} + 2\pi\upsilon_{12}t_{12} ;$$

the TFRs $C_{x_0}^{\pm}(t,f)$ are defined via their correlative duals $\hat{C}_{x_0}^{\pm}(\tau,\upsilon)$ by

$$\hat{C}_{x_0}^{\pm}(\tau,\upsilon) = \Psi_c(\tau\pm\tau_{12},\upsilon\pm\upsilon_{12})\, A_{x_0}(\tau,\upsilon) . \tag{11.7}$$

Again, (11.6) does not necessarily imply that the IT is indeed located around the center point (t_{12},f_{12}); this will only be the case if the ambiguity kernel $\Psi_c(\tau,\upsilon)$ is non-oscillatory (the GWD with $\Psi_{W^{(\alpha)}}(\tau,\upsilon) = e^{j2\pi\alpha\tau\upsilon}$ is a counter example). We note that the IT subterms are oscillatory, with oscillation frequency in the time direction equal to $\pm\upsilon_{12}$ and oscillation "frequency" in the frequency direction equal to $\pm\tau_{12}$. Another interesting point, evident from (11.7), is the fact that the IT is controlled by the values of the ambiguity kernel $\Psi_c(\tau,\upsilon)$ in the vicinity of $(\pm\tau_{12},\pm\upsilon_{12})$. In particular, the IT will be small if $\Psi_c(\tau,\upsilon)$ is itself small around $(\pm\tau_{12},\pm\upsilon_{12})$. This fact is important for the definition of "smoothed WD versions" (cf. Section 13).

Energy distributions. It has been demonstrated above that the oscillation of ITs, with oscillation frequency in the time (frequency) direction equal to the frequency (time) distance between the interfering signal components, is a general characteristic of shift-invariant TFRs. Even more about ITs can be said in the case of an "energy

distribution," i.e., a shift-invariant TFR $C_{x,y}(t,f)$ satisfying the marginal properties (cf. (4.1))

$$\int_f C_{x,y}(t,f)\,df = p_{x,y}(t)\,, \quad \int_t C_{x,y}(t,f)\,dt = P_{x,y}(f)\,, \quad \iint_{tf} C_{x,y}(t,f)\,dt\,df = E_{x,y}\,.$$

Since the marginal properties hold for signal terms and ITs separately, it follows that an IT's integral over frequency, time, or both time and frequency is given by the corresponding IT of the energetic quantities $p_{x,y}(t)$, $P_{x,y}(f)$, and $E_{x,y}$, respectively:

$$\int_f C_{kl}^{(I)}(t,f)\,df = p_{kl}^{(I)}(t) = 2\,\mathrm{Re}\left\{c_k c_l^*\, x_k(t)\, x_l^*(t)\right\},$$

$$\int_t C_{kl}^{(I)}(t,f)\,dt = P_{kl}^{(I)}(f) = 2\,\mathrm{Re}\left\{c_k c_l^*\, X_k(f)\, X_l^*(f)\right\},$$

$$\iint_{tf} C_{kl}^{(I)}(t,f)\,dt\,df = E_{kl}^{(I)} = 2\,\mathrm{Re}\left\{c_k c_l^* \int_t x_k(t)\, x_l^*(t)\,dt\right\}.$$

These IT integrals are hence *independent of the specific energy distribution C*; in particular, they equal the respective IT integrals of the WD. We also conclude that the marginal properties enforce the existence of a nonzero IT in the TFR C whenever at least one of the ITs $p_{kl}^{(I)}(t)$ and $P_{kl}^{(I)}(f)$ is not identically zero (this has already been mentioned in the context of the WD in Section 4). The ITs must again be oscillatory in general; this is easily seen by studying the simple example of two complex sinusoids, $x_1(t) = e^{j2\pi f_1 t}$ and $x_2(t) = e^{j2\pi f_2 t}$, where the IT's frequency integral is obtained as

$$\int_f C_{12}^{(I)}(t,f)\,df = p_{12}^{(I)}(t) = 2\,\mathrm{Re}\left\{c_1 c_2^*\, e^{j2\pi(f_1-f_2)t}\right\} = 2\,|c_1||c_2|\,\cos\left(2\pi\upsilon_{12}t + \varphi_{12}\right)$$

with $\varphi_{12} = \arg\{c_1\} - \arg\{c_2\}$ (cf. the "beat effect" discussed in Section 4). Since the IT's frequency integral is oscillatory with oscillation frequency $\upsilon_{12} = f_1 - f_2$, the IT must itself feature this type of oscillation.

It is interesting to note that both the shift-invariance property and the marginal property enforce a specific type of IT oscillation but do not specify other important IT features such as the IT's location and concentration in the time-frequency plane. Indeed, we have seen that the ITs of, e.g., the WD and RD (which both satisfy the shift-invariance property and the marginal property) show the same type of oscillation but quite different time-frequency location and concentration properties. These properties depend on the specific shape of the kernel functions $\varphi_C(t,\tau)$ etc.; they will be discussed in some detail in the next two sections.

12. THE SHIFT-SCALE-INVARIANT CLASS

The *shift-scale-invariant class* of bilinear TFRs [34,14,36] is a subclass of the shift-invariant class (bilinear Cohen class) discussed in the previous section. In addition to bilinearity and shift invariance, we here assume the following *scale-invariance property*: if the signals are time-frequency scaled as

$$x_a(t) = \sqrt{|a|}\, x(at) , \quad X_a(f) = \frac{1}{\sqrt{|a|}} X(\frac{f}{a})$$

and

$$y_a(t) = \sqrt{|a|}\, y(at) , \quad Y_a(f) = \frac{1}{\sqrt{|a|}} Y(\frac{f}{a})$$

with $a \neq 0$, then the TFR $C_{x,y}(t,f)$ reacts according to

$$C_{x_a,y_a}(t,f) = C_{x,y}(at, \frac{f}{a}) .$$

We shall see that this scale-invariance property entails characteristic IT properties.

It can be shown [34] that the kernels of a shift-scale-invariant TFR $C_{x,y}(t,f)$ assume the following special forms:

$$\varphi_c(t,\tau) = \int_\alpha \gamma_c(\alpha)\, \delta(t-\alpha\tau)\, d\alpha = \frac{1}{|\tau|} \gamma_c(\frac{t}{\tau}) \tag{12.1}$$

$$\Phi_c(f,\upsilon) = \int_\alpha \gamma_c(\alpha)\, \delta(f+\alpha\upsilon)\, d\alpha = \frac{1}{|\upsilon|} \gamma_c(-\frac{f}{\upsilon}) \tag{12.2}$$

$$\psi_c(t,f) = \int_\alpha \gamma_c(\alpha) \frac{1}{|\alpha|} e^{-j2\pi\frac{tf}{\alpha}}\, d\alpha \tag{12.3}$$

$$\Psi_c(\tau,\upsilon) = \int_\alpha \gamma_c(\alpha)\, e^{-j2\pi\alpha\tau\upsilon}\, d\alpha = \Gamma_c(\tau\upsilon) , \tag{12.4}$$

where the "kernel functions" $\gamma_c(\alpha)$ and $\Gamma_c(\xi)$, each of which characterizes the TFR C, are related by a Fourier transform,

$$\Gamma_c(\xi) = \int_\alpha \gamma_c(\alpha)\, e^{-j2\pi\xi\alpha}\, d\alpha .$$

The GWD is a prominent member of the shift-scale-invariant class. For the GWD $W_{x,y}^{(\alpha_0)}(t,f)$ with parameter α_0, the kernel functions are

$$\gamma_{W(\alpha_0)}(\alpha) = \delta(\alpha+\alpha_0) , \qquad \Gamma_{W(\alpha_0)}(\xi) = e^{j2\pi\alpha_0\xi} ,$$

and for the WD ($\alpha_0 = 0$), we have

$$\gamma_W(\alpha) = \delta(\alpha) , \qquad \Gamma_W(\xi) = 1 .$$

The marginal properties will be satisfied if

$$\int_\alpha \gamma_c(\alpha)\, d\alpha = \Gamma_c(0) = 1 .$$

Since this condition simply expresses a normalization of $\gamma_c(\alpha)$, we shall assume it to be met and, in the following, thus restrict our discussion to shift-scale-invariant *energy distributions*.

The specific forms (12.1)-(12.4) of the kernel functions $\varphi_c(t,\tau)$ etc. entail a characteristic type of interference geometry. Let us first study the interference of two

time-domain impulses $x_1(t) = \delta(t-t_1)$ and $x_2(t) = \delta(t-t_2)$. We here obtain the signal terms and IT as follows:

$$C_1^{(S)}(t,f) = |c_1|^2 \delta(t-t_1) , \qquad C_2^{(S)}(t,f) = |c_2|^2 \delta(t-t_2) , \tag{12.5}$$

$$C_{12}^{(I)}(t,f) = |c_1||c_2| \frac{1}{|\tau_{12}|} \left[\gamma_c\left(\frac{t-t_{12}}{\tau_{12}}\right) e^{j(-2\pi\tau_{12}f+\varphi_{12})} + \gamma_c\left(-\frac{t-t_{12}}{\tau_{12}}\right) e^{j(2\pi\tau_{12}f-\varphi_{12})} \right] \tag{12.6}$$

with $\varphi_{12} = \arg\{c_1\} - \arg\{c_2\}$. The signal terms are Dirac impulses at the correct time locations t_1 and t_2; they are independent of the specific TFR C. The ideal time concentration of the signal components is reflected by an equally ideal time concentration of the signal terms.

The IT shows the usual oscillation with respect to frequency. Apart from this, the IT features a characteristic "scaling property" which is a direct consequence of the TFR's scale invariance. We note that the envelopes of the two IT subterms are controlled by the function

$$\tilde{\gamma}_c(t;\tau_{12}) = \frac{1}{|\tau_{12}|} \gamma_c\left(\frac{t}{\tau_{12}}\right) .$$

Let us assume that $\gamma_c(\alpha)$ is a function with maximum (height) $\gamma_0 < \infty$ and effective length (spread) $\Delta\alpha > 0$. (This assumption is not valid in the case of the GWD where $\gamma_0 = \infty$ and $\Delta\alpha = 0$.) Then, for given time distance $|\tau_{12}|$ between the two signal components, the height and time spread of the IT envelope function $\tilde{\gamma}_c(t;\tau_{12})$ are $\gamma_0/|\tau_{12}|$ and $\Delta t = |\tau_{12}|\,\Delta\alpha$, respectively. This shows that the IT's height is inversely proportional to the time distance $|\tau_{12}| = |t_1-t_2|$ between the interfering signal components whereas the IT's time spread is proportional to the distance $|\tau_{12}|$. For signal components whose time distance is large, the IT will thus be very small in amplitude but very much spread out in the time direction.

Dual results are obtained in the case of two complex sinusoids (frequency-domain impulses) $x_1(t) = e^{j2\pi f_1 t}$ and $x_2(t) = e^{j2\pi f_2 t}$:

$$C_1^{(S)}(t,f) = |c_1|^2 \delta(f-f_1) , \qquad C_2^{(S)}(t,f) = |c_2|^2 \delta(f-f_2) ,$$

$$C_{12}^{(I)}(t,f) = |c_1||c_2| \frac{1}{|\upsilon_{12}|} \left[\gamma_c\left(-\frac{f-f_{12}}{\upsilon_{12}}\right) e^{j(2\pi\upsilon_{12}t+\varphi_{12})} + \gamma_c\left(\frac{f-f_{12}}{\upsilon_{12}}\right) e^{-j(2\pi\upsilon_{12}t+\varphi_{12})} \right] . \tag{12.7}$$

For growing frequency distance $|\upsilon_{12}| = |f_1-f_2|$ between the interfering signal components, the IT's amplitude will decrease and the IT's frequency spread will increase.

The two dual situations discussed above illustrate the "scaling property" of the ITs of shift-scale-invariant TFRs. They are, however, not sufficient for a complete characterization of the interference geometry. In particular, they are misleading in one respect: while it is true that, *in the case of time-domain or frequency-domain impulses*, the TFR signal terms preserve the time or frequency concentration of the signal components, a similar property does not generally hold in the practical situation where the signal components are not perfect impulses. An example is the GWD of a chirp signal (cf. Figure 22). We shall say more about concentration properties in Section 13.

In the general case, a partial characterization of the interference geometry can be derived from the fact that *any shift-scale-invariant TFR is a superposition of GWDs*. This is easily seen by combining (12.1) with (11.5), from which it follows that $\varphi_C(t,\tau) = \int \gamma_C(-\alpha)\, \varphi_{W(\alpha)}(t,\tau)\, d\alpha$ and thus

$$C_{x,y}(t,f) = \int_\alpha \gamma_C(-\alpha)\, W_{x,y}^{(\alpha)}(t,f)\, d\alpha \ . \tag{12.8}$$

We have shown in Section 9 that, for two "signal points" (t_1,f_1) and (t_2,f_2), the IT of the GWD is located around the time-frequency points $(t_{12}-\alpha\tau_{12}, f_{12}+\alpha\upsilon_{12})$ and $(t_{12}+\alpha\tau_{12}, f_{12}-\alpha\upsilon_{12})$. Due to the superposition relation (12.8), the IT of the shift-scale-invariant TFR C will then be located around the line segment l_{12} made up of all points $(t_{12}\mp\alpha\tau_{12}, f_{12}\pm\alpha\upsilon_{12})$ with α inside the effective support of $\gamma_C(\alpha)$. *Figure 27* shows this line segment for the case where the effective support of $\gamma_C(\alpha)$ is the interval $-1/2 < \alpha < 1/2$. Note, however, that the IT's amplitude will often be small if both $|\tau_{12}|$ and $|\upsilon_{12}|$ are not close to zero (cf. Section 13); the region shown in Figure 27 should therefore be interpreted as the *potential* support of the IT component corresponding to the "signal points" (t_1,f_1) and (t_2,f_2).

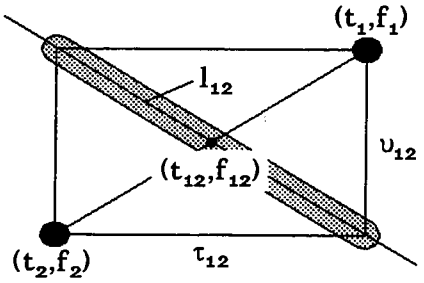

Figure 27. Pointwise construction of the potential IT support of a shift-scale-invariant TFR.

The time length and frequency length of the IT line segment l_{12} are approximately $\Delta t = |\tau_{12}|\,\Delta\alpha$ and $\Delta f = |\upsilon_{12}|\,\Delta\alpha$, respectively, where $\Delta\alpha$ is the effective spread of the function $\gamma_C(\alpha)$. Thus, the spread of $\gamma_C(\alpha)$ again controls the IT's spread in the time-frequency plane. Due to the normalization $\int \gamma_C(\alpha)\, d\alpha = 1$, an increase of IT spread is accompanied by a proportional decrease of IT height.

13. SMOOTHED VERSIONS OF WIGNER DISTRIBUTION

The interference structure of the WD is a basic limitation of the WD's practical usefulness. Since the number of *outer ITs* grows quadratically with the number of signal components, the WD's signal terms (which, after all, represent the greatest part of signal energy) will often be covered by outer ITs and will thus become hardly visible. In a similar way, *inner ITs* tend to occupy larger regions of the time-frequency plane, thus burying smaller signal terms. In practice, therefore, it is often

mandatory to suppress or attenuate at least part of the ITs. Since ITs are oscillatory, this can easily be done by *smoothing* the WD with respect to the time and/or frequency variable.

Shift-invariant smoothing. If the WD smoothing is to be linear and independent of time and frequency, which is assumed in the following, then the *smoothed WD* (SWD) is derived from the WD by a convolution

$$C_{x,y}(t,f) = \int\int_{t'f'} \psi_c(t-t',f-f')\, W_{x,y}(t',f')\, dt'\, df' \; . \tag{13.1}$$

Comparing with (11.2), we see that this is just the general formulation of a shift-invariant TFR. The SWD (13.1) is hence guaranteed to be bilinear and shift-invariant. However, this does not say that, conversely, all shift-invariant TFRs are SWDs: for an SWD, we have to require that the Wigner kernel $\psi_c(t,f)$ is a smooth, non-oscillatory function (i.e., a lowpass function). For example, a TFR which is shift-invariant but cannot be considered as an SWD is the GWD whose Wigner kernel, $\psi_{W(\alpha)}(t,f) = \frac{1}{|\alpha|} \exp(j2\pi \frac{tf}{\alpha})$, is oscillatory. Indeed, in the case of the GWD the convolution (13.1) effects essentially a time-frequency displacement, rather than attenuation, of ITs (cf. Section 9).

A compact characterization of smoothing can be given in the dual (correlative) domain [3,14,15,16]. According to (11.4), the correlative dual of the SWD $C_{x,y}(t,f)$ is given by the product of the AF and the ambiguity kernel $\Psi_c(\tau,\upsilon)$,

$$\hat{C}_{x,y}(\tau,\upsilon) = \Psi_c(\tau,\upsilon)\, A_{x,y}(\tau,\upsilon) \; . \tag{13.2}$$

The advantage of this description is the fact that the convolution is here replaced by a simple multiplication. Note that the Wigner kernel and the ambiguity kernel are a Fourier transform pair,

$$\Psi_c(\tau,\upsilon) = \int\int_{t\,f} \psi_c(t,f)\, e^{-j2\pi(\upsilon t-\tau f)} dt\, df \; ;$$

the same relation holds between the WD and the AF, as well as between $C_{x,y}(t,f)$ and $\hat{C}_{x,y}(\tau,\upsilon)$.

In the correlative domain, the smoothing property is expressed by the fact that the magnitude of the ambiguity kernel $\Psi_c(\tau,\upsilon)$ decays for larger values of $|\tau|$ and/or $|\upsilon|$. (Again, this is not true in the case of the GWD where $|\Psi_{W(\alpha)}(\tau,\upsilon)| = |e^{j2\pi\alpha\tau\upsilon}| \equiv 1$.) In the following, we assume that $\Psi_c(\tau,\upsilon)$ has its maximum at the origin (0,0) of the (τ,υ)-plane. We also assume the normalization

$$\Psi_{c,max} = \Psi_c(0,0) = \int\int_{t\,f} \psi_c(t,f)\, dt\, df = 1$$

which guarantees the property $\int\int C_{x,y}(t,f)\, dt\, df = E_{x,y}$, and

$$\psi_c(t,f) \in \mathbb{R} \; , \qquad \Psi_c^*(-\tau,-\upsilon) = \Psi_c(\tau,\upsilon)$$

which guarantees that the auto-TFR $C_x(t,f)$ is real-valued.

Interference geometry of SWDs. Since an SWD is a shift-invariant TFR, its ITs exhibit the type of oscillation discussed in Section 11. Due to this oscillation, the smoothing operation will generally produce an attenuation of ITs.

For a *given kernel* $\psi_c(t,f)$ or, equivalently, $\Psi_c(\tau,\upsilon)$, this attenuation will be more pronounced for faster oscillation of the ITs. Recalling that larger time distance $|\tau_{12}|$ and/or frequency distance $|\upsilon_{12}|$ between the interfering signal points (t_1,f_1) and (t_2,f_2) causes faster IT oscillation, we obtain the general rule that *the IT of more distant signal points will be attenuated more.*

This rule must be applied with caution, however, since a substantial IT attenuation can be achieved only if the direction of IT oscillation and the direction of smoothing are not orthogonal: if, for example, the IT oscillates in the time direction (i.e., the interfering signal components are displaced with respect to frequency but not with respect to time) and the smoothing occurs mainly in the frequency direction (i.e., the Wigner kernel $\psi_c(t,f)$ has a large frequency spread but a small time spread), then little or no IT attenuation will be obtained.

The attenuation of a *given IT* will be stronger if the Wigner kernel $\psi_c(t,f)$ has a larger spread in the time and/or frequency direction, which means that the ambiguity kernel $\Psi_c(\tau,\upsilon)$ is more concentrated around the origin of the (τ,υ)-plane.

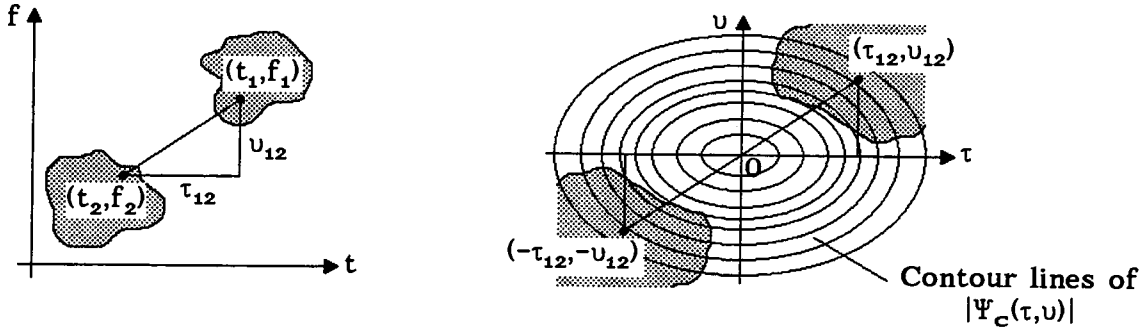

Figure 28. Correlative-domain analysis of IT attenuation.

A detailed, quantitative analysis of IT attenuation can be derived from the correlative-domain formulation (13.2), combined with the AF's interference geometry as discussed in Section 10. Suppose that the two interfering signal points are (t_1,f_1) and (t_2,f_2) as illustrated in *Figure 28.* We know from Section 3 that the WD's IT is located around the center point (t_{12},f_{12}) and oscillates in the time direction with frequency $|\upsilon_{12}|$ and in the frequency direction with "frequency" $|\tau_{12}|$. Passing into the correlative domain, the corresponding IT of the AF is located around the points $(\tau_{12},\upsilon_{12})$ and $(-\tau_{12},-\upsilon_{12})$. We now construct the correlative dual of the SWD by multiplying the AF with the ambiguity kernel according to (13.2). By this, the IT's magnitude is reduced by the factor $|\Psi_c(\tau_{12},\upsilon_{12})| = |\Psi_c(-\tau_{12},-\upsilon_{12})| \leq 1$. This attenuation factor is preserved when passing back into the energetic domain since energetic and correlative domains are related by the *linear* Fourier transform. Hence, the IT corresponding to signal points (t_1,f_1) and (t_2,f_2) will be reduced by the factor $|\Psi_c(\tau_{12},\upsilon_{12})|$. Of course, this statement is valid in an approximate sense only since

a strict pointwise localization is not possible; the IT attenuation factor will thus be influenced also by the values of $\Psi_c(\tau,\upsilon)$ in a local neighborhood of the point $(\tau_{12},\upsilon_{12})$.

From the above construction, we also conclude that an IT of the WD corresponding to the signal points (t_1,f_1) and (t_2,f_2) will be suppressed altogether if the corresponding "lag point" $(\tau_{12},\upsilon_{12})$ is located outside the effective support $\hat{R}_\Psi$ of the ambiguity kernel $\Psi_c(\tau,\upsilon)$ (see *Figure 29*). For general signal components $x_1(t)$ and $x_2(t)$ with effective time-frequency supports R_1 and R_2, respectively, the IT $C_{12}^{(I)}(t,f)$ of the SWD C will be approximately zero if the effective support $\hat{R}_{12}$ of the AF's IT lies entirely outside $\hat{R}_\Psi$. This situation is shown in Figure 29 (recall that, according to Section 10, $\hat{R}_{12}$ consists of all lag points $(\tau_{12},\upsilon_{12})$ and $(-\tau_{12},-\upsilon_{12})$ with $\tau_{12}=t_1-t_2$ and $\upsilon_{12}=f_1-f_2$, where $(t_1,f_1)\in R_1$ and $(t_2,f_2)\in R_2$).

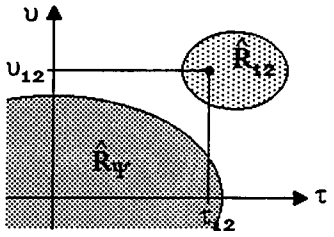

Figure 29. Suppression of IT in the SWD: analysis in the correlative domain.

Time-frequency concentration. The price paid for the attenuation of ITs is a loss in time-frequency concentration. This is an obvious consequence of the fact that a smoothing broadens the non-oscillatory WD signal terms and the envelopes of the oscillatory ITs. Closely spaced signal terms and ITs which, before smoothing, are well separated in the WD may hence overlap after smoothing [37].

For a very rough quantitative analysis, let us assume that the Wigner kernel $\psi_c(t,f)$ can be characterized by a time spread Δt and a frequency spread Δf. Such a characterization is possible if $\psi_c(t,f)$ is a "simple" function such as, for example, a two-dimensional Gaussian. (We stress, however, that this excludes shift-scale-invariant SWDs for which a separate discussion will be given later.) In this case, roughly the same spreads Δt and Δf will be obtained for the "marginals"

$$\int_f \psi_c(t,f)\,df = \varphi_c(t,0)\ , \qquad \int_t \psi_c(t,f)\,dt = \Phi_c(f,0)$$

of the Wigner kernel $\psi_c(t,f)$.

As a basic example, we now consider the time-domain impulse $x(t)=\delta(t-t_0)$ whose ideal time concentration is preserved in the WD $W_x(t,f)=\delta(t-t_0)$, a fact highlighting the WD's perfect time concentration. In contrast, the SWD represents the impulse as

$$C_x(t,f) = \varphi_c(t-t_0,0)\ ,$$

i.e., with time spread Δt. A dual result is obtained for a complex sinusoid (frequen-

cy-domain impulse) $e^{j2\pi f_0 t}$: while the WD $W_x(t,f) = \delta(f-f_0)$ is perfectly concentrated, the SWD is

$$C_x(t,f) = \Phi_c(f-f_0, 0)$$

and thus has frequency spread Δf.

More generally, if a WD signal term has effective time length T, then the smoothing (convolution) operation will roughly increase this time length by Δt; an analogous statement can be made with respect to frequency. The spreads Δt and Δf of the smoothing kernel $\psi_c(t,f)$ can thus be interpreted as "analysis uncertainties" of the SWD C with respect to time and frequency, respectively. An increase of these spreads or analysis uncertainties means a loss in time-frequency concentration.

In the correlative domain, the broadening of signal terms can be viewed as a consequence of the multiplication of the AF by the ambiguity kernel $\Psi_c(\tau,\upsilon)$. While it is true that the AF's signal terms are located around the origin of the (τ,υ)-plane, they yet extend to regions corresponding to larger values of $|\tau|$ and/or $|\upsilon|$. These components are attenuated if $\Psi_c(\tau,\upsilon)$ is small in the corresponding regions, which results in a broadening of the signal terms of the SWD. Note that, since $\psi_c(t,f)$ and $\Psi_c(\tau,\upsilon)$ are a Fourier transform pair, a large time spread Δt of $\psi_c(t,f)$ means that $\Psi_c(\tau,\upsilon)$ is very narrow with respect to υ; similarly, a large frequency spread Δf entails a $\Psi_c(\tau,\upsilon)$ which is very narrow with respect to τ.

At this point, it is evident that the WD smoothing is governed by a fundamental tradeoff of IT attenuation versus time-frequency concentration: for good IT attenuation, the ambiguity kernel $\Psi_c(\tau,\upsilon)$ should be as narrow as possible around the origin of the (τ,υ)-plane; however, due to the Fourier transform relationship connecting $\psi_c(t,f)$ and $\Psi_c(\tau,\upsilon)$, this will result in a broad Wigner kernel $\psi_c(t,f)$ with large spreads Δt and Δf and, consequently, poor time-frequency concentration. Thus, as a general rule, better IT attenuation entails poorer time-frequency concentration, and vice versa.

For practical applications, the kernels $\psi_c(t,f)$ or $\Psi_c(\tau,\upsilon)$ should be designed such that they produce sufficient IT attenuation while impairing the WD's time-frequency concentration as little as possible. Such a design necessitates some *a-priori* knowledge about the signal under analysis. Suppose, for example, that the signal components are known to be displaced mainly with respect to time such that their ITs oscillate mainly in the frequency direction. Obviously, a Wigner kernel with large time spread Δt is then a bad choice since it impairs the WD's time concentration without producing any IT attenuation.

There is thus a demand for SWDs which, besides permitting an efficient implementation, allow the time spread Δt and the frequency spread Δf to be adjusted *independently of each other* in a simple way. The *smoothed pseudo Wigner distribution*, to be discussed presently, largely meets these requirements.

The pseudo Wigner distribution. By way of preparation, we first discuss the *pseudo Wigner distribution* (PWD) [1]

$$\hat{W}_{x,y}^{(h)}(t,f) = \int_\tau x(t+\tfrac{\tau}{2}) y^*(t-\tfrac{\tau}{2})\, h^2(\tfrac{\tau}{2})\, e^{-j2\pi f\tau}\, d\tau \,. \qquad (13.3)$$

The PWD is a short-time version of the WD using a running analysis window h(t). We assume the window h(t) to be real-valued, even, normalized as $h(0) = 1$ (this assures the normalization $\int\int \psi_{\hat{W}}(t,f)\, dtdf = 1$), and finite-length such that $h(t) = 0$ for $|t| > T_h/2$, where T_h is the window length. Note that the integration in (13.3) then reduces to an integration over the finite interval $[-T_h, T_h]$. Formally, the WD is a limiting case of the PWD with infinite window length $T_h = \infty$ and the all-constant window $h(t) \equiv 1$.

The PWD can be expressed as [1]

$$\hat{W}^{(h)}_{x,y}(t,f) = \int_{f'} \xi_h(f-f')\, W_{x,y}(t,f')\, df'$$

with

$$\xi_h(f) = W_h(0,f) = \int_{\tau} h^2\left(\frac{\tau}{2}\right) e^{-j2\pi f\tau}\, d\tau \; ;$$

it is thus an SWD, where the smoothing occurs with respect to the frequency variable only. A stronger frequency smoothing will be obtained for a broader smoothing function $\xi_h(f)$, i.e., for a shorter analysis window h(t). Since the PWD does not effect any time smoothing, the ideal *time* concentration of the WD is preserved, and ITs are attenuated only if they have an oscillation component in the frequency direction, i.e., if the interfering signal components are displaced *in time*.

The kernels of the PWD are given by

$$\varphi_{\hat{W}(h)}(t,\tau) = \delta(t)\, h^2\left(\frac{\tau}{2}\right) , \qquad \Phi_{\hat{W}(h)}(f,\upsilon) = \xi_h(f) ,$$

$$\psi_{\hat{W}(h)}(t,f) = \delta(t)\, \xi_h(f) , \qquad \Psi_{\hat{W}(h)}(\tau,\upsilon) = h^2\left(\frac{\tau}{2}\right) .$$

In particular, $\Psi_{\hat{W}(h)}(\tau,\upsilon)$ is independent of the frequency lag υ, decreasing for increasing time lag $|\tau|$ (for usual windows), and zero for $|\tau| > T_h$. Evidently, the IT of two time-disjoint signals will be totally suppressed if the gap between the signals' (effective) time supports exceeds the window length T_h. Here, the finite-length window h(t) never catches both signals simultaneously (see *Figure 30*).

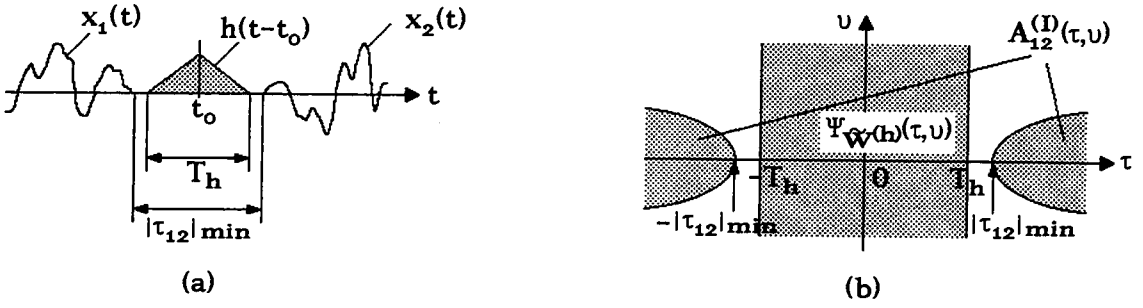

Figure 30. Signals producing zero IT in PWD: (a) time domain, (b) correlative domain.

A simple approximate expression can be given for the PWD of an AM-FM signal

$$x(t) = a(t)\, e^{j\varphi(t)} , \qquad a(t) \geq 0 , \qquad \varphi(t) \in \mathbb{R}$$

provided that the PWD window h(t) is sufficiently short and the variations of the instantaneous amplitude a(t) and instantaneous frequency $f_i(t) = \varphi'(t)/2\pi$ are sufficiently slow. Specifically, we assume that, inside the local window interval $[t_o-T_h/2, t_o+T_h/2]$ corresponding to each analysis time point t_o, the instantaneous amplitude a(t) is approximately constant and the instantaneous frequency $f_i(t)$ can be approximated by a linear function (linear FM, "local chirp approximation"),

$$a(t) \approx a(t_o) \quad \text{and} \quad f_i(t) \approx f_i(t_o) + f_i'(t_o)\,(t-t_o) \quad \text{for} \quad t_o-\frac{T_h}{2} < t < t_o+\frac{T_h}{2} .$$

This approximation results in the following approximate expression for the PWD,

$$\hat{W}_x^{(h)}(t,f) \approx a^2(t)\,\xi_h\big(f-f_i(t)\big) ,$$

according to which the PWD is concentrated along the instantaneous-frequency curve and does not contain inner ITs.

If the linear approximation of $f_i(t)$ is not sufficient, a second-order (linear+quadratic FM) approximation can be used. For each analysis time point, the PWD is here approximated in the frequency direction by the convolution of an Airy function (cf. Section 7) with $\xi_h(f)$, i.e., by a smoothed Airy function. The Airy-function approximation shows inner ITs on the concave side of the instantaneous-frequency curve (cf. Figure 14). In any case, the local extension of the PWD's inner ITs with respect to frequency can be (approximately) derived from the instantaneous-frequency curve by applying the laws of WD interference geometry while taking into account the fact that signal points whose time distance exceeds the window length T_h cannot produce ITs (see *Figure 31*). From the geometric construction shown in Figure 31, it is clear that the PWD's ITs will be more spread out with respect to frequency if, inside the local window interval $[t_o-T_h/2, t_o+T_h/2]$, the *curvature* of the instantaneous frequency is stronger.

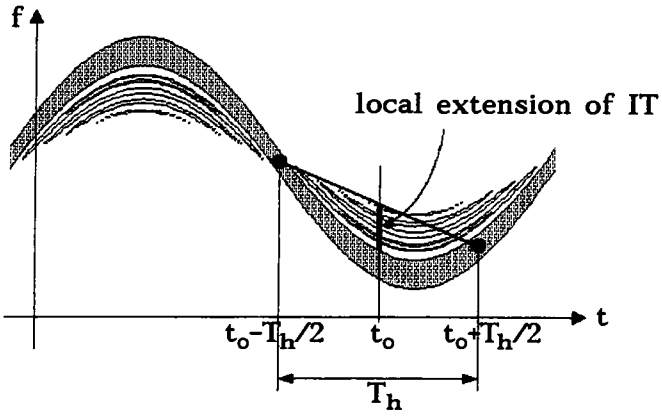

Figure 31. PWD of FM signal.

The smoothed pseudo Wigner distribution. Since the PWD does not effect any smoothing with respect to time, it is incapable of attenuating ITs which oscillate

in the time direction only, i.e., which are caused by signal components displaced only with respect to frequency. This drawback can be overcome by an explicit time smoothing of the PWD; this leads to the *smoothed pseudo Wigner distribution* (SPWD) defined as [38,39]

$$\hat{W}_{x,y}^{(g,h)}(t,f) = \int_{t'} g(t-t')\, \hat{W}_x^{(h)}(t',f)\, dt' = \int_{t'}\int_{f'} g(t-t')\, \xi_h(f-f')\, W_{x,y}(t',f')\, dt'df' .$$

Here, g(t) is a smoothing (or lowpass) function which we assume to be real-valued and normalized as $\int g(t)\, dt = 1$. Both the WD and the PWD are special cases of the SPWD; in particular, the PWD is obtained for $g(t) = \delta(t)$. In general, of course, the time smoothing contained in the SPWD will produce a loss in time concentration as compared to the WD or PWD.

The SPWD's smoothing characteristics in the time and frequency direction can be controlled arbitrarily and independently of each other by the choice of the time smoothing function g(t) and the PWD window h(t). A broader time smoothing function g(t) will produce more time smoothing and thus better IT attenuation but poorer time concentration. The smoothing in the frequency direction equals that of the PWD: a broader PWD window h(t) will produce less frequency smoothing, which results in poorer IT attenuation but better frequency concentration.

The kernels of the SPWD are given by

$$\varphi_{\hat{W}^{(g,h)}}(t,\tau) = g(t)\, h^2(\tfrac{\tau}{2}) , \qquad \Phi_{\hat{W}^{(g,h)}}(f,\upsilon) = \xi_h(f)\, G(\upsilon) ,$$

$$\psi_{\hat{W}^{(g,h)}}(t,f) = g(t)\, \xi_h(f) , \qquad \Psi_{\hat{W}^{(g,h)}}(\tau,\upsilon) = h^2(\tfrac{\tau}{2})\, G(\upsilon) ,$$

where $G(\upsilon)$ is the Fourier transform of g(t). Note that all kernels are *separable* functions; this structure facilitates the independent adjustment of the smoothing properties in the time and frequency directions. As in the case of the PWD, the IT of two time-disjoint signal components will be altogether suppressed if the gap between the signal components is broader than the length T_h of the PWD window h(t). As a difference from the PWD, the IT of two frequency-disjoint signal components will be effectively suppressed if the length $|\upsilon_{12}|_{min}$ of the gap separating the two signal bands falls outside the effective support of $G(\upsilon)$, i.e., if the length of the "frequency gap" exceeds the bandwidth of the time-smoothing window g(t).

In order to further illustrate the IT attenuation and time-frequency concentration properties of the SPWD, we again consider the cases of two time-domain and frequency-domain impulses. For two time-domain impulses $x_1(t) = \delta(t-t_1)$ and $x_2(t) = \delta(t-t_2)$, the SPWD's signal terms and IT are

$$\hat{W}_1^{(g,h)(S)}(t,f) = |c_1|^2\, g(t-t_1) , \qquad \hat{W}_2^{(g,h)(S)}(t,f) = |c_2|^2\, g(t-t_2) ,$$

$$\hat{W}_{12}^{(g,h)(I)}(t,f) = 2\, |c_1|\, |c_2|\, g(t-t_{12})\, h^2(\tfrac{\tau_{12}}{2})\, \cos(2\pi\tau_{12}f - \varphi_{12})$$

with $\varphi_{12} = \arg\{c_1\} - \arg\{c_2\}$. We see that the time spreads of both the signal terms and the IT are directly given by the spread of the time smoothing window g(t).

Besides, the IT is weighted by the factor $h^2(\frac{\tau_{12}}{2})$ which, for h(t) being a usual window, decays for growing time distance $|\tau_{12}|$ and is altogether zero for $|\tau_{12}| > T_h$.

In the dual case of two complex sinusoids (frequency-domain impulses) $x_1(t) = e^{j2\pi f_1 t}$ and $x_2(t) = e^{j2\pi f_2 t}$, we obtain

$$\tilde{W}_1^{(g,h)(S)}(t,f) = |c_1|^2 \, \xi_h(f-f_1) \;, \qquad \tilde{W}_2^{(g,h)(S)}(t,f) = |c_2|^2 \, \xi_h(f-f_2) \;,$$

$$\tilde{W}_{12}^{(g,h)(I)}(t,f) = 2\,|c_1|\,|c_2|\;\xi_h(f-f_{12})\;G(\upsilon_{12})\;\cos(2\pi\upsilon_{12}t+\varphi_{12}) \;.$$

Here, the frequency spreads of both the signal terms and the IT equal the spread of $\xi_h(f)$, and the IT is weighted by the factor $G(\upsilon_{12})$ which will be small for large frequency distance $|\upsilon_{12}|$.

The spectrogram. The auto-spectrogram [29,40,18,19] is defined as the squared magnitude of the short-time Fourier transform,

$$S_x^{(h)}(t,f) = |X^{(h)}(t,f)|^2 \qquad \text{with} \qquad X^{(h)}(t,f) = \int_{t'} x(t')\,h(t'-t)\,e^{-j2\pi f t'}\,dt' ;$$

it is thus everywhere non-negative. The cross-spectrogram is defined as

$$S_{x,y}^{(h)}(t,f) = X^{(h)}(t,f)\;Y^{(h)*}(t,f) \;. \tag{13.4}$$

Here, h(t) is an analysis window which we assume to be real-valued, even, of finite length T_h, and normalized with respect to its energy such that $E_h = \int h^2(t)\,dt = 1$.

For a real-valued and even window h(t), the spectrogram can be written as

$$S_{x,y}^{(h)}(t,f) = \int_{t'}\int_{f'} W_h(t-t',f-f')\;W_{x,y}(t',f')\;dt'df' \;;$$

it is thus recognized to be an SWD since, for a "good" window h(t), the window's WD $W_h(t,f)$ is a lowpass function. The spectrogram's kernels are obtained as

$$\varphi_{S(h)}(t,\tau) = h\left(t+\tfrac{\tau}{2}\right)h\left(t-\tfrac{\tau}{2}\right) \;, \qquad \Phi_{S(h)}(f,\upsilon) = H\left(f+\tfrac{\upsilon}{2}\right)H\left(f-\tfrac{\upsilon}{2}\right) \;,$$

$$\psi_{S(h)}(t,f) = W_h(t,f) \;, \qquad \Psi_{S(h)}(\tau,\upsilon) = A_h(\tau,\upsilon) \;.$$

The spectrogram is in fact a very special SWD since its Wigner kernel equals the WD of the analysis window h(t). As a consequence, the time spread Δt and the frequency spread Δf cannot be chosen independently of each other. Indeed, a long (short) window h(t) produces a Wigner kernel $\psi_{S(h)}(t,f) = W_h(t,f)$ with large (small) time spread Δt and small (large) frequency spread Δf, yielding good attenuation of ITs oscillating in the time direction (frequency direction) but poor time concentration (frequency concentration). This is illustrated in *Figure 32.*

Furthermore, the spreads Δt and Δf cannot both be made arbitrarily small since the uncertainty principle prohibits the WD of h(t) from being ideally concentrated both in the time direction and in the frequency direction. Assuming proper definition

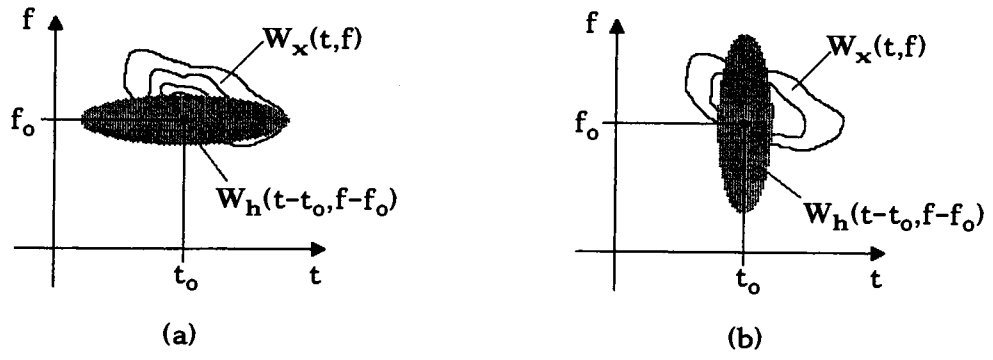

Figure 32. Time-frequency concentration tradeoff of spectrogram: (a) "long" window, (b) "short" window.

of the spreads Δt and Δf, the uncertainty relation states that the product of Δt and Δf is bounded from below as [23]

$$\Delta t \, \Delta f \geq \frac{1}{4\pi} .$$

Thus, the spectrogram effects a fixed minimal overall smoothing. In contrast to the SPWD where the time smoothing and frequency smoothing can be adjusted independently and without restrictions, the spectrogram merely permits a trading-off of time smoothing against frequency smoothing. As a consequence, the overall time-frequency concentration is limited, and the spectrogram suffers from a tradeoff between time concentration and frequency concentration (see Figure 32).

On the other hand, the substantial smoothing in the spectrogram produces a strong attenuation of ITs [18,19]. In fact, the smoothing is so strong that most ITs will be suppressed and, furthermore, the auto-spectrogram becomes nonnegative ("smoothing for positivity"). The identity

$$\left| S_{x,y}^{(h)}(t,f) \right|^2 = S_x^{(h)}(t,f) \, S_y^{(h)}(t,f) ,$$

which follows from the definition (13.4), can be used for deriving an upper bound on the magnitude of the spectrogram's ITs [10,21]: for a two-component signal $x(t) = x_1(t) + x_2(t)$, the IT's magnitude is

$$\left| S_{12}^{(h)(I)}(t,f) \right| = \left| 2 \, \mathrm{Re}\left\{ S_{x_1,x_2}^{(h)}(t,f) \right\} \right| \leq 2 \left| S_{x_1,x_2}^{(h)}(t,f) \right| = 2 \sqrt{S_{x_1}^{(h)}(t,f) \, S_{x_2}^{(h)}(t,f)} . \qquad (13.5)$$

This shows that, at a given time-frequency point, the IT's magnitude cannot be larger than twice the geometric mean of the corresponding auto-spectrograms (signal terms). In particular, the IT is seen be restricted to those regions of the time-frequency plane where the corresponding signal terms overlap. Thus, the IT will always be superimposed on the signal terms; it will never appear as a separate structure. If the signal terms are effectively non-overlapping, then $S_{x_1}^{(h)}(t,f) \, S_{x_2}^{(h)}(t,f) \approx 0$ for all (t,f) and, due to (13.5), the IT is approximately zero (see *Figure 33*),

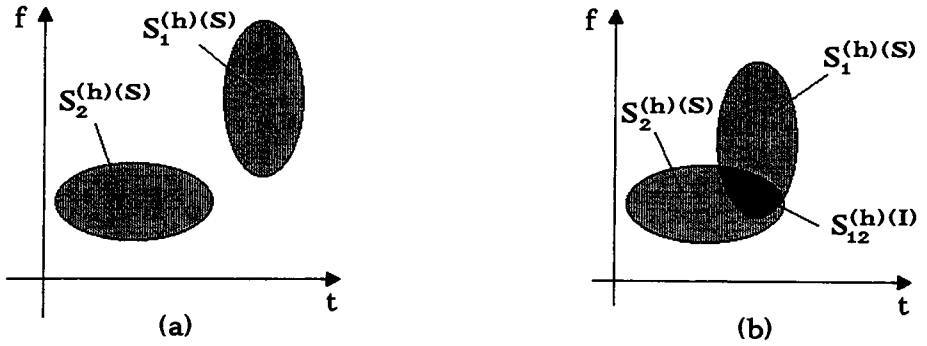

Figure 33. ITs of the spectrogram: (a) non-overlapping signal terms and zero IT; (b) overlapping signal terms and non-zero IT.

$$S_{12}^{(h)(I)}(t,f) \approx 0 \quad \text{for} \quad S_1^{(h)(S)}(t,f)\, S_2^{(h)(S)}(t,f) \approx 0 .$$

The general properties of the spectrogram discussed above are illustrated by the simple example of two complex sinusoids $x_1(t) = e^{j2\pi f_1 t}$ and $x_2(t) = e^{j2\pi f_2 t}$. Signal terms and IT are obtained as

$$S_1^{(h)(S)}(t,f) = |c_1|^2 H^2(f-f_1) , \qquad S_2^{(h)(S)}(t,f) = |c_2|^2 H^2(f-f_2) ,$$

$$S_{12}^{(h)(I)}(t,f) = 2\,|c_1||c_2|\, H(f-f_1)\, H(f-f_2) \cos(2\pi \upsilon_{12} t + \varphi_{12})$$

with $\varphi_{12} = \arg\{c_1\} - \arg\{c_2\}$. We see that the frequency spread of the signal terms increases with decreasing length of the window h(t), causing a loss in frequency concentration. The IT is restricted to those frequencies f where $H(f-f_1)\, H(f-f_2) \neq 0$, i,e, where the signal terms overlap. The IT will be altogether suppressed if the effective bandwidth of the window h(t) is smaller than the frequency distance $|\upsilon_{12}| = |f_1 - f_2|$. The overall two-component signal is shown in *Figure 34* for two different windows: a "long" window (Figure 34.a) results in non-overlapping signal terms and, consequently, a zero IT; in contrast, a "short" window (Figure 34.b) causes the signal terms to overlap and the IT to be nonzero. The oscillatory IT is here superimposed on the signal terms; signal terms and IT are combined into an overall oscillatory (but non-negative) structure which, of course, reflects the "beat" between the two frequencies f_1 and f_2 (cf. the "beat effect" discussed for the WD in Section 4).

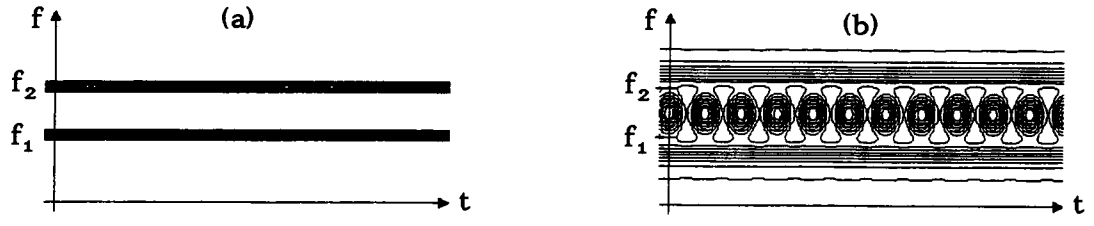

Figure 34. Spectrogram of superposition of two complex sinusoids: (a) "long" window, (b) "short" window.

Dual results are obtained for the case of two time-domain impulses $x_1(t) = \delta(t-t_1)$ and $x_2(t) = \delta(t-t_2)$:

$$S_1^{(h)(S)}(t,f) = |c_1|^2 h^2(t-t_1) , \qquad S_2^{(h)(S)}(t,f) = |c_2|^2 h^2(t-t_2) ,$$

$$S_{12}^{(h)(I)}(t,f) = 2 |c_1||c_2| h(t-t_1) h(t-t_2) \cos(2\pi\tau_{12}f - \varphi_{12}) .$$

The signal terms' time spread here increases with growing window length, causing a loss in time concentration. The IT is confined to the time interval where the signal terms overlap; it will be zero for non-overlapping signal terms, i.e., if the window length T_h is smaller than the time distance $|\tau_{12}| = |t_1-t_2|$ between the two impulses.

Shift-scale-invariant smoothing. So far, we have considered SWDs $C_{x,y}(t,f)$ whose Wigner kernel $\psi_c(t,f)$ is a "simple" two-dimensional function which can be roughly characterized by a time spread Δt and a frequency spread Δf; these spreads can then be interpreted as "analysis uncertainties" in the sense that they characterize the SWD's time concentration and frequency concentration, respectively.

We now study *shift-scale-invariant* SWDs which feature a somewhat more sophisticated type of smoothing. According to (12.3), the Wigner kernel $\psi_c(t,f)$ here is a function of the product tf and thus cannot be characterized by simple spread quantities. In fact, shift-scale-invariant TFRs have been shown in Section 12 to possess some very special properties regarding time-frequency concentration and interference geometry. These properties will now be considered in more detail.

According to (12.4), the ambiguity kernel of a shift-scale-invariant TFR C is

$$\Psi_c(\tau,\upsilon) = \int_\alpha \gamma_c(\alpha)\, e^{-j2\pi\alpha\tau\upsilon}\, d\alpha = \Gamma_c(\tau\upsilon) \tag{13.6}$$

and thus a function of the product $\tau\upsilon$. Again, not every shift-scale-invariant TFR is an SWD; recalling that the magnitude of $\Psi_c(\tau,\upsilon)$ has to decay for larger values of $|\tau|$ and/or $|\upsilon|$, we obtain the requirement that the magnitude of $\Gamma_c(\xi)$ decays for larger values of $|\xi|$. This again excludes the GWD $W_{x,y}^{(\alpha)}(t,f)$ which is shift-scale-invariant but, due to $|\Gamma_{W(\alpha)}(\xi)| = |e^{j2\pi\alpha\xi}| \equiv 1$, cannot be counted as an SWD.

Let us assume that the effective support of the kernel function $\Gamma_c(\xi)$ is the interval $|\xi| < \xi_o$, i.e., there is $\Gamma_c(\xi) \approx 0$ for $|\xi| > \xi_o$. Due to (13.6), the ambiguity kernel $\Psi_c(\tau,\upsilon)$ will then be approximately zero for all (τ,υ) with $|\tau\upsilon| > \xi_o$. The resulting effective support of $\Psi_c(\tau,\upsilon)$ is "cross-shaped" as shown in *Figure 35.* The cross shape of the ambiguity kernel $\Psi_c(\tau,\upsilon)$ is a direct consequence of the "product structure" $\Psi_c(\tau,\upsilon) = \Gamma_c(\tau\upsilon)$ and thus a distinctive feature of shift-scale-invariant SWDs.

We note that

$$\Psi_c(\tau,0) = \Psi_c(0,\tau) = \Psi_c(0,0) = 1 ;$$

thus, the ambiguity kernel $\Psi_c(\tau,\upsilon)$ is constant both on the τ axis and on the υ axis, and a decay of $|\Psi_c(\tau,\upsilon)|$ occurs only for lag points (τ,υ) off the axes. This simple fact largely determines the interference geometry of shift-scale-invariant SWDs [36]. Indeed, suppose that the interfering signal points (t_1,f_1) and (t_2,f_2) are displaced

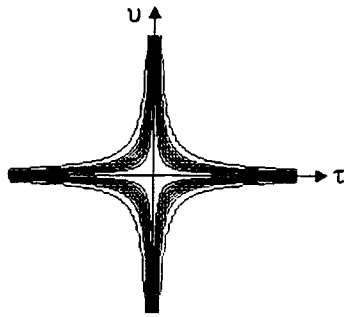

Figure 35. Ambiguity kernel $\Psi_c(\tau,\upsilon)$ of a shift-scale-invariant SWD.

with respect to both time and frequency so that *both* $|\tau_{12}| = |t_1-t_2|$ and $|\upsilon_{12}| = |f_1-f_2|$ are not close to zero. This situation is shown in *Figure 36.a*. The corresponding IT is here attenuated by the factor $|\Gamma_c(\tau_{12}\upsilon_{12})| < 1$. On the other hand, if the signal points are displaced only with respect to time, we have $\upsilon_{12} = 0$ and the IT is weighted by $|\Gamma_c(\tau_{12}\upsilon_{12})| = |\Gamma_c(0)| = 1$ which does not cause an attenuation (see *Figure 36.b*). An analogous result is obtained for signal points which are displaced only with respect to frequency ($\tau_{12} = 0$).

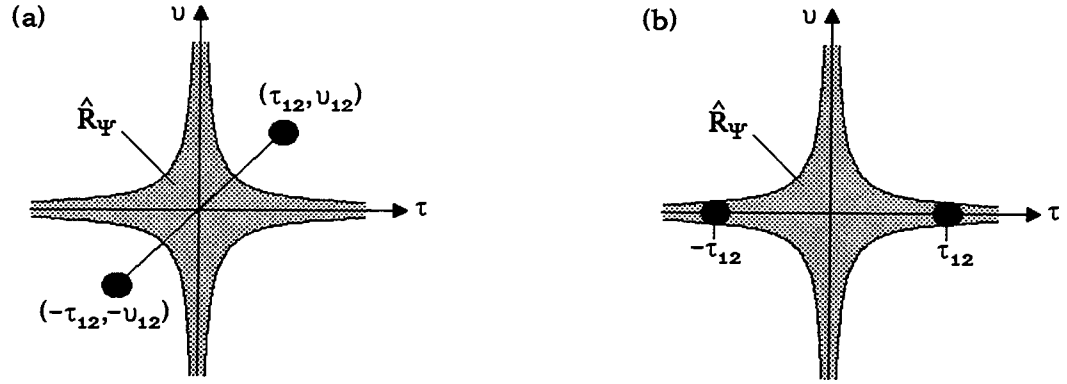

Figure 36. Correlative-domain analysis of shift-scale-invariant SWD: (a) case of IT attenuation, (b) case of no IT attenuation.

Of course, the above analysis is overly simplified since a strict pointwise localization of signal terms and ITs is not possible. Still, it is justified to draw the conclusion that shift-scale-invariant SWDs are capable of producing good IT attenuation for signal components displaced with respect to both time and frequency, whereas the IT attenuation will be poor for signal components displaced either only with respect to time or only with respect to frequency (or, in other words, for signal components occurring either at the same frequency or at the same time).

Further interesting properties of shift-scale-invariant SWDs can be derived from the example of two time-domain impulses $x_1(t) = \delta(t-t_1)$ and $x_2(t) = \delta(t-t_2)$. This example has already been studied for general shift-scale-invariant TFRs in Section

12. For simplicity, we now suppose that $\gamma_c(\alpha)$ is real-valued and even. From (12.5) and (12.6), the signal terms and IT are then obtained as

$$C_1^{(S)}(t,f) = |c_1|^2 \delta(t-t_1) , \qquad C_2^{(S)}(t,f) = |c_2|^2 \delta(t-t_2) ,$$

$$C_{12}^{(I)}(t,f) = 2|c_1||c_2| \frac{1}{|\tau_{12}|} \gamma_c\left(\frac{t-t_{12}}{\tau_{12}}\right) \cos(2\pi\tau_{12}f-\varphi_{12}) \tag{13.7}$$

with $\varphi_{12} = \arg\{c_1\}-\arg\{c_2\}$. As mentioned in Section 12, the signal terms feature perfect time concentration independent of the specific $\gamma_c(\alpha)$. In contrast, the IT is spread out in time, with increasing spread for growing time distance $|\tau_{12}| = |t_1-t_2|$. This increase of spread is compensated by a proportional decrease of the IT's height. The IT's *integral* with respect to time is fixed, i.e., independent of τ_{12} and even independent of the specific $\gamma_c(\alpha)$. In fact, due to

$$\int_t \frac{1}{|\tau_{12}|} \gamma_c\left(\frac{t-t_{12}}{\tau_{12}}\right) dt = \int_\alpha \gamma_c(\alpha)\, d\alpha = \Gamma_c(0) = 1 \qquad \text{for all } \tau_{12} \text{ and all normalized } \gamma_c(\alpha),$$

the IT's time integral equals the corresponding IT of the spectral energy density,

$$\int_t C_{12}^{(I)}(t,f)\, dt = P_{12}^{(I)}(f) = 2|c_1||c_2| \cos(2\pi\tau_{12}f-\varphi_{12}) . \tag{13.8}$$

While the IT's amplitude is reduced for growing time distance $|\tau_{12}| = |t_1-t_2|$, the IT's time spread increases such that the IT's time integral remains constant. In this sense, the IT is not attenuated at all. Note that (13.8) reflects the fact that C satisfies the marginal properties; this is a consequence of our initial normalization assumption $\Gamma_c(0) = \int \gamma_c(\alpha)\, d\alpha = 1$.

Completely analogous results are obtained for two complex sinusoids $x_1(t) = e^{j2\pi f_1 t}$ and $x_2(t) = e^{j2\pi f_2 t}$ (cf. (12.7)). Here, for growing frequency distance $|\upsilon_{12}| = |f_1-f_2|$, the IT's amplitude is reduced while the IT's frequency spread is increased proportionally such that the IT's frequency integral remains constant.

Just as the interference geometry of a shift-scale-invariant SWD is rather complex, so are the time-frequency concentration properties. In contrast to "simple" SWDs like the SPWD or the spectrogram, the time-frequency concentration of a shift-scale-invariant SWD depends on the signal itself; this is the reason why it cannot be globally characterized by a time spread and a frequency spread.

We first consider impulses in the time domain and in the frequency domain, $x(t) = \delta(t-t_0)$ and $y(t) = e^{j2\pi f_0 t}$. We obtain

$$C_x(t,f) = \delta(t-t_0) \qquad \text{and} \qquad C_y(t,f) = \delta(f-f_0) ,$$

which shows that, independently of $\gamma_c(\alpha)$, the impulses' perfect time or frequency concentration is preserved. However, this does not say that, in general, a shift-scale-invariant SWD features perfect time-frequency concentration. On the contrary, *for all other signals* a concentration impairment will be incurred. The singular role of impulses is easily understood by noting that, for the time-domain impulse $x(t) = \delta(t-t_0)$, $A_x(\tau,\upsilon) = \delta(\tau)$ is perfectly concentrated on the υ axis ($\tau = 0$) where $\Psi_c(0,\upsilon) =$

$\Gamma_c(0) = 1$ such that the multiplication of the AF $A_x(\tau,\upsilon)$ by the ambiguity kernel $\Psi_c(\tau,\upsilon)$ does not make any difference. Similarly, the AF of the frequency-domain impulse $y(t) = e^{j2\pi f_0 t}$ is perfectly concentrated on the τ axis where the ambiguity kernel is again 1. Obviously, these two cases exhaust the situations where the AF is invariant to the multiplication by the ambiguity kernel $\Psi_c(\tau,\upsilon)$. In all other cases, this multiplication will effect a windowing which causes a smearing of $C_x(t,f)$ and thus a loss in concentration as compared to the WD.

We illustrate this windowing effect for the case of a chirp signal with instantaneous frequency $f_i(t) = ct$. The WD, $W_x(t,f) = \delta(f-ct)$, is perfectly concentrated along the instantaneous-frequency line. The AF, $A_x(\tau,\upsilon) = \delta(\upsilon-c\tau)$, also exhibits perfect concentration. We assume that the effective support of $\Gamma_c(\xi)$ is the interval $|\xi| < \xi_0$; for simplicity, we further assume a rectangular $\Gamma_c(\xi)$, i.e., $\Gamma_c(\xi) = 1$ for $|\xi| < \xi_0$ and $\Gamma_c(\xi) = 0$ for $|\xi| > \xi_0$. The correlative dual of $C_x(t,f)$ is then obtained as

$$\hat{C}_x(\tau,\upsilon) = \Psi_c(\tau,\upsilon)\, A_x(\tau,\upsilon) = \Gamma_c(\tau\upsilon)\, \delta(\upsilon-c\tau) = \Gamma_c(c\tau^2)\, \delta(\upsilon-c\tau) = \begin{cases} \delta(\upsilon-c\tau), & |\tau| < \tau_0 \\ 0, & |\tau| > \tau_0 \end{cases}$$

with $\tau_0 = \sqrt{\xi_0/|c|}$. This is illustrated in *Figure 37*. Transforming back into the energetic domain according to (11.3) yields the following result for the SWD,

$$C_x(t,f) = \int_\tau \int_\upsilon \hat{C}_x(\tau,\upsilon)\, e^{j2\pi(t\upsilon-f\tau)} d\tau\, d\upsilon = \int_{-\tau_0}^{\tau_0} e^{-j2\pi(f-ct)\tau} d\tau = 2\tau_0 \frac{\sin[2\pi\tau_0(f-ct)]}{2\pi\tau_0(f-ct)}.$$

Thus $C_x(t,f)$, too, is concentrated along the instantaneous-frequency line $f = ct$; however, the concentration is not perfect since the frequency characteristic is a sinc function. The frequency spread increases with decreasing τ_0, i.e., for smaller "cutoff parameter" ξ_0 and/or larger chirp rate $|c|$. To achieve good frequency concentration (which, in the chirp case considered, also means good time concentration), we have to choose a large value for the cutoff parameter ξ_0; unfortunately, this entails a broad ambiguity kernel $\Psi_c(\tau,\upsilon)$ and thus yields poor IT attenuation. This shows that, in general, the fundamental tradeoff between good IT attenuation and good time-frequency concentration is not removed by the property of shift-scale invariance.

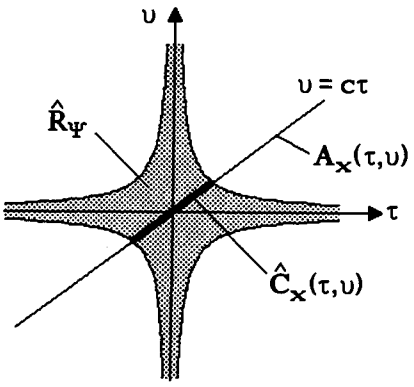

Figure 37. Shift-scale-invariant SWD of a chirp signal: windowing effect in the correlative domain.

While the property of shift-scale invariance does not seem to afford a marked improvement with respect to IT attenuation and time-frequency concentration in the general case, it is true that shift-scale-invariant SWDs do possess a theoretical advantage. In the case of SWDs which are not shift-scale-invariant, the smoothing usually destroys most of the nice theoretical properties of the WD (except for shift-invariance and real-valuedness). In contrast, a shift-scale-invariant SWD, besides being shift-invariant and scale-invariant, will satisfy many other nice properties with only mild restrictions regarding $\gamma_c(\alpha)$ [14,16,36]. In fact, it is real-valued (in the auto case) and satisfies the marginal, instantaneous-frequency, and group-delay properties [1] if $\gamma_c(\alpha)$ is real-valued, even, and normalized such that $\int \gamma_c(\alpha)\,d\alpha = \Gamma_c(0) = 1$. In addition, the finite-support properties (cf. Section 3) are obtained if $\gamma_c(\alpha) = 0$ for $|\alpha| > 1/2$. Other properties, such as the convolution and multiplication property [1] and unitarity [41] (validity of Moyal's formula [1]) cannot be satisfied by any SWD since they are incompatible with the smoothing characteristic (i.e., the requirement that $|\Psi_c(\tau,\upsilon)|$ decays for large values of $|\tau|$ and/or $|\upsilon|$).

On the other hand, a disadvantage of shift-scale-invariant SWDs is the fact that they do not allow the amounts of smoothing in the time direction and frequency direction to be chosen independently. For example, more time smoothing will be achieved by a narrower $\Gamma_c(\xi)$; due to the "product structure" $\Psi_c(\tau,\upsilon) = \Gamma_c(\tau\upsilon)$ of the ambiguity kernel, this automatically produces more frequency smoothing as well.

Examples of shift-scale-invariant SWDs. Shift-scale-invariant SWDs which have been proposed in the literature are the Choi-Williams distribution, the Born-Jordan distribution, and the class of "reduced-interference distributions."

In the case of the *exponential distribution* or *Choi-Williams distribution* (CWD) [42,16,43,14], the kernel functions $\gamma_c(\alpha)$ and $\Gamma_c(\xi)$ are Gaussians,

$$\gamma_{CWD}(\alpha) = \sqrt{\pi\xi_0^2}\, e^{-(\pi\xi_0\alpha)^2}, \qquad \Gamma_{CWD}(\xi) = e^{-(\xi/\xi_0)^2}. \tag{13.9}$$

The parameter $\xi_0 > 0$ controls the amount of smoothing; a smaller value of ξ_0 produces a stronger smoothing with respect to both time and frequency. In the extreme case of no smoothing, $\xi_0 \to \infty$, we have $\Gamma_{CWD}(\xi) \to 1$ and the CWD thus reduces to the WD. The CWD is real-valued in the auto case and satisfies the marginal properties as well as the instantaneous-frequency and group-delay properties. However, due to $\gamma_{CWD}(\alpha) \neq 0$ for $|\alpha| > 1/2$, the finite-support properties are not satisfied. This means that ITs will generally be spread over the entire time or frequency axis (although they will decay according to a Gaussian law). For example, the IT of two time-domain impulses at time points t_1 and t_2 follows with (13.7) as

$$CWD_{12}^{(I)}(t,f) = 2|c_1||c_2|\sqrt{\pi\xi_0^2}\,\frac{1}{|\tau_{12}|}\exp\left[-\left(\pi\xi_0\frac{t-t_{12}}{\tau_{12}}\right)^2\right]\cos(2\pi\tau_{12}f-\varphi_{12})\,;$$

it is a Gaussian with respect to time, with spread proportional to τ_{12}/ξ_0 (see *Figure 38.a*).

The *Born-Jordan distribution* (BJD) [44] is defined by a rectangular $\gamma_c(\alpha)$ or, equivalently, a $\Gamma_c(\xi)$ with sinc shape,

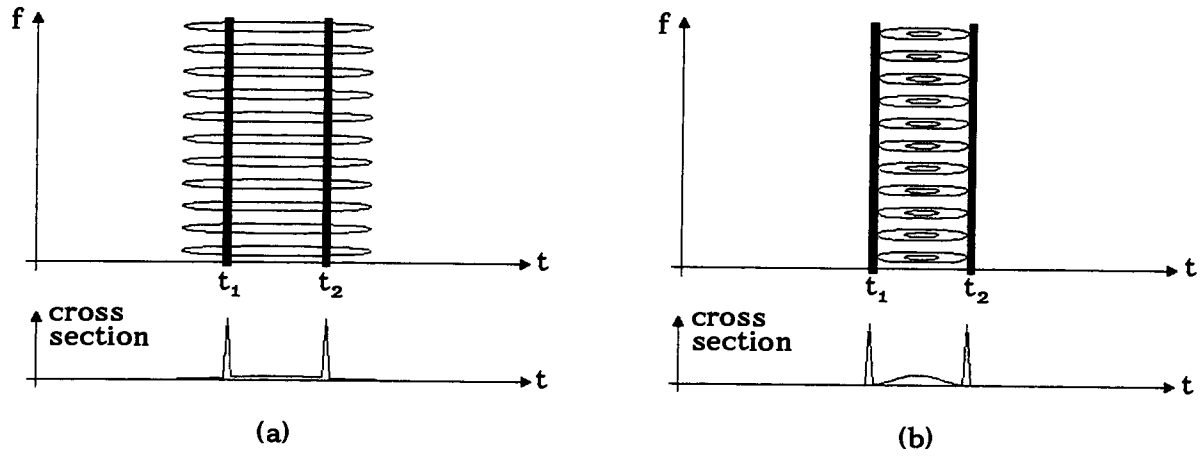

Figure 38. Signal terms and IT for two time-domain impulses: (a) CWD and (b) RID with Hamming window.

$$\gamma_{BJD}(\alpha) = \begin{cases} 1, & |\alpha| < 1/2 \\ 0, & |\alpha| > 1/2 \end{cases}, \qquad \Gamma_{BJD}(\xi) = \frac{\sin(\pi\xi)}{\pi\xi}.$$

The BJD satisfies also the finite-support properties; however, its IT attenuation is poorer than that of the CWD due to the relatively slow decay and the "sidelobes" of the sinc-shaped $\Gamma_{BJD}(\xi)$.

The class of *"reduced-interference" distributions* (RIDs) [16] is simply defined as the class of all shift-scale-invariant SWDs that are real-valued in the auto case and satisfy the marginal, instantaneous-frequency, group-delay, and finite-support properties. Thus, as mentioned above, apart from the general "smoothing condition" that $\Gamma_c(\xi)$ decays for larger $|\xi|$, the function $\gamma_c(\alpha)$ has to be real-valued, even, normalized such that $\int \gamma_c(\alpha)\,d\alpha = \Gamma_c(0) = 1$, and zero for $|\alpha| > 1/2$. This excludes the CWD (which does not satisfy the finite-support properties) but includes the BJD. As proposed in [16], standard finite-support windows can be used to construct a $\gamma_c(\alpha)$ satisfying the RID requirements; the BJD then corresponds to the rectangular window.

We note that the finite-support properties have an influence on the interference geometry since the IT corresponding to two signal components displaced in time can never extend beyond the total time support of the overall two-component signal. This is illustrated in *Figure 38.b* for an RID using a Hamming window for $\gamma_c(\alpha)$. Note that the improved time concentration of the IT (as compared to the CWD shown in Figure 38.a) is paid for by an increase of the IT's height. An analogous statement holds with respect to frequency.

Other SWDs. The definition of SWDs with sophisticated smoothing kernels continues to be a current research topic. In the following, we give a brief survey of some smoothing schemes that have been proposed recently.

The *cone-kernel representation* (CKR) [12,45,43,14] is defined by the ambiguity kernel

$$\Psi_{CKR}(\tau,\upsilon) = g(\tau)\,|\tau|\,\frac{\sin(\pi\tau\upsilon)}{\pi\tau\upsilon},$$

where $g(\tau)$ is some window function. In contrast to the ambiguity kernel of conventional SWDs, $\Psi_{CKR}(\tau,\upsilon)$ is zero at the origin of the (τ,υ)-plane, and attains its maximum at those points on the τ-axis where the function $g(\tau)\,|\tau|$ is maximal. Hence, the CKR implements a directional bandpass filtering, rather than lowpass filtering, of the WD. This can lead to significant residual ITs between signal terms occurring around the same frequency, for some range of the time lag $|\tau_{12}| = |t_1 - t_2|$ between the interfering signal components. A remarkable feature of the CKR is that it satisfies the temporal finite-support property and is yet capable of attenuating ITs oscillating in the time direction. The CKR achieves good time-frequency concentration and good IT attenuation in the case of multiple sinosoidal bursts with quasi-stationary instantaneous frequencies. The CKR's integral with respect to the frequency variable, and thus also the integral over the entire time-frequency plane, is zero; hence, the CKR is not an "energy distribution."

An obvious extension of the smoothing discussed so far is a "directional" smoothing [9,10,46] where the Wigner kernel $\psi_c(t,f)$ is oriented in a given direction of the time-frequency plane and, consequently, the smoothing is maximal in this direction. Such a directional smoothing is advantageous if the ITs are known to oscillate mainly in a specific, slanted direction. We note that directional smoothing is inconsistent with both the separable structure of the SPWD kernels and the product structure of shift-scale-invariant SWDs.

A recent extension of the Choi-Williams distribution is the *generalized exponential distribution* (GED) [17,14] for which

$$\Psi_{GED}(\tau,\upsilon) = \exp\left[-\left(\frac{\tau}{\tau_o}\right)^{2M}\left(\frac{\upsilon}{\upsilon_o}\right)^{2N}\right].$$

The GED is shift-scale-invariant only if M=N. The parameters τ_o, υ_o, M, and N permit an adjustment of the smoothing characteristics that is more flexible than in the CWD. The CWD is a special case corresponding to the parameters M=N=1. An SWD following a similar philosophy is the *Butterworth distribution* [17,14].

A general disadvantage of these more sophisticated SWD definitions is that, often, they perform well for certain types of signals but may perform poorly for other signal types. In many cases, a significant performance gain can be achieved by adapting the smoothing kernel to the specific signal under analysis. An example is given by the *radially-Gaussian kernel distribution* [11,14] whose ambiguity kernel is a Gaussian in each radial direction of the (τ,υ)-plane,

$$\Psi_{RGD,x}(\tau,\upsilon) = \exp\left[-\frac{(\tau/\tau_o)^2+(\upsilon/\upsilon_o)^2}{2\,\sigma_x^2(\Theta)}\right], \qquad \Theta = \arctan\frac{\upsilon/\upsilon_o}{\tau/\tau_o},$$

and where the Gaussian's spread, $\sigma_x(\Theta)$, depends on the radial direction (Θ) and is optimally adapted to the signal $x(t)$ under analysis. This scheme is particularly suited for multicomponent signals consisting of linear FM (chirp) components with

various chirp rates. Other signal-adaptive SWDs are discussed in [20,46-48]. Note, however, that if the signal-adaptive control mechanism is considered part of the SWD definition, then the SWD is no longer quadratic with respect to the signal.

Another extension of the WD smoothing discussed so far is the use of different smoothing kernels for different points of the time-frequency plane. For example, if a detailed *a-priori* knowledge about the signal is available, then it may be advantageous to use different kernel spreads and/or directions in different regions of the time-frequency plane [9,10, 46-48]. An important special case of this philosophy is the use of an *affine* smoothing, which implements a "constant-Q" time-frequency analysis where the time and frequency concentrations are better and poorer, respectively, for growing analysis frequency [13,14]. An alternative approach to constant-Q time-frequency analysis is proposed in [49,48]. We emphasize, however, that these "time-frequency-varying" SWDs are no longer members of the shift-invariant class (bilinear Cohen class).

Comparison of SWDs. An in-depth comparison of different SWDs [14, 43,50] is beyond the scope of this work. In the following, we concentrate on some essential points and illustrate some of the properties and effects discussed previously by means of computer simulations. We shall also compare the WD, PWD, SPWD, spectrogram, and CWD for a few specific signals.

As has been stated above, the IT attenuation and time-frequency concentration properties of an SWD depend on the shape of the ambiguity kernel $\Psi_c(\tau,\upsilon)$. *Figure 39* compares schematic representations of the effective supports of the ambiguity kernels of various SWDs. An IT falling outside these effective supports will be effectively suppressed. Also, the concentration loss in a signal term will be larger if a larger part of the corresponding AF lies outside the effective support of $\Psi_c(\tau,\upsilon)$.

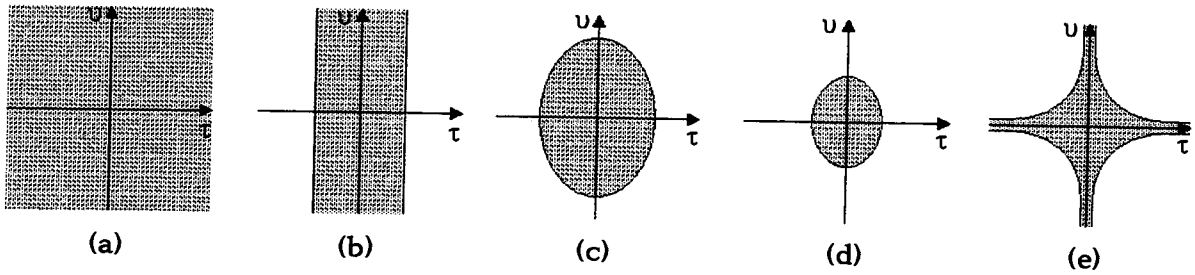

Figure 39. Effective support of ambiguity kernel $\Psi_c(\tau,\upsilon)$: (a) WD (no smoothing), (b) PWD, (c) SPWD, (d) spectrogram with Gaussian window, (e) shift-scale-invariant SWD.

We next consider "simple" SWDs for which the amounts of smoothing in the time and frequency directions can be roughly characterized by the time spread Δt and the frequency spread Δf, respectively, of the Wigner kernel $\psi_c(t,f)$. This class includes the PWD, SPWD, and spectrogram but not shift-scale-invariant SWDs like the CWD or BJD. *Figure 40* compares possible choices of the spreads Δt and Δf for various "simple" SWDs. In the extreme case of the WD (case of no smoothing),

Δt and Δf are both zero, which results in perfect time-frequency concentration but no IT attenuation at all. The PWD permits frequency smoothing ($\Delta f \geq 0$) but no time smoothing ($\Delta t = 0$), and thus yields an attenuation of ITs oscillating in the frequency direction at the cost of impaired frequency concentration. The SPWD allows a free and independent choice of the smoothing spreads Δt and Δf, and thus an arbitrary control of IT attenuation and time-frequency concentration (apart from the fundamental tradeoff relating these two properties). Finally, in the spectrogram the spreads are constrained by the uncertainty relation $\Delta t \, \Delta f \geq 1/(4\pi)$ and thus cannot both be made arbitrarily small. This leads to a fixed minimal amount of overall smoothing, corresponding to substantial IT attenuation but poor time-frequency concentration.

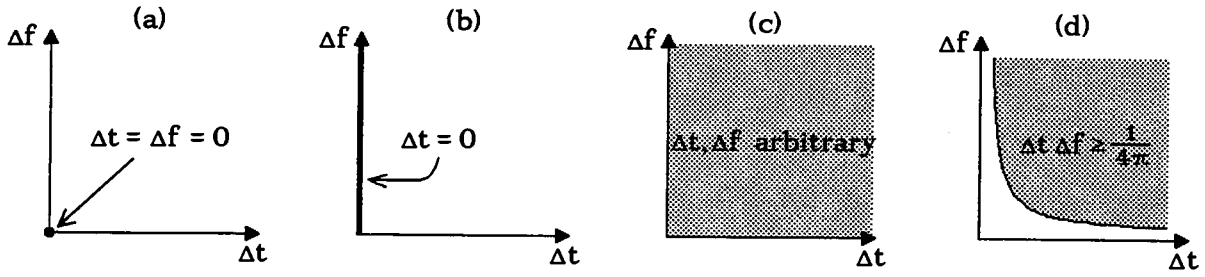

Figure 40. Possible smoothing spreads Δt and Δf for (a) WD, (b) PWD, (c) SPWD, and (d) spectrogram.

The following four figures illustrate the characteristic interference-geometric properties of shift-scale-invariant SWDs. They also show a comparison of the results obtained with a specific shift-scale-invariant SWD (the CWD) with corresponding results of the SPWD. For a fair comparison, the dynamic ranges of all contour-line plots have been chosen strictly identical (10 contour lines with linear spacing between the maximum height and 1% of the maximum).

Figure 41 compares the results of the SPWD and the CWD for the case of two chirp signals. Note that the CWD's concentration is poorer than that of the SPWD although the CWD's ITs are considerably stronger. Of course, the CWD's ITs could be reduced in height by choosing a smaller value for the spread parameter ξ_o

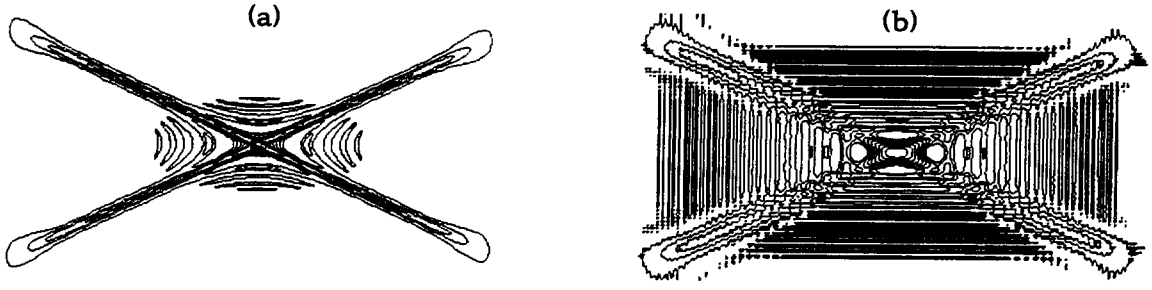

Figure 41. (a) SPWD and (b) CWD of two chirp signals.

in (13.9); however, this would produce a further broadening of the chirp signal terms and an even greater spreading-out of the ITs in the time or frequency direction. The CWD result nicely illustrates the interference geometry of shift-scale-invariant SWDs. Specifically, the ITs are observed to oscillate either only in the time direction or only in the frequency direction. This follows from the fact that, as explained further above, only signal points occurring either at the same time or at the same frequency produce an IT; due to the general interference geometry, the IT will then oscillate in the time direction (in the first case) or in the frequency direction (in the second case).

We next compare the results of the SPWD and CWD obtained for a signal consisting of four time-frequency-shifted Gaussian components [14]. Two different signals are considered: the first signal, shown in *Figure 42*, consists of Gaussians which all occur at different times and frequencies. In contrast, the second signal (see *Figure 43*) contains Gaussians of which two occur at the same time and two occur at the same frequency.

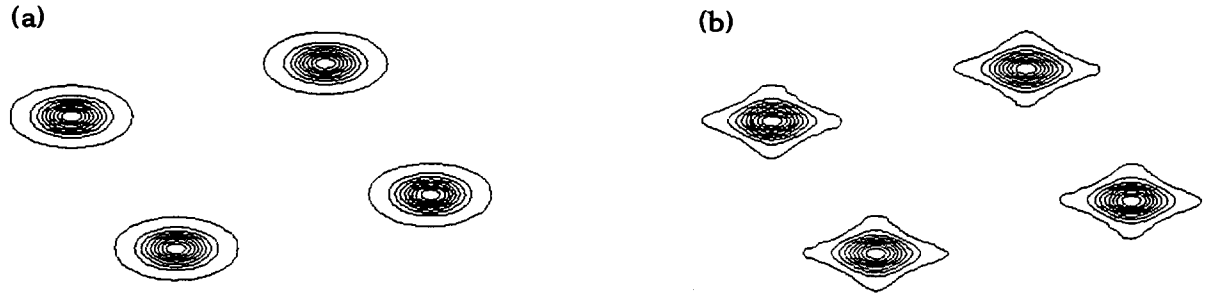

Figure 42. (a) SPWD and (b) CWD for a signal consisting of four Gaussians, all of which occur at different times and frequencies.

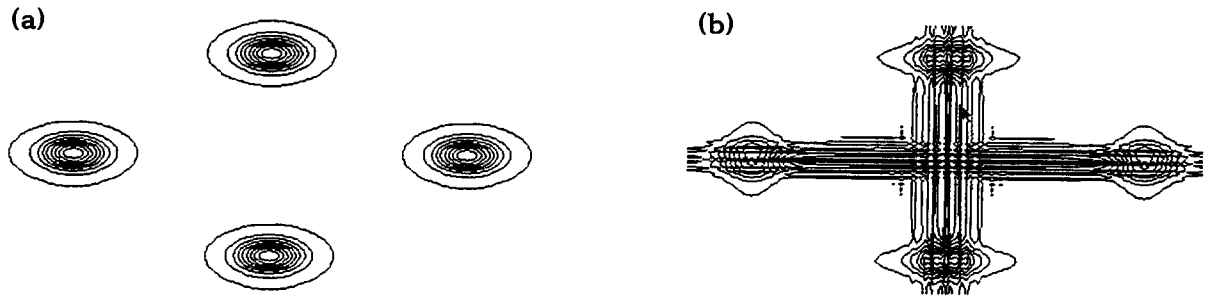

Figure 43. (a) SPWD and (b) CWD for a signal consisting of four Gaussians, of which two coincide in time and two coincide in frequency. (Note that in (b) the ITs of the CWD have been truncated; they actually extend beyond the signal terms.)

In the SPWD, the two situations lead to similar results; in particular, the ITs are nicely suppressed in both cases. In contrast, the CWD shows satisfactory IT sup-

pression only in the first case; in the second case, substantial ITs are seen to exist. Again, the reason is that the CWD yields poor IT attenuation for signal components occurring either at the same time or at the same frequency (cf. Figure 36). Note, also, the large time and frequency spreads of the CWD's ITs. This confirms the result, derived previously, that an attenuation of IT amplitude is paid for by a proportional increase of IT spread.

Figure 44 shows the results of the SPWD, CWD, and spectrogram for two "parallel" chirp signals. The time distance between the two chirp signals is varied whereas the smoothing characteristic of each representation is held constant. The results confirm the general rule that an IT corresponding to signal components with larger distance in the time-frequency plane features a faster oscillation and will

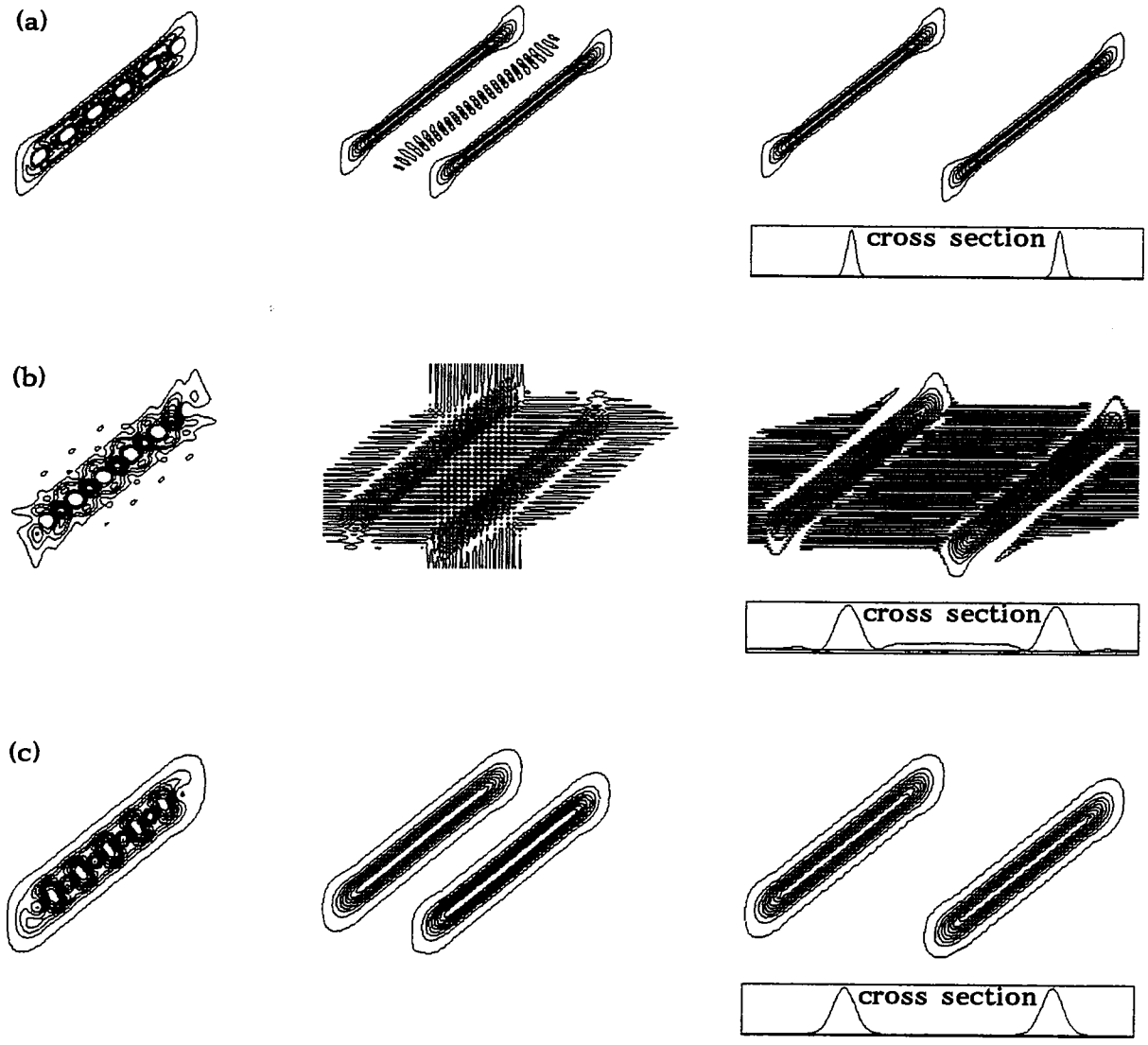

Figure 44. Results of (a) SPWD, (b) CWD, and (c) spectrogram for two "parallel" chirp signals with various time distances.

hence be attenuated more in an SWD. Note that, in the CWD, the time spread of the IT increases with the time distance of the signal terms. Also, the IT of the spectrogram is seen to be zero for non-overlapping signal terms.

Finally, *Figure 45* illustrates the IT-attenuation/concentration tradeoff by comparing the results of different "simple" SWDs obtained for a given signal. The WD (Figure 45.a) represents the extreme case of no smoothing and, consequently, perfect time-frequency concentration but no IT attenuation. The PWD features smoothing in the frequency direction only; hence, ITs oscillating only in the time direction are not attenuated (see Figure 45.b). Figures 45.c-e show results of the SPWD with various window lengths. It is verified that more smoothing yields a better attenuation of ITs but causes a stronger broadening of the signal terms, i.e., poorer time-frequency concentration. Spectrogram results are shown in Figures 45.f and 45.g. The similarity of Figures 45.e and 45.f shows that the SPWD is capable of simulating a spectrogram if the smoothing in the SPWD is chosen sufficiently strong. All in all, these results demonstrate the great flexibility of the SPWD which, on the one hand, contains the WD and PWD as special cases and, on the other, can also realize an extensive smoothing comparable to that of the spectrogram.

14. CONCLUSION

Throughout this work, we have emphasized the geometrical properties of interference terms (ITs) since it is this "interference geometry" which is most important for practical applications. Often, we are in the "interpretation" situation where we have to interpret the Wigner distribution (WD) of an otherwise unknown signal: by inspecting the signal's WD, we want to obtain information about the signal's time-frequency structure, i.e., decide in what regions of the time-frequency plane the signal's energy is located. However, a large WD value at some time-frequency point does not necessarily mean that the signal has any energy around this point. It is exactly this fact (closely related with the uncertainty principle which *a-priori* prohibits the pointwise energetic interpretation of any time-frequency representation) that necessitates the distinction between *signal terms* and *ITs*. In interpreting a large WD value, we need to decide whether it is part of a signal term (which carries energy) or an oscillatory IT (which usually carries little or no energy). The laws of interference geometry allow us not only to identify signal terms and ITs but also to associate an IT with the corresponding signal terms: given two signal terms, we know where the associated IT is located; conversely, given an IT, we can derive the time-frequency locations of the associated pair of signal terms.

This application of interference geometry is possible whenever the signal consists of energetic components which are sufficiently concentrated and separated in the time-frequency plane. Examples of "concentrated" signals are signals of the AM-FM type where the signal energy is concentrated along the curve of instantaneous frequency, or Gaussian signals which are concentrated around some time-frequency point.

There exist, however, signals which do not have such a "simple" time-frequency

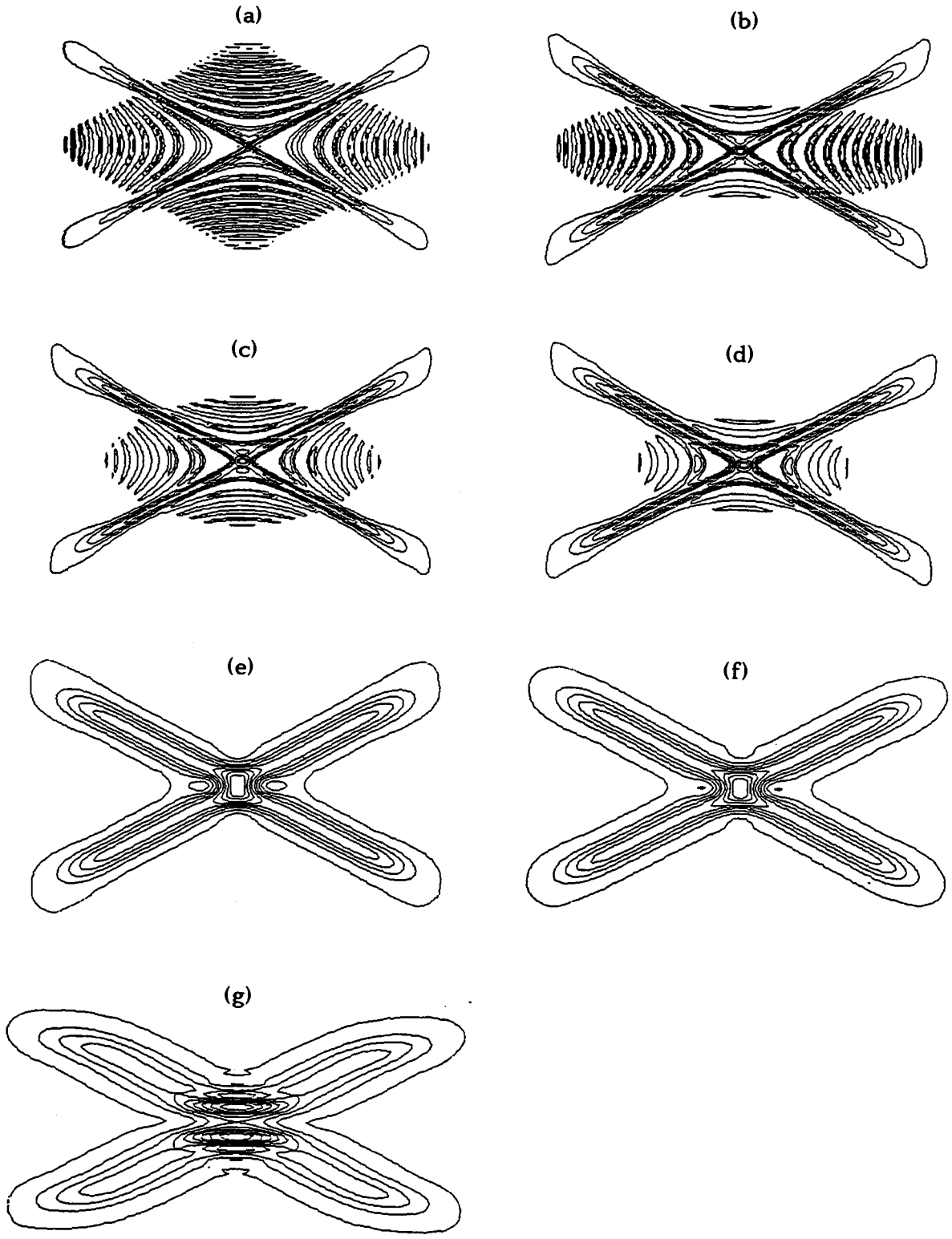

Figure 45. SWD results for two crossed chirps. (a) WD, (b) PWD, (c) SPWD with mild smoothing, (d) SPWD with stronger smoothing, (e) SPWD with strong smoothing, (f) spectrogram with "good" window, (g) spectrogram with "too long" window.

structure. Extreme cases are noise signals whose energy is irregularly spread over larger regions of the time-frequency plane. Here, a distinction between "signal terms" and ITs is hardly possible.

In any case, it should be noted that the distinction between signal terms and ITs is not based on a mathematically strict criterion. (In the last instance, any WD point is made up by "interference" of other points - cf. the inner interference formula (5.1).) Rather, the definition of ITs is based on the ITs' oscillation and is thus a phenomenological one. In the case of outer interference, the definition of ITs as bilinear cross terms is not unique either since any signal can be split into signal components in an infinity of ways, and the concept of a "multicomponent signal" is not a mathematically strict one. Still, in many situations it is intuitively clear what the signal components are, and in these cases the distinction between signal terms and ITs, as well as the laws of interference geometry, are indispensable for a proper interpretation of WD results and an appropriate choice of a WD smoothing kernel.

From a theoretical viewpoint, the occurrence of oscillatory ITs in the WD is not surprising since the ITs are *enforced* by the marginal properties, i.e., by the fact that the WD is an energy distribution. In many situations, the marginal properties impart an energetic interpretation to ITs; hence, it does not seem justified to call ITs "artifacts" of the signal representation WD. We note that in general oscillatory components *must* exist in other energy distributions as well, even in the case of the "positive" distributions [51,52] which are non-bilinear. The differences between the ITs of various energy distributions are essentially differences with respect to interference geometry. These differences in interference geometry have a heavy influence on the results obtained with different representations. For example, the comparison of the WD and the Rihaczek distribution clearly shows that representations with very similar general properties but different interference geometries will generally produce very different results for the same signal (cf. Figure 22). The aspect of interference geometry is thus an important criterion for selecting a specific time-frequency representation for a given application.

In some situations, ITs are important since they provide specific information which is not contained in the signal terms. In particular, the relative phase of two signal components is visible only in the IT (via the phase of its oscillation). Time-frequency methods for optimal detection and estimation are often based on the unitarity (validity of Moyal's formula) of the time-frequency representation used [53]; this necessitates the occurrence of ITs since the unitarity property is incompatible with IT attenuation by means of smoothing [41]. Also, ITs often allow the identification of small signal components in contour-line plots: if a signal component is so small that its signal term falls below the lowest contour line, the signal term itself will be invisible; however, the IT caused by interference of this signal component with a larger signal component may still be visible.

Even though some arguments in favor of ITs do exist, the fact remains that ITs are a nuisance in many applications since they tend to conceal the signal terms on which a signal's interpretation usually relies. A smoothing of the WD results in an

attenuation of ITs at the cost of impaired time-frequency concentration and the sacrifice of at least some of the nice mathematical properties of the WD. In many applications, however, these properties are not really utilized and can thus be sacrificed in favor of improved clearness and readability of analysis results (this is especially the case in applications where a time-frequency representation is interpreted by a human analyst).

Our treatment of WD smoothing has been placed in a deterministic framework. We note, however, that a WD smoothing can also be motivated from a stochastic viewpoint, namely, the viewpoint of time-varying spectral estimation [38,39,54]. Here, the various smoothed WDs (SWDs) can be interpreted as estimators of the Wigner-Ville spectrum of a nonstationary random process. In this framework, the IT attenuation/time-frequency-concentration tradeoff becomes a variance/bias tradeoff: more smoothing reduces the estimator's variance while increasing its bias.

A classical SWD is the spectrogram (or, in the context of spectrum estimation, the periodogram) which, however, allows only a very restricted control over the smoothing characteristics. Due to its flexibility in adjusting the smoothing characteristics, the smoothed pseudo WD (SPWD) has a clear advantage over the spectrogram. Shift-scale-invariant SWDs like the Choi-Williams distribution, on the other hand, are theoretically attractive since they preserve a maximal number of nice mathematical WD properties. They do not, however, appear to produce clearer results than the SPWD in the general case. Of course, it is impossible to make a general statement in favor of a specific SWD. The "best" SWD always depends on the application at hand and, in the last instance, is also a matter of personal predilection.

The development of sophisticated smoothing methods continues to be a current research topic. Examples of recently proposed SWDs are the cone-kernel representation, the generalized exponential distribution, and the radially-Gaussian kernel distribution. Although we have here considered shift-invariant smoothing schemes where the smoothing kernel does not depend on the time-frequency point of evaluation, there also exist "time-frequency varying" SWDs such as "constant-Q" SWDs which are members of the affine class of bilinear time-frequency representations. In all cases, the smoothing kernel contains one or more parameters (e.g., window lengths or spread parameters) which influence the smoothing characteristics and need to be adjusted. This adjustment is either done "manually" by the signal analyst or automatically via an adaptive algorithm; the latter case corresponds to a truly signal-adaptive SWD.

While we have concentrated in this chapter on smoothing schemes for attenuating the WD's ITs, we note that several alternative approaches for IT suppression have been proposed. Relevant references are [55-58], to name but a few.

Finally, a issue which has not been addressed in this chapter is that of *positivity*. We have mentioned that the WD's local negativity can be viewed as an interference phenomenon. Also, it is clear that a smoothing of the WD will usually reduce the amount of negativity (a prominent example is the spectrogram which is always nonnegative). An in-depth discussion of positivity issues may be found in [59].

ACKNOWLEDGEMENT

The authors wish to express their thanks to R.L. Urbanke who prepared most of the figures and simulation plots contained in this work. Also, the support of the *Fonds zur Förderung der wissenschaftlichen Forschung* (grant No. P7354-PHY) is gratefully acknowledged.

REFERENCES

[1] T.A.C.M. Claasen and W.F.G. Mecklenbräuker, "The Wigner distribution - A tool for time-frequency signal analysis, Part I: Continuous-time signals." *Philips J. Res.*, Vol. 35, pp. 217-250, 1980.

[2] A.J.E.M. Janssen, "On the locus and spread of pseudo-density functions in the time-frequency plane." *Philips J. Res.*, Vol. 37, pp. 79-110, 1982.

[3] P. Flandrin, "Some features of time-frequency representations of multicomponent signals." *Proc. IEEE ICASSP-84*, San Diego (CA), pp. 41.B.4.1-4, March 1984.

[4] F. Hlawatsch, "Interference terms in the Wigner distribution." *Proc. 1984 Int. Conf. Digital Signal Processing*, Florence (Italy), pp. 363-367, Sept. 1984.

[5] P. Flandrin, "Representations des signaux dans le plan temps-frequence." These D.I., Grenoble, 1982.

[6] P. Flandrin and B. Escudie, "Geometrie des fonctions d'ambiguite et des representations conjointes de Ville: l'approche de la theorie des catastrophes." *8e Coll. Trait. Signal GRETSI*, Nice (France), pp. 69-74, 1981.

[7] P. Flandrin and F. Hlawatsch, "Signal representations geometry and catastrophes in the time-frequency plane." In *Mathematics in Signal Processing*, Eds. T.S. Durrani et al., Clarendon Press, Oxford, pp. 3-14, 1987.

[8] W. Wokurek, F. Hlawatsch, and G. Kubin, "Wigner distribution analysis of speech signals." *Proc. 1987 Int. Conf. Digital Signal Processing*, Florence (Italy), pp. 294-298, Sept. 1987.

[9] J.C. Andrieux, M.R. Feix, G. Mourgues, P. Bertrand, B. Izrar, and V.T. Nguyen, "Optimum smoothing of the Wigner-Ville distribution." *IEEE Trans. Acoust., Speech, Signal Processing*, Vol. 35, No. 6, June 1987, pp. 769-806.

[10] M.D. Riley, "Time-frequency representations for speech signals." PhD Dissertation, MIT Artificial Intelligence Laboratory, Cambridge, MA, May 1987, also as *Speech Time-Frequency Representations*, Boston: Kluwer, 1989.

[11] R.G. Baraniuk and D.L. Jones, "A radially Gaussian, signal-dependent time-frequency representation." *Proc. IEEE ICASSP-91*, Toronto, Canada, May 1991, pp. 3181-3184.

[12] Y. Zhao, L.E. Atlas, and R.J. Marks, II, "The use of cone-shaped kernels for generalized time-frequency representations of nonstationary signals." *IEEE Trans. Acoust., Speech, Signal Processing*, Vol. 38, No. 7, July 1990, pp. 1084-1091.

[13] O. Rioul and P. Flandrin, "Time-scale energy distributions: A general class extending wavelet transforms." *IEEE Trans. Signal Processing*, Vol. 40, No. 7, July 1992, pp. 1746-1757.

[14] F. Hlawatsch and G.F. Boudreaux-Bartels, "Linear and quadratic time-frequency signal representations." *IEEE Signal Processing Mag.*, Vol. 9, Apr. 1992, pp. 21-67.

[15] F. Hlawatsch, "Time-frequency methods for signal processing." Technical Report 1291-0001, Dept. Elec. Eng., Univ. of Rhode Island, Kingston, RI, Dec. 1991.

[16] J. Jeong and W.J. Williams, "Kernel design for reduced interference distributions." *IEEE Trans. Signal Processing*, Vol. 40, No. 2, Feb. 1992, pp. 402-412.

[17] A. Papandreou and G.F. Boudreaux-Bartels, "Distributions for time-frequency analysis: A generalization of Choi-Williams and the Butterworth distribution." *Proc. IEEE ICASSP-92*, San Francisco, CA, Mar. 1992, Vol. V, pp. 181-184.

[18] S. Kadambe and G.F. Boudreaux-Bartels, "A comparison of the existence of "cross terms" in the Wigner distribution and the squared magnitude of the wavelet transform and the short time Fourier transform." *IEEE Trans. Signal Processing*, Vol. 40, No. 10, Oct. 1992, pp. 2498-2517.

[19] J. Jeong and W.J. Williams, "Mechanism of the cross-terms in spectrograms." *IEEE Trans. Signal Processing*, Vol. 40, No. 10, Oct. 1992, pp. 2608-2613.

[20] R.G. Baraniuk and D.L. Jones, "A signal-dependent time-frequency representation, Part I." *IEEE Trans. Signal Processing*, vol. 41, no. 4, Apr. 1993, pp. 1589-1602.

[21] F. Hlawatsch, "A simple upper bound on the cross terms of the spectrogram and the scalogram." Tech. Rep. 92-01, INTHFT, Vienna Univ. Technol., Sept. 1992.

[22] T.A.C.M. Claasen and W.F.G. Mecklenbräuker, "On the time-frequency discrimination of energy distributions: Can they look sharper than Heisenberg?" *Proc. IEEE ICASSP-84*, San Diego (CA), pp. 41.B.7.1-4, 1984.

[23] A. Papoulis, *Signal Analysis*. McGraw-Hill, 1977.

[24] M.V. Berry, "Semi-classical mechanics in phase-space: A study of Wigner's function." *Phil. Trans. Roy. Soc.* London A 287, pp. 237-271, 1977.

[25] T. Poston and I. Stewart, *Catastrophe Theory and Its Application*. London: Pitman, 1978.

[26] M. Abramowitz and I.A. Stegun, *Handbook of Mathematical Functions*. New York: Dover Publications, 1965.

[27] T.A.C.M. Claasen and W.F.G. Mecklenbräuker, "The Wigner distribution - A tool for time-frequency signal analysis, Part II: Discrete-time signals." *Philips J. Res.*, Vol. 35, pp. 276-300, 1980.

[28] F. Peyrin and R. Prost, "A unified definition for the discrete-time, discrete-frequency, and discrete time/frequency Wigner distributions." *IEEE Trans. Acoust., Speech, Signal Processing*, Vol. 34, Aug. 1986, pp. 858-867.

[29] T.A.C.M. Claasen and W.F.G. Mecklenbräuker, "The Wigner distribution - A tool for time-frequency signal analysis, Part III: Relations with other time-frequen-

cy signal transformations." *Philips J. Res.*, Vol. 35, pp. 372-389, 1980.

[30] W. Rihaczek, "Signal energy distribution in time and frequency." *IEEE Trans. Information Theory*, Vol. 14, pp. 369-374, 1968.

[31] R.D. Hippenstiel and P.M. De Oliveira, "Time-varying spectral estimation using the instantaneous power spectrum (IPS)." *IEEE Trans. Acoust., Speech, Signal Processing*, Vol. 38, No. 10, Oct. 1990, pp. 1752-1759.

[32] H.H. Szu and J.A. Blodgett, "Wigner distribution and ambiguity function." In *Optics in Four Dimensions*, L.M. Narducci, Ed., New York: American Institute of Physics, 1981, pp. 355-381.

[33] H.L. Van Trees, *Detection, Estimation, and Modulation Theory, Part III: Radar-Sonar Signal Processing and Gaussian Signals in Noise.* Malabar, FL: Krieger Publishing Company, 1992.

[34] F. Hlawatsch, "Duality and classification of bilinear time-frequency signal representations." *IEEE Trans. Signal Processing*, Vol. 39, July 1991, pp. 1564-1574.

[35] L. Cohen, "Generalized phase-space distribution functions." *J. Math. Phys.*, Vol. 7, pp. 781-786, 1966.

[36] F. Hlawatsch and R. L. Urbanke, "Bilinear time-frequency representations of signals: The shift-scale invariant class." *IEEE Trans. Signal Processing*, vol. 42, no. 2, Feb. 1994, pp. 357-366.

[37] D.L. Jones and T.W. Parks, "A resolution comparison of several time-frequency representations." *IEEE Trans. Signal Processing*, Vol. 40, No. 2, Feb. 1992, pp. 413-420.

[38] P. Flandrin and W. Martin, "Pseudo-Wigner estimators for the analysis of nonstationary processes." *Proc. IEEE Spectr. Est. Workshop II*, Tampa, FL, pp. 181-185, Nov. 1983.

[39] W. Martin and P. Flandrin, "Wigner-Ville spectral analysis of nonstationary processes." *IEEE Trans. Acoust., Speech, Signal Processing*, Vol. ASSP-33, No. 6, Dec. 1985, pp. 1461-1470.

[40] R.A. Altes, "Detection, estimation, and classification with spectrograms." *J. Acoust. Soc. Am.*, Vol. 67, pp. 1232-1246, Apr. 1980.

[41] F. Hlawatsch, "Regularity and unitarity of bilinear time-frequency signal representations." *IEEE Trans. Information Theory*, Vol. 38, No. 1, Jan. 1992, pp. 82-94.

[42] H.-I. Choi and W.J. Williams, "Improved time-frequency representation of multicomponent signals using exponential kernels." *IEEE Trans. Acoust., Speech, Signal Processing*, Vol. 37, No. 6, June 1989, pp. 862-871.

[43] F. Hlawatsch, T.G. Manickam, R. L. Urbanke, and W. Jones, "Smoothed pseudo-Wigner distribution, Choi-Williams distribution, and cone-kernel representation: Ambiguity-domain analysis and experimental comparison," *Signal Processing*, vol. 43, no. 2, May 1995, pp. 149-168.

[44] L. Cohen, "Time-frequency distributions - A review." *Proc. IEEE*, Vol. 77, No. 7, pp. 941-981, July 1989.

[45] S. Oh and R.J. Marks, II, "Some properties of the generalized time-frequency representation with cone-shaped kernels." *IEEE Trans. Signal Processing*, Vol. 40, No. 7, July 1992, pp. 1735-1745.

[46] D.L. Jones and T.W. Parks, "A high-resolution data-adaptive time-frequency representation." *IEEE Trans. Acoust., Speech, Signal Processing*, Vol. 38, No. 12, Dec. 1990, pp. 2127-2135.

[47] S. Kadambe, G.F. Boudreaux-Bartels, and P. Duvaut, "Window length selection for smoothing the Wigner distribution by applying an adaptive filter technique." *Proc. IEEE ICASSP-89*, pp. 2226-2229, 1989.

[48] Proceedings of the *IEEE-SP International Symposium on Time-Frequency and Time-Scale Analysis*, Victoria, BC, Canada, Oct. 1992.

[49] A. Papandreou, F. Hlawatsch, and G.F. Boudreaux-Bartels, "The hyperbolic class of quadratic time-frequency representations - Part I." *IEEE Trans. Signal Processing*, vol. 41, Dec. 1993, pp. 3425-3444; see also vol. 45, Feb. 1997, pp. 303-315.

[50] C. Griffin and A.H. Nuttall, "Comparison of two kernels for the modified Wigner distribution function." *SPIE Conf.*, San Diego, CA, July 1991.

[51] L. Cohen and T. Posch, "Positive time-frequency distributions." *IEEE Trans. Acoust., Speech, Signal Processing*, Vol. 33, Feb. 1985, pp. 31-38.

[52] A.J.E.M. Janssen, "A note on 'Positive Time-Frequency Distributions'." *IEEE Trans. Acoust., Speech, Signal Processing*, Vol. 35, May 1987, pp. 701-703.

[53] P. Flandrin, "A time-frequency formulation of optimum detection." *IEEE Trans. Acoust., Speech, Signal Processing*, Vol. 36, Sept. 1988, pp. 1377-1384.

[54] P. Flandrin and W. Martin, "The Wigner-Ville spectrum of nonstationary random signals." In *The Wigner distribution - Theory and Applications in Signal Processing*, W. Mecklenbräuker and F. Hlawatsch, Eds., Amsterdam: Elsevier, 1997.

[55] F. Hlawatsch and W. Krattenthaler, "A new approach to time-frequency signal decomposition." *Proc. IEEE ISCAS-89*, Portland, Oregon, pp. 1248-1251, May 1989.

[56] M. Sun, C.C. Li, L.N. Sekhar, and R.J. Sclabassi, "Elimination of cross-components of the discrete pseudo Wigner distribution via image processing." *Proc. IEEE ICASSP-89*, Glasgow (Scotland), pp. 2230-2233, May 1989.

[57] R.S. Orr, J.M. Morris, and S.E. Qian, "Use of the Gabor representation for Wigner distribution crossterm suppression." *Proc. IEEE ICASSP-92*, San Francisco, CA, Mar. 1992, Vol. V, pp. 29-31.

[58] S. Barbarossa and A. Zanalda, "A combined Wigner-Ville and Hough transform for cross-terms suppression and optimal detection and parameter estimation." *Proc. IEEE ICASSP-92*, San Francisco, CA, Mar. 1992, Vol. V, pp. 173-176.

[59] A.J.E.M. Janssen, "Positivity and spread of bilinear time-frequency distributions," In *The Wigner distribution - Theory and Applications in Signal Processing*, W. Mecklenbräuker and F. Hlawatsch, Eds., Amsterdam: Elsevier, 1997.